Navigating the Depths: Pioneering water depth measurements through distributed acoustic sensing

A new method for monitoring the water-mud interface and water column height using passive noise and fibre optical cables

Buisman, M.

DOI
10.4233/uuid:6fbf12a7-f5df-4c46-9312-b8a061122f4d

Publication date
2025

Document Version
Final published version

Citation (APA)
Buisman, M. (2025). *Navigating the Depths: Pioneering water depth measurements through distributed acoustic sensing: A new method for monitoring the water-mud interface and water column height using passive noise and fibre optical cables* . [Dissertation (TU Delft), Delft University of Technology]. https://doi.org/10.4233/uuid:6fbf12a7-f5df-4c46-9312-b8a061122f4d

Navigating the Depths: Pioneering Water Depth Measurements Through Distributed Acoustic Sensing

A new method for monitoring the water-mud interface and water column height using passive noise and fibre optical cables

Navigating the Depths: Pioneering Water Depth Measurements Through Distributed Acoustic Sensing

A new method for monitoring the water-mud interface and water column height using passive noise and fibre optical cables

Dissertation

for the purpose of obtaining the degree of doctor
at Delft University of Technology
by the authority of the Rector Magnificus, Prof. dr. ir. T.H.J.J. van der Hagen,
chair of the Board for Doctorates
to be defended publicly on
Monday 27 January 2025 at 17:30 o'clock

by

Menno BUISMAN

This dissertation has been approved by the promotors.

Composition of the doctoral committee:

Dr. D.S. Draganov,	Delft University of Technology, *promotor*
Dr. C. Chassagne,	Delft University of Technology, *promotor*
Dr. A. Kirichek,	Delft University of Technology, *copromotor*

Independent members:

Prof. dr. M. van der Baan	U. of Alberta, Canada
Prof. dr. ir. E. C. Slob	Delft University of Technology
Prof. dr. ir. L. V. Socco	Delft University of Technology
Prof. dr. ir. M. van Koningsveld	Delft University of Technology

Keywords: Distributed Acoustic Sensing, fibre optics, nautical depth, Burial Depth

Printed by: Gildeprint

Front & back: Fibre optical cable and a seismic trace

ISBN 000-00-0000-000-0

An electronic copy of this dissertation is available at
https://repository.tudelft.nl/.

Just keep swimming.

Dori

Contents

Summary

Maritime transport facilitates close to 80 % of global trade, standing as an unparalleled cornerstone in international commerce. Projections herald a further increase in maritime activity, due to the low carbon footprint and cost-effectiveness, elevating the need for ensuring navigational safety within ports and waterways. At the heart of safe maritime navigation lies the pivotal concept of maintaining adequate nautical-depth, a threshold where a ship's keel encounters navigational constraints. However, this necessity inherently demands incessant monitoring and recurring dredging operations, resulting in high costs amounting to millions of euros and, contributing significantly to carbon emissions. These factors underscore an urgent call for optimization of monitoring the nautical-depth to reduce monitoring and dredging costs, and increase marine navigational safety.
Presently, common methods for nautical-depth monitoring rely heavily on acoustic echo sounders, rooted in dated methodologies with limited innovation over nearly a century. Acoustic echo sounders measure the two-way travel time of sound pulses, assuming a known propagation velocity of the acoustic energy. However, accurately approximating the pressure-wave velocity in shallow marine environments poses challenges due to variations in temperature and salinity among different water layers, leading to depth-measurement inaccuracies. Furthermore, this method is limited by vessel availability and requires access to quay walls, often occupied by loading or unloading ships.

At the center of the work we present, lies the exploration and application of advanced geophysical techniques, notably the harnessing of Distributed Acoustic Sensing (DAS) for nautical-depth monitoring. DAS, a technology that converts optical fibres into an array of seismic sensors, shows great promise to either complement or supplant current nautical-depth monitoring methodologies.
One method we propose involves combining DAS with an attenuation-based approach, distinguishing materials like water and fluid mud by their differing acoustical characteristics.

We first demonstrate the combination of DAS with an attenuation-based approach in a controlled laboratory setting. This experimental setup comprises of a transparent cylinder housing a PVC pipe with a fibre coiled on it, designed to emulate a vertical seismic profile (VSP). The cylinder is partly filled with mud, and partly filled with water. A dual echo sounder is placed on top of the cylinder, serving as an acoustic source for pressure waves. Signal acquisition involves a single-mode standard communication fibre and a DAS interrogator. Large amplitude disparities between water and mud, emphasise the potential in the attenuation-based approach coupled with DAS technology.

We further deploy a similar VSP in the Port of Rotterdam. Here, we use a 24-m-long steel pole, driven into the subsurface, housing a 2.4-m-long mantle with a 960 m standard single-mode coiled fibre. Passive noise generated by vessel movements substitutes the active source. The noise is recorded by the fibre, yielding similar findings. These recording show larger amplitudes in fibre section in the water-column in contrast to the fibre section in mud. Notably, we show that higher-frequency signals experience rapid attenuation beyond the water-mud interface, while lower-frequency signals display a small increase in amplitudes. This discrepancy in attenuation for different bandwidths hints at the potential existence of diverse waves types, potentially including surface waves within the mud, or this difference could be related to varying coupling conditions between the fibre sections immersed in water and mud.

Following the first field experiment, we make modifications to the field setup. We the standard communication fibre with a direct burial cable, and add a second 24-m-long steel pole, housing another mantel with coiled fibre is added. Furthermore, on both mantles rings are welded allowing for horizontal segments between the two mantles. Our aim of this setup is to create a more realistic setup for monitoring the nautical-depth in ports and waterways by adding horizontal fibres between the two poles.

Our analysis of the data of the horizontal sections highlight the capability to estimate the water-mud interface near real-time through the resonance of multiple sources, including vessel movements, water flow, and likely infra-gravity waves, seafloor compliance or bow and stern waves. Notably, signal attenuation at the sections where the fibre is in contact with the mud, providing an exceptional vertical resolution unparalleled by alternative surveying methods. However, it is essential to note that the fibre hangs at varying depth increments of 30 to 50 centimeters, restricting interface measurements to these specific locations.

Finally, we estimate the water-column height change is estimated by showing oscillating frequency patterns which match the tidal duration. Furthermore, calibration of a water depth would then allow to measure the absolute water-column height, instead of only relative water-column height's change due to the tides.

Collectively, our findings underscore the development of a comprehensive monitoring system focused at tracking the water-mud interface and water-column height. Our study identifies both passive and active sources suitable for these measurements, elucidating their respective bandwidth characteristics.

SAMENVATTING

Ongeveer 80 % van alle goederen worden via het water verzonden. Hierdoor is maritiem transport een bijzonder belangrijke schakel in de internationale handel. De zeevaart zal naar alle waarschijnlijkheid alleen maar toenemen door de lage kosten en lage CO2 uitstoot. Dit zorgt ervoor dat de noodzaak van het bevaarbaar houden van rivieren en haven als maar toeneemt. Voor het bevaarbaar houden van rivieren en kanalen wordt een nautische diepte behouden, een diepte die gedefinieerd wordt als een grens waar de kiel van een schip geen navigatieproblemen ondervindt.
Echter, het behouden en garanderen van een nautische diepte vereist herhaaldelijke monitoringscampagnes en baggerwerkzaamheden, dat jaarlijks miljoenen kost.
Deze factoren laten zien dat het van groot belang is om het monitoren van aanslibbing te optimaliseren om zo bagger en monitoringskosten te reduceren, en de bevaarbaarheid nog beter te kunnen meten.

Momenteel worden echoloden voornamelijk gebruikt om de diepte te bepalen. Deze methode is meer dan 100 jaar geleden uitgevonden, en beperkt door ontwikkeld. Het principe van echoloden is berust op het sturen van een geluidsgolf, en het tijdverschil meten tussen het sturen en het opnemen van deze geluidsgolf door het echolood. De snelheid van de geluidsgolf moet hiervoor bekend zijn.
Echter, de snelheid van een geluidsgolf kan variëren door een verschil in zoutgehalte of temperatuur. Dit kan weer voor onzekerheid zorgen in de metingen.
Daarbij is deze methode ook beperkt door de beschikbaarheid van een schip en toegang tot kademuren, die vaak bezet zijn door (ont)ladende containerschepen.

Ons onderzoek focust op het toepassen van nieuwe geofysische methodes voor het meten van de nautische diepte. Wij focussen op een techniek genaamd Distributed Acoustic Sensing (DAS). DAS is een techniek die een glasvezel omzet in een rij trilsensoren. Deze technologie is veel belovend als toevoeging of vervanging voor de huidige hydrografische metingen.
Voor een van de methodes voor het meten van de nautische diepte met DAS evalueren wij het verschil in het afzwakken van (geluids)golven om water van slib te onderscheiden.

De combinatie van DAS en het analyseren van signaalverzwakking demonsteren wij in dit onderzoek eerst met een laboratorium opstelling. Deze opstelling bestaat uit transparante cilinder met daarin een pvc-buis. Deze pvc-buis heeft eromheen een glasvezel gewikkeld, om zo een verticaal seismisch profiel (VSP) na te bootsen. Wij vullen de cilinder gedeeltelijk met slib en water. Daarna plaatsen wij een dual echolood bovenop om als bron te dienen voor geluidsgolven. Vervolgens nemen de geluidsgolven op met de glasvezel en een DAS interrogator. Wij nemen grote amplitude verschillen waar in de

metingen en demonstreren hiermee de potentie van een verzwakkingsmethode gecombineerd met DAS.

Vervolgens installeren wij een vergelijkbare VSP in de haven van Rotterdam. Hierbij worden twee 24 m lange stalen palen in de ondergrond geheid. Deze stalen palen dienen als een houder voor een 2.4m lange mantel met glasvezel eromheen gewikkeld. Met deze opstellingen vervangen wij de actieve bron door ruis van passerende schepen. Deze opnames laten dezelfde resultaten zien als in het laboratorium.
Met deze opnames demonstreren wij dat de secties van de glasvezel in water hoge amplitudes meet, in tegenstelling tot de secties glasvezel in slib die lage amplitudes meet. Hierbij is het opvallend dat de hoogfrequente signalen snel verzwakken voorbij de water-slib grens. Daarentegen nemen laagfrequente signalen juist geleidelijk toe in amplitude. Dit verschil in signaalverzwakking per bandbreedte zou een indicatie voor de aanwezigheid van oppervlakte golven kunnen zijn, of is een verschil in koppelingseffect van de glasvezel tussen het water en slib.

Na de VSP-opstelling in de haven van Rotterdam zorgen wij voor aanpassingen aan de opstelling om ook horizontale vezels tussen de palen te kunnen spannen. We gebruiken een 'direct burial' glasvezel om de standaard glasvezel. Daarbij worden op beide mantels ringen gelast om het horizontale gedeelte van de glasvezel er doorheen te rijgen. Het doel van deze nieuwe opstelling is om een realistischere opstelling na te bootsen die haalbaar is in havens en rivieren voor het meten van de nautische diepte.
Onze data-analyses laten zien dat het mogelijk is om vrijwel direct en continue het onderscheid te maken tussen de glasvezelsecties in water en slib. Meerdere trillingsbronnen zoals passerende schepen en stromingen hebben we hiervoor kunnen gebruiken. Wij laten een duidelijk verschil in signaal afzwakking zien tussen de vezel in contact met slib en de vezel in contact met water. Dit geeft een zeer hoge verticale resolutie in vergelijking met andere methodes, gezien deze dan gelijk staat aan de dikte van de vezel. Echter is het wel belangrijk om de onzekerheid van de kabel positie in acht te nemen, en dat er met deze opstelling kabels op verschillende hoogtes hangen met hoogte intervallen van 30 cm of 50 cm.
Als laatst laten we een verschil zien in de waterkolom hoogte door een verschil in oscillaties die we relateren aan een waterkolom hoogteverschil veroorzaakt door het getij. Wanneer er een hoogte kalibratie wordt toegepast kunnen deze metingen vervolgens gebruikt worden om hoogteverschil naar absolute waterkolom hoogte om te zetten.
Met de bevindingen in dit proefschrift geven weer hoe een meetsysteem ontwikkeld kan worden dat de water-slib grens en waterkolomhoogte kan meten. Verder worden de verschillende ruisbronnen voor deze doelstelling geïdentificeerd en worden de desbetreffende bandbreedtes besproken.

1

INTRODUCTION

The maritime industry serves as the primary conduit for nearly 80 % of global trade, signifying its key role in international commerce. With projections indicating a continual increase in maritime activity, the critical need for ensuring navigational safety in ports and waterways is ever growing. Maintaining adequate nautical-depth, defined as the level at which a ship's keel encounters navigational constraints, stands as a pivotal aspect of safe maritime navigation. However, this necessitates frequent monitoring and dredging operations, which not only incur high costs running into millions of euros but also contribute significantly to carbon emissions, thus underscoring the urgency for optimization.

Current methods employed for monitoring nautical-depth largely trace back to techniques commercialized nearly a century ago. This lack of innovation and reliance on old methodologies underlines the need for enhancing nautical-depth monitoring processes. Addressing this need is the focus of this dissertation, which aims to introduce novel geophysical methods capable of vastly improving the precision and efficiency of nautical-depth monitoring.

Central to this dissertation is the exploration of advanced geophysical techniques, notably leveraging distributed acoustic sensing (DAS). DAS operates by utilizing optical fibers to create an array of seismic sensors, presenting a promising technique to either complement or change current nautical-depth monitoring methods. The dissertation outlines a framework for employing these innovative DAS-based methods to continuously monitor nautical-depth, offering a paradigm shift from conventional approaches towards a more sophisticated and sustainable solution.

Within this introduction, fundamental concepts pertinent to maritime navigation and dredging operations are introduced. The forthcoming sections will delve deeper into the intricacies of DAS-based monitoring systems, exploring their potential to not only enhance accuracy but also significantly reduce the environmental footprint associated with dredging operations.

1

1.1. NAUTICAL-DEPTH MONITORING

PORTS and waterways subjected to high siltation rates need consistent surveys to ascertain adequate nautical-depths. Defining this nautical-depth often revolves around a density criterion ranging between 1.15 kg/l to 1.3 kg/l, as shown by [1]. The variability of this criterion stems from the non-linear correlation between shear strength and the density of fluid mud, a suspension of fine particles in the water column, as demonstrated by [2].
To estimate the depth of the density boundary layer(s), (dual) echo-sounders are frequently used complemented by intrusive point measurements for calibration [3]. Echo-sounding techniques, initially conceived and patented by the German physicist Alexander Behm in 1913, were subsequently commercialized in 1924 [4]. Modern echo-sounders typically deploy multiple frequencies, encompassing a high frequency range spanning 180 kHz to 240 kHz and a lower-frequency range between 15 kHz to 40 kHz. This dual-frequency emission strategy allows for the detection of distinct layers, enabling the identification of a fluid mud top layer and a consolidated bottom layer[5], as shown in Figure 1.1.

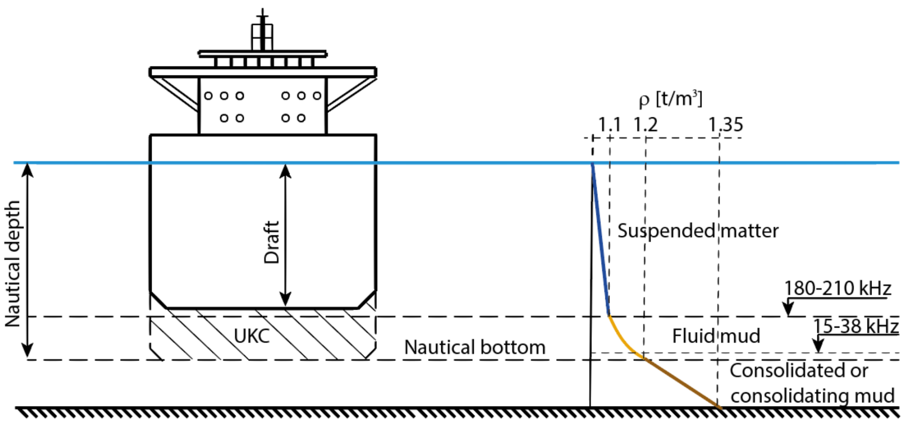

Figure 1.1: Visualization depicting the essence of nautical-depth determination: a ship over layers with varying density, showcasing echo-sounder emissions and frequency reflections off fluid and consolidated mud beds. [6].

The echo-sounding technique, albeit augmented with additional emitted frequencies, remains entrenched in its original framework pioneered by Alexander Behm. This stagnation in innovation perpetuates the persistent inaccuracies inherent in these methodologies. Moreover, their reliance on the availability of surveying vessels and access to quay walls further limits the temporal resolution. The lack of innovation also means that the same problems inherent with these echo-sounding techniques causing inaccuracies still persevere.
Given that there have been limited developments in monitoring and the increase in marine transport volumes, this raises the question of whether there is a more practical approach to monitoring the nautical-depth. Even more so, given that

ports are very accessible, meaning access to electricity, data infrastructure, and sight access for sensors, it does have all the means to facilitate a continuous monitoring system with suitable sensors. This raises the following questions:

1. Which sensors exhibit the potential for large-scale deployment in this context?
2. What physical phenomena can be effectively measured to estimate water-depth accurately and reliably?

The answer to the first question hinges on factors like survey-area size and desired spatial resolution. Conventional piezoelectric transducers and pressure gauges afford a certain level of accuracy in depth measurement. However, their susceptibility to corrosion and individual wiring requirements, alongside costs ranging from a few hundred to several thousands of euros per sensor, render it economically impractical to install sensors at frequent intervals within ports or waterways.

A novel technique uses optical cables as sensors. Optical fibres come with many advantages over conventional sensors. Because these fibres are made of glass, they are non-conductive, immune to electromagnetic interference, non-corrosive, easy to deploy, and maybe most importantly, they are very cheap [7–9]. Due to these many advantages, optical fibres could serve as a prime candidate for monitoring the nautical-depth on a large scale.

The second question inadvertently raises a few challenges. Distinguishing between water and mud with conventional geophysical methods is arduous. Acoustic or seismic methods relying on pressure wave (P-wave) velocities for subsurface imaging encounter difficulties due to subtle differences in these velocities between water and (fluid) mud. Water has a P-wave velocity between 1470 - 1520 m/s, depending on salinity and temperature. [10] showed that (fluid) mud has a P-wave velocity of around 1590 m/s, just 6 % above that of water. The minute difference, in P-wave velocities, introduces uncertainties in inversion methodologies, compounded by temperature fluctuations and imprecise receiver locations.

High-frequency sources (around 200 kHz) with wide beam angles for reliable inversion do exist but are typically vessel-mounted, impeding continuous measurements, and only capture the top of the (fluid) mud layer.

An alternative approach involves exploring signal muting by mud. The fine grains and gas bubbles within fluid mud layers significantly dampen acoustic signals, resulting in a low signal-to-noise ratio (SNR), as will be shown later. Harnessing this signal's attenuation as a parameter, especially in conjunction with fibre installations in both water and mud, could offer valuable insights, leveraging the abundant acoustic energy in seaports for monitoring purposes.

1.2. PROBLEM DESCRIPTION AND KNOWLEDGE GAPS

Approximately 80 % of the world's trade volume is reliant on maritime transport, with this volume anticipated to continually increase in absolute terms. The need to accommodate ship traffic necessitates regular surveys and dredging operations by port authorities. However, these activities often require quay walls being vacated, leading to reduced occupancy and operational downtime. A potential remedy lies in the installation of sensors capable of continuous nautical-depth monitoring, even during vessel-docking periods. Such sensors could reduce the necessity for surveying vessels to access quay walls and might aid in minimizing safety buffers that result from inadequate measurements.

Moreover, after storms, large bathymetrical changes can occur, leading to extensive, time-consuming survey campaigns to ensure sustained nautical-depth. Given the mounting pressure to increase the occupancy rate and reduce CO2 emissions, port authorities are looking to innovate and develop new monitoring techniques to facilitate these improvements.

That is why the primary objective of this dissertation is to develop new techniques for continuously monitoring of the nautical-depth. Moreover, this dissertation shows the development of such a system on both laboratory scale, and field setup scale. The latter could easily be extended for port-wide deployment Notably, this thesis not only delves into the continuous-monitoring aspects but also shows the resolution capabilities of such a method, laying the groundwork for its large-scale implementation within port infrastructures.

1.3. RESEARCH QUESTIONS AND THESIS OUTLINE

In order to develop a new system to monitor the nautical-depth, I posed my research questions as follows:

1. What is the best parameter to use to measure the water depth with optical fibres? This research question is addressed in Chapter 3 Here we created a vertical seismic profile (VSP) and looked at the acoustic energy throughout the VSP.
2. What would be the depth resolution in the field using distributed acoustic sensing and passive noise? Chapters 3 - 7 answer this question. What is worth noting is that in Chapter 3 - 5 a VSP is used, whereas in Chapter 6 horizontal fibres are used.
3. How can we implement a continuously-monitoring system on a large scale? Chapter 6 shows how to measure on a large scale. The field setup could easily be extended to a much larger scale. Additionally, both the horizontal and vertical resolution are shown. This is further summarised in chapter 8.

REFERENCES

[1] W. H. McAnally, R. Kirby, S. H. Hodge, T. L. Welp, N. Greiser, P. Shrestha, D. McGowan, and P. Turnipseed. "Nautical depth for US navigable waterways: A review". In: *Journal of Waterway, Port, Coastal, and Ocean Engineering* 142.2 (2016), p. 04015014.

[2] A. Shakeel, A. Kirichek, and C. Chassagne. "Is density enough to predict the rheology of natural sediments?" In: *Geo-Marine Letters* 39 (2019), pp. 427–434.

[3] W. H. McAnally, A. Teeter, D. Schoellhamer, C. Friedrichs, D. Hamilton, E. Hayter, P. Shrestha, H. Rodriguez, A. Sheremet, R. Kirby, *et al.* "Management of fluid mud in estuaries, bays, and lakes. II: Measurement, modeling, and management". In: *Journal of Hydraulic Engineering* 133.1 (2007), pp. 23–38.

[4] A. Behm. "Die Entstehung des Echolots [The emergence of the echo sounder]". In: *Naturwissenschaften* 16.45-47 (1928), pp. 962–969.

[5] J. Granboulan, A. Feral, M. Villerot, and J. Jouanneau. "Study of the sedimentological and rheological properties of fluid mud in the fluvio-estuarine system of the Gironde estuary". In: *Ocean and Shoreline Management* 12.1 (1989), pp. 23–46.

[6] A. Kirichek, C. Chassagne, H. Winterwerp, and T. Vellinga. "How navigable are fluid mud layers?" In: *Terra et Aqua* (Aug. 2018), pp. 6–18.

[7] M. Shao, X. Qiao, X. Zhao, Y. Zhang, and H. Fu. "Liquid Level Sensor Using Fiber Bragg Grating Assisted by Multimode Fiber Core". In: *IEEE Sensors Journal* 16.8 (2016), pp. 2374–2379. DOI: https://doi.org/10.1109/JSEN.2015.2513413.

[8] W. Xu, J. Wang, J. Zhao, C. Zhang, J. Shi, X. Yang, and J. Yao. "Reflective Liquid Level Sensor Based on Parallel Connection of Cascaded FBG and SNCS Structure". In: *IEEE Sensors Journal* 17.5 (2017), pp. 1347–1352. DOI: https://doi.org/10.1109/JSEN.2016.2629488.

[9] C. Yang, S. Chen, and G. Yang. "Fiber optical liquid level sensor under cryogenic environment". In: *Sensors and Actuators A: Physical* 94 (Oct. 2001), pp. 69–75. DOI: https://doi.org/10.1016/S0924-4247(01)00663-X.

[10] X. Ma, A. Kirichek, K. Heller, and D. Draganov. "Estimating P-and S-Wave Velocities in Fluid Mud Using Seismic Interferometry". In: *Frontiers in earth science* 10 (2022), p. 251.

2

MATERIALS AND METHODS

The objective of this chapter is to explain the methodologies employed and the materials used to carry out the study. First, a concise overview of the characteristics and origin of the mud samples is given. Afterwards, a detailed explanation on the methodology grounded in muting-based approaches is explained. Further, the underlying principles behind DAS is explained, accompanied by overview of the various interrogators used for this study. lastly, the field experiment conducted in the Port of Rotterdam its location and setup is described, encompassing its location and the specifics of its experimental setup.

2.1. MUD SAMPLING AND SYNTHETIC CLAY

THis study uses diverse mud samples sourced from both the Port of Rotterdam and the Port of Hamburg. An acoustic standpoint highlights the paramount disparity between these samples, primarily rooted in their organic matter composition. The organic degradation within these samples instigates the formation of gas pockets, notably accentuated during the summer season, creating a heightened gas content within the mud matrix. By conducting experiments on both freshwater and saline mud variants, this investigation demonstrates the versatility of the muting approach across varying environmental contexts.

Moreover, the study delves into the impact of gas presence on the efficacy of the muting-based methodology. Findings indicate a limited advantageous influence of gas pockets on the muting approach, affirming its robust functionality across seasons, unaffected by fluctuations attributed to seasonal variations.

Additionally, a synthetic clay suspension comprising bentonite serves as a key component in this study, facilitating an exploration of increasing shear stresses on acoustic wave behavior. Unlike natural mud, bentonite exhibits minimal density changes over a short time spans of 24 hours. However, a rapid increase in shear strength is observed within the initial 24-hour period post-mixing, presenting an opportunity to discern the impact of this increase in shear stresses on acoustic wave propagation.

2.2. ATTENUATION-BASED APPROACH

Lacking a standardized definition within the field, within the scope of this study, an attenuation-based approach is defined as follows: '*A method predicated on exploiting amplitude differences to infer subsurface parameters.*'

The unconventional nature of utilizing passive noise amplitudes for subsurface parameter estimation may appear nonintuitive within geophysical methodologies. To elaborate on this approach, consider an illustrative scenario: envision a scenario contrasting air and insulation material, as depicted in Figure 2.1. Suppose paths a and b share the same lengths, with path a traversing solely through air, while Path b partially navigates through insulation material comprising 95 % air and 5 % polystyrene. Given that both paths primarily traverse air and a substantial portion of the insulation material comprises air, the travel time from the source to the receivers is approximately the same. Although triangulation using numerous receivers could potentially estimate velocities, this task is intricate and demands high precision of source localization—typically unattainable when employing passive noise.

An alternative, more intuitive approach emerges when assessing the amplitude discrepancy of the signal between receivers a and b. Receiver b, affected by muting induced by the insulation material, exhibits reduced amplitudes compared to receiver a. Similarly, within our geophysical context involving water and mud layers, comprising of predominantly water with a fraction of fine sediments, even a thin layer of mud exerts muting effects on signals. Leveraging this principle enables us to discern between water and mud within our amplitude data, akin to the conceptual scenario illustrated in Figure 2.1.

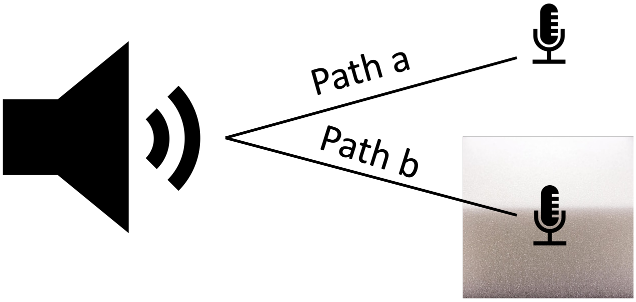

Figure 2.1: A schematic overview of a muting-based approach. A source generates acoustic energy. This energy propagates to the receivers. The top receiver is in the air, while the bottom receiver is in insulation foam. Path a is equal in length to path b. The top receiver will record much higher amplitudes than the bottom receiver, even though most of the path towards the bottom is also in the air, and the foam, in which the bottom receiver is located, also consists of 95 % air.

2.3. DISTRIBUTED ACOUSTIC SENSING

DAS measures the dynamic strain or strain-rate along optical fibres. This measurement stems from alterations in the photon path length of Rayleigh-backscattered light emitted by a laser source detected by a receiver in an interrogator [1]. The underlying principle behind DAS mirrors that of optical time domain reflectometry (OTDR). However, the highly non-linear transfer function of the backscattered signal's phase change renders it unsuitable for seismic applications. To circumvent this limitation, the phase difference between two points, referred to as the gauge length, is used instead [2]. Despite averaging the phase difference over the gauge length, DAS retains waveform fidelity, enabling the retrieval of both amplitude and phase information, whereas preceding OTDR methodologies solely captured amplitude.

This capacity to retrieve phase information is why DAS has been successfully used in various fields of research, including teleseismic earthquake monitoring [3, 4], vertical seismic profiling [5–7], and earthquake phase identification [8].
It should be noted that, in contrast to geophones, DAS measures axial strain along the fibre, characterizing it a 1C sensor with directional sensitivity [9, 10]. Owing to this directional sensitivity, DAS records directional strain rather than true amplitudes, occasionally necessitating conversion of strain or strain-rate data to particle displacement for specific algorithms. A common assumption to aid in a conversion is assuming alignment of acoustic energy with the fibre, thereby enabling subsequent application of various algorithmic methodologies like full-waveform inversion to DAS data in specific scenarios involving near-offset VSPs. [11, 12].
Nevertheless, it should be noted that the absence of multiple components leads to (cross)correlation of different waveforms [13]. This feature, if mishandled, can potentially yield misleading results.

Commercially available DAS instruments often utilize short-pulse coherent lasers, where the pulse width constrains spatial resolution [1]. Additionally, such systems are prone to optical nonlinearities like self-phase modulation and modulation instabilities, limiting the energy output per pulse and consequently constraining the backscattered signal [14]. Monitoring large seaports, necessitating high spatial resolution over vast distances, poses challenges for short-pulse systems.

Recent advancements in coherent detection employing linear frequency modulation [15] and bi-directional distributed Raman amplification [16] have broadened the dynamic range of DAS interrogators. Notably, linear frequency-modulated signals compressed via chirp compression techniques, akin to radar applications [17], significantly augment the energy launched into the fibre [18]. This innovation is of great importance for large-scale monitoring, reducing financial barriers by minimizing the number of interrogators needed for continuous monitoring across expansive areas, and improving overal data quality.

2.3.1. Interrogators used in this study

This study utilizes three distinct interrogators: Silixa's iDAS v2, Febus' A1, and ASN's OptoDAS, each exhibiting unique sensitivities and individual strengths. The iDAS v2 stands out for its user-friendly interface, rendering it the most easily deployable and operationally straightforward interrogator within this context. The Febus A1 system offers variable gauge length capability and the storage of optical phase data, facilitating post-processing adjustments in gauge length and channel spacing. The OptoDAS has the highest sensitivity and the largest dynamic range.
However, each system also has specific drawbacks. The iDAS v2 comes at a significant cost. The Febus A1, while versatile, presents challenges with its less user-friendly interface. Furthermore, its post-processed gauge length dependency on the laser's pulse width, which is fixed during data acquisition, limits its adaptability to specific gauge lengths. The OptoDAS, despite its superior sensitivity and range, requires approximately an hour for laser stabilization and is the bulkiest among the three systems, posing handling challenges.

2.3.2. Field setup

The field setup is positioned within the Port of Rotterdam, delineated in Figure 2.2. Situated in close proximity to Het Scheur, De Geulhaven, Botlek, and The Third Petroleum Harbor, this location experiences high vessel traffic due to its adjacency to bustling maritime zones. At this site, a car jetty with two bollards in the water facilitates the loading and unloading of cars onto ships.
For the field setup, I arrange for two solid steel poles to be driven into the subsurface to serve as anchorage points for securing a mantle coiled with an optical fibre next to the car jetty and behind the most northern bollard. Initially, I designed the mantles coiled with a loose fibre jacket. After this fibre proved to be impractical due

to its fragility, I switched to a direct burial fibre. The reason why I chose the location near the Geulhaven was because it is positioned adjacent to the car jetty and behind a bollard, thereby shielding the setup from potential collisions and interference with maritime vessels. The selection of this location accounts for both its high traffic volume and safety considerations.
For installation process I hired and supervised multiple crane ships, one of which was equipped with a vibratory hammer. I required this specialised equipment for driving two 24-meter steel poles into the subsurface to a depth of approximately 18 m and 20 m.

The initial setup was focused on creating a VSP with a very dense spacing. To

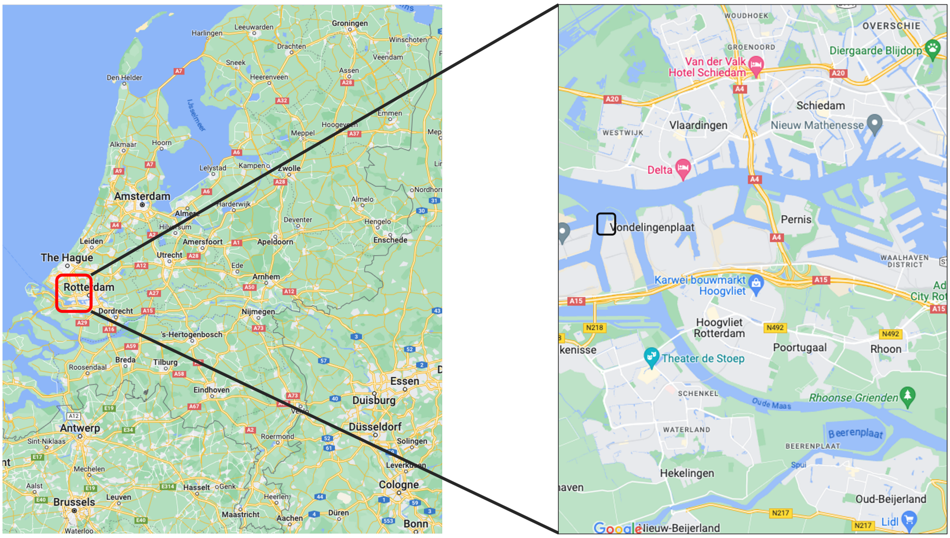

Figure 2.2: A map of the Netherlands (left) with the location of the field setup highlighted by the red rectangle. A zoomed in section of a part of the Port of Rotterdam (right) with the field location highlighted by the black rectangle.

achieve this dense spacing, the first fibre coiled on the mantle was thin, measuring only 1.6 mm in diameter, enabling a very fine wrapping around the mantles. A subsequent drone inspection revealed the complete coverage of the mantles in mud. Consequently, to address this issue, the mantles were lifted, allowing for partial submersion into water and mud. However, in the process of raising the mantles, the connecting fibre laying on the sediments fractured, leading to the utilization of only one mantle for creating the VSP. Subsequently, the fibre on the remaining mantle also suffered a break, compelling the lifting of the mantle again to splice the fibre back together.
Following the completion of the VSP experiments, the configuration was changed, concentrating on creating horizontal fibre sections between the two poles. This was achieved by welding rings on the mantle providing a pathway to traverse in

an upward zig-zag pattern. Lessons learned from the utilization of the smaller, less robust 1.6 mm fiber led to the decision to transition to a sturdier solution: an acrylic armored direct-burial fiber with a diameter of 6 mm, commonly employed by the telecom industry due to its cost-effectiveness and heightened durability. To execute this experimental setup, two crane vessels were indispensable to simultaneously lower the two mantels. Additionally, a work platform was essential to facilitate movement between the two crane ships, as depicted in Figure 2.3.

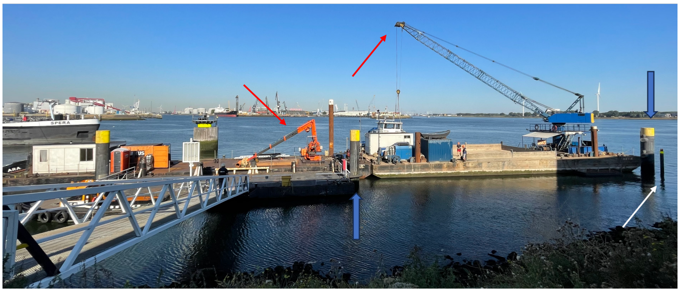

Figure 2.3: A picture of the vessels and cranes used to lower the mantles onto the steel poles. The white arrow indicates a steel pole that has been driven into the subsurface and acting as a mount for the mantle. The blue arrows show the two docking bollards. The red arrows show the cranes.

REFERENCES

[1] N. Lindsey, H. Rademacher, and J. Ajo-Franklin. “On the Broadband Instrument Response of Fiber-Optic DAS Arrays”. In: *Journal of Geophysical Research: Solid Earth* 125.2 (2020), e2019JB018145. DOI: https://doi.org/10.1029/2019JB018145.

[2] A. Hartog, B. Frignet, D. Mackie, and M. Clark. “Vertical seismic optical profiling on wireline logging cable”. In: *Geophysical Prospecting* 62.4-Vertical Seismic Profiling and Microseismicity Frontiers (2014), pp. 693–701.

[3] J. B. Ajo-Franklin, S. Dou, N. J. Lindsey, I. Monga, C. Tracy, M. Robertson, V. Rodriguez Tribaldos, C. Ulrich, B. Freifeld, T. Daley, and X. Li. “Distributed Acoustic Sensing Using Dark Fiber for Near-Surface Characterization and Broadband Seismic Event Detection”. In: *Scientific Reports* 9.1 (2019), p. 1328. ISSN: 2045-2322. DOI: https://doi.org/10.1038/s41598-018-36675-8.

[4] P. Jousset, T. Reinsch, T. Ryberg, H. Blanck, A. Clarke, R. Aghayev, G. P. Hersir, J. Henninges, M. Weber, and C. M. Krawczyk. “Dynamic strain determination using fibre-optic cables allows imaging of seismological and structural features”. In: *Nature Communications* 9.1 (2018), p. 2509. ISSN: 2041-1723. DOI: https://doi.org/10.1038/s41467-018-04860-y.

[5] T. Daley, D. Miller, K. Dodds, P. Cook, and B. Freifeld. “Field testing of modular borehole monitoring with simultaneous distributed acoustic sensing and geophone vertical seismic profiles at Citronelle, Alabama”. In: *Geophysical Prospecting* 64.5 (2016), pp. 1318–1334. DOI: https://doi.org/10.1111/1365-2478.12324.

[6] E. Martuganova, M. Stiller, K. Bauer, J. Henninges, and C. M. Krawczyk. “Cable reverberations during wireline distributed acoustic sensing measurements: their nature and methods for elimination”. In: *Geophysical Prospecting* 69.5 (2021), pp. 1034–1054. DOI: https://doi.org/10.1111/1365-2478.13090.

[7] A. Mateeva, J. Lopez, H. Potters, J. Mestayer, B. Cox, D. Kiyashchenko, P. Wills, S. Grandi, K. Hornman, B. Kuvshinov, W. Berlang, Z. Yang, and R. Detomo. “Distributed acoustic sensing for reservoir monitoring with vertical seismic profiling”. In: *Geophysical Prospecting* 62.4 (2014), pp. 679–692. DOI: https://doi.org/10.1111/1365-2478.12116.

[8] N. Lindsey, E. Martin, D. Dreger, B. Freifeld, S. Cole, S. James, B. Biondi, and J. Ajo-Franklin. “Fiber-optic network observations of earthquake wavefields: Fiber-optic earthquake observations”. In: *Geophysical Research Letters* 44.23 (Nov. 2017), pp. 11, 792–11, 799. DOI: https://doi.org/10.1002/2017GL075722.

2

[9] A. Baird, A. Stork, S. Horne, G. Naldrett, J.-M. Kendall, J. Wookey, J. Verdon, and A. Clarke. "Characteristics of microseismic data recorded by distributed acoustic sensing systems in anisotropic mediaMicroseismic DAS in anisotropic media". In: *Geophysics* 85.4 (2020), KS139–KS147.

[10] Z. Zhan. "Distributed acoustic sensing turns fiber-optic cables into sensitive seismic antennas". In: *Seismological Research Letters* 91.1 (2020), pp. 1–15.

[11] A. Egorov, J. Correa, A. Bóna, R. Pevzner, K. Tertyshnikov, S. Glubokovskikh, V. Puzyrev, and B. Gurevich. "Elastic full-waveform inversion of vertical seismic profile data acquired with distributed acoustic sensors". In: *Geophysics* 83.3 (2018), R273–R281.

[12] P. G. Hubbard, J. P. Vantassel, B. R. Cox, J. W. Rector, M. B. Yust, and K. Soga. "Quantifying the Surface Strain Field Induced by Active Sources with Distributed Acoustic Sensing: Theory and Practice". In: *Sensors* 22.12 (2022), p. 4589.

[13] E. R. Martin, N. J. Lindsey, J. B. Ajo-Franklin, and B. L. Biondi. "Introduction to interferometry of fiber-optic strain measurements". In: *Distributed Acoustic Sensing in Geophysics: Methods and Applications* (2021), pp. 111–129.

[14] J. Toulouse. "Optical nonlinearities in fibers: review, recent examples, and systems applications". In: *Journal of lightwave technology* 23.11 (2005), pp. 3625–3641.

[15] O. H. Waagaard, E. Rønnekleiv, A. Haukanes, F. Stabo-Eeg, D. Thingbø, S. Forbord, S. E. Aasen, and J. K. Brenne. "Real-time low noise distributed acoustic sensing in 171 km low loss fiber". In: *OSA Continuum* 4.2 (Feb. 2021), pp. 688–701. DOI: https://doi.org/10.1364/OSAC.408761.

[16] D. Chen, Q. Liu, and Z. He. "Distributed Fiber-optic Acoustic Sensor with Long Sensing Range over 100 km and Sub-nano Strain Resolution". In: *2019 IEEE International Instrumentation and Measurement Technology Conference (I2MTC)*. IEEE. 2019, pp. 1–5.

[17] M. A. Richards. *Fundamentals of radar signal processing*. McGraw-Hill Education, 2014.

[18] S. Wang, X. Fan, Q. Liu, and Z. He. "Distributed fiber-optic vibration sensing based on phase extraction from time-gated digital OFDR". In: *Optics Express* 23.26 (2015), pp. 33301–33309.

3

CAPTURING THE WATER-MUD INTERFACE IN LABORATORY USING DAS

Laboratory experiments serve as a critical phase in the validation of emerging monitoring methodologies. While Distributed Acoustic Sensing (DAS) traditionally finds application in lower frequencies, demanding substantial spatial dimensions due to larger wavelengths, this chapter presents an innovative perspective. It showcases the adaptability of DAS, leveraging the cost-effectiveness and compact nature of optical fibers to enable dense, high-frequency measurements at a confined scale.
The laboratory measurements for this study were conducted were to assess the sensitivity of DAS for capturing the water-mud interface. Utilizing mud samples sourced from the ports of Rotterdam and Hamburg, the measurements were performed during various stages of sedimentation and consolidation. Additionally, this study derived depth accuracy for an active acoustic experiment conducted in this laboratory setting. Moreover, these laboratory investigations lay the groundwork for forthcoming field experiments, establishing a fundamental framework for the progression of this research endeavor.

Parts of this chapter have been published in Journal of Soils and Sediments, **22**, (11) (2022) [1].

3.1. INTRODUCTION

Port authorities regularly survey ports and waterways to measure the water depth. Current non-intrusive surveying methods are limited in accuracy due to, for instance, temperature fluctuations in water layers, but also in time due to their dependency on the availability of surveying vessels [2]. The latter case especially poses problems after storm or dredging-related bathymetrical changes. A permanent monitoring system that can be operated remotely could be of special interest at busy docks, i.e., docks that are often occupied by ships. If one could monitor the depth at these locations on demand, the availability of these docks would increase.

Fadel et al. (2021) [3] and Ma et a. (2021) [4] showed that non-intrusive seismic measurements can be used for estimating shear strength in fluid mud.

DAS could be used to create a VSP and using ambient-noise sources for subsurface imaging. This would allow one to measure the bathymetry on demand without the need to be at a monitor location. Multiple VSP setups could be installed. Such VSP setups would consist of no more than 300 meter of optical fiber, which costs a little over 100 euros. In addition to their relatively low cost, optical fibres offer many other advantages over conventional sensors, e.g., being non-corrosive and non-conductive, making them well-suited with regard to safety and durability for long-term bathymetry monitoring. During the last decade, there has been an ever growing interest in DAS in geoscience [5–7]. One of the primary uses of DAS is to record VSPs in boreholes. Because in boreholes the fibre is permanently installed, there is no need to reopen the borehole or to keep the borehole open, which has significant economical benefits [8–11]. In a borehole, the fibre is often cemented inside the casing, in order to increase the coupling with the borehole. There are also various recordings where a temporarily installed wireline cable was used [12–14]. Here the fibre is not properly coupled, meaning it has a certain degree of freedom to move around. One clear difference between these two conditions, is that in the latter case, ringing noise is observed [15, 16].

This ringing noise appears as waves that propagate with infinite velocity, and is related to standing waves, which depend on the length of the fibre and the frequency. The source of this ringing noise was first identified by [17]. In this paper, the authors also proposed an elegant solution to filter these standing waves. They also showed that the length of the standing waves is related to the fundamental frequencies. This is important to note, because a similar approach could be used with a VSP setup to monitor the water-mud interface using standing waves. Standing waves could develop between the water-mud interface and the water/air interface due to constructive interference. For illustrative purposes, in Figure 3.1 we show a schematic overview of standing-wave modes that could develop between two closed ends.

3.2. SETUP

We want to measure reverberations, also known as standing waves, using a fibre-optical cable. For this aim, we use a standard single-mode optical fibre, which is coiled around a PVC pipe with a diameter of 0.125 m, which in turn is installed

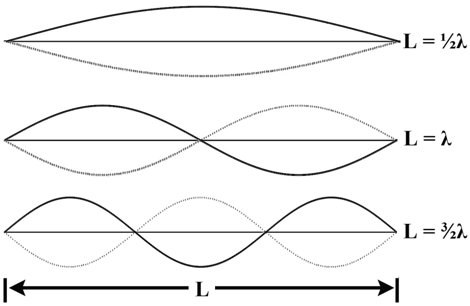

Figure 3.1: A schematic explanation of the relation between the first three modes of standing waves that can develop between two closed ends, the wavelength λ, and the physical body length L with two fixed ends.

in a transparent column with a diameter of 0.4 m. In this way, we obtain a VSP setup. We partly fill the column with mud from the Port of Rotterdam, with an initial density of 1.17 kg l^{-1} and a yield point of 35 Pa. The transparent column allows us to visually track the water-mud interface. A sketch of our setup can be viewed in Figure 3.2 and a picture of the setup is shown in Figure 3.3.
Optical fibers are then converted into seismic sensors using a Silixa iDAS interrogator, and a Febus A1 interrogator [18]. DAS uses elastic Rayleigh scattering to measure the elongation and contraction of the fiber, which can be expressed in units of strain-rate. For a more detailed explanation, the interested reader is referred to [19], who give a clear overview of the measuring principle of DAS, and iDAS in particular. On top of our column, we install a dual frequency echo-sounder. This device is commonly used to measure the water depth in ports and waterways. The echo-sounder we use has two transducers: one with a center frequencies of 38 kHz, and another with a center frequency of 200 kHz (SIMRAD 38/200 COMBI C). Due to the limited time sampling of 100 kHz, we only use the transducer with a 38 kHz center frequency. We connect this transducer to a wave/function generator, which allows one to choose for the source signal at any center frequency within the bandwidth of the generator. The signal is then amplified by a power amplifier.
We record for 0.1 s at 100 kHz with the iDAS interrogator, and 0.3 s with the Febus interrogator. The recording is repeated 10 times for a 0.1 s recording, and 30 times for a 0.3 s recording, which allows stacking the individual recordings 10 or 30 times, respectively. This stacking suppresses random noise and increase the SNR.

3.3. MEASUREMENTS

The result from the stacked recordings using the 38 kHz center frequency, set at 30 kHz with the wave generator, can be seen in Figure 3.4. One feature that is very apparent in this figure is that the data seem to be partly aliased. This is likely related to the fact that the higher frequencies of the source signal are close to the

Nyquist frequency for a time sampling of 100 kHz. We also observe oscillations which appear to propagate at an infinite velocity. This phenomenon can clearly be observed after 0.006 s, and seems to be bound to the water-mud interface, indicated by the blue line in Figure 3.4. It can even be seen before the source pulse arrives, which is counter-intuitive but is possible because a triggering system was missing, and thus there are oscillations from previous measurements before the pulse arrives from the current measurement. A part of this phenomenon appears a few cm below the water-mud interface. This can be related to the measuring principle of the iDAS system, which uses a gauge length of 10 m, meaning it averages measurements over 10 m of fibre.

It appears that there are more arrivals, and thus more energy, in the water layer

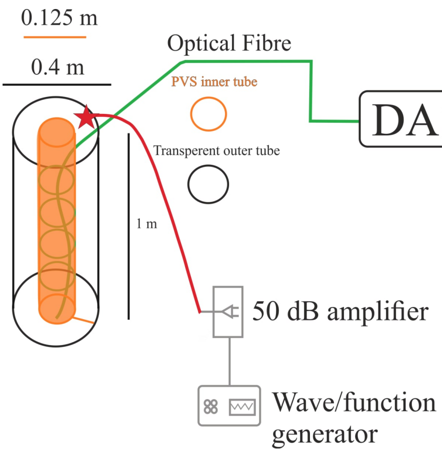

Figure 3.2: Sketch of the laboratory VSP setup. During the measurements, the column is partly filled with water and mud.

than in the mud layer. If indeed so, we should be able to observe the same in a Power Spectral Density (PSD) plot. To obtain a PSD plot, we transform the data using Welch's method [20], which uses a discrete Fourier transform to transform data from the time-space domain to the frequency-space domain. The PSD can be viewed in Figure 3.5. In this figure, we can observe a striking difference in the spectral density between the water, above the red line, and the mud, below the red line. It appears that there is far more energy in the water layer, than in the mud layer at almost any frequency. This is likely due to attenuation of the wave energy in mud. The PSD also shows that there are dominant frequencies at approximately 11 kHz, 22 kHz and 33 kHz. Especially the 22 kHz signal is very strong and seems to cease to exist 2 cm below the water-mud interface. To validate that the waves with a high apparent velocity can be used for estimating the depth of the water-mud interface, we do the same experiment with a source frequency of 23 kHz in the same column but this time filled only with water. We perform these measurements using the Febus A1 interrogator instead of the Silixa iDAS interrogator. The PSD of this setup can be viewed in Figure 3.6. In Figure 3.6, we can see that high energy, characteristic of

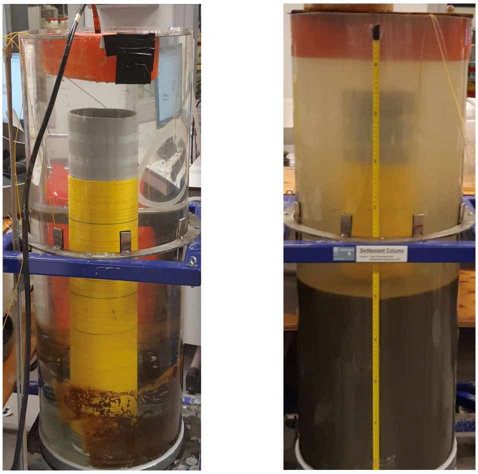

Figure 3.3: Photographs of the laboratory VSP setup. On the left, the column is filled with water, and on the right, the column is partially filled with mud and water.

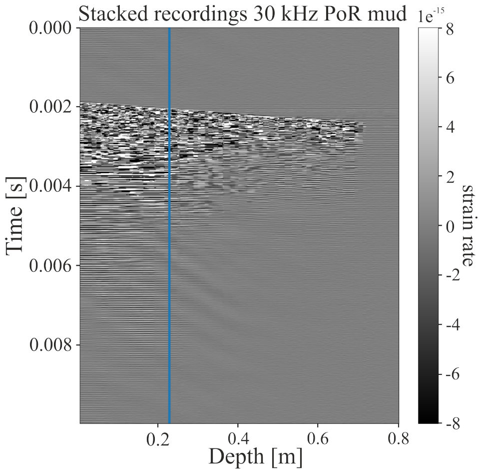

Figure 3.4: Stacked traces along the optical fibre using a 30 kHz signal. The blue line indicates the water-mud interface; PoR stands for Port of Rotterdam

the waves with the very high apparent velocity, is now present along the complete length of the column. This shows that there is no water-mud interface, but only a water layer.

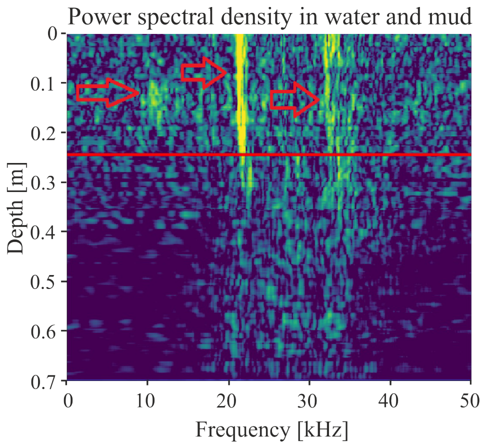

Figure 3.5: Power Spectrum Density of Figure 3.4 with a source signal with center frequency of 30 kHz center. The red line indicates the water-mud interface. The arrows point to dominant frequencies at approximately 11 kHz, 22 kHz and 33 kHz.

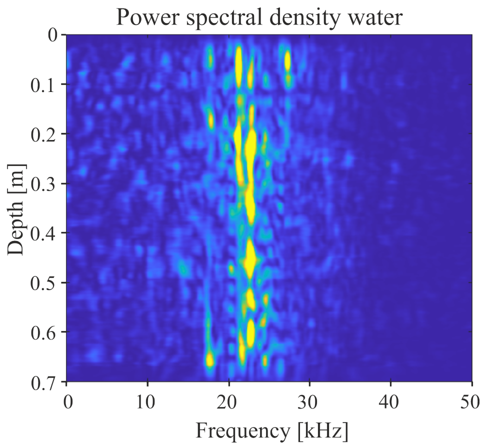

Figure 3.6: Power Spectral Density of the same column as in Figure 3.5, but filled only with water, and a source signal with center frequency of 23 kHz.

3.4. DISCUSSION

Figures 3.4 and 3.5 clearly show that there is a large difference in arrivals and energy inside the water and the mud layers. When we zoom into the arrivals after 0.007 s in Figure 3.4, arrivals with apparent velocities over 500000 m s^{-1} can be observed, as can be seen in Figure 3.7. This is far above the normal longitudinal (P-) wave velocity in water, which is around 1480 m s^{-1}. Unlike the late oscillations, the first arrival from the source signal does propagate at approximately 1480 m s^{-1}. Clearly,

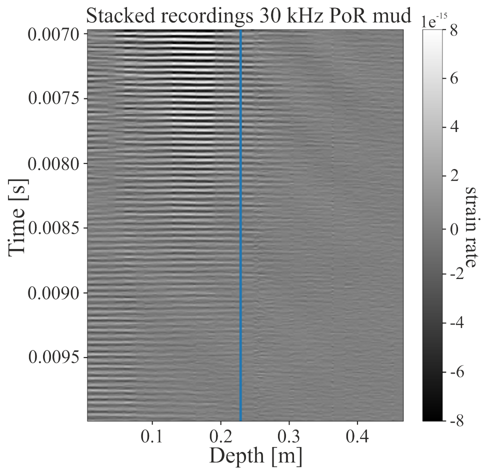

Figure 3.7: Zoom in of the oscillations in Figure 3.4, which are likely standing waves. The blue line indicates the water-mud interface

these oscillations are not P-waves, and must be something else.

The most probable explanation for this oscillating phenomenon, is that standing waves have developed in the water column , which in turn means that this extremely high velocity is related to an apparent velocity. [17] showed that standing waves can be measured when they have developed with a loosely coupled fibre. This happens if the fundamental frequency coincides with the physical length of the body in which these standing waves occur, or when an overtone has developed. They also showed that there are harmonics related to the physical length in their wireline VSP. In Figure 3.5, we observe 3 harmonics, namely at 11 kHz, 22 kHz and at 33 kHz. Because we send a frequency of 30 kHz, the harmonic at 11 kHz, which is the furthest away from the center frequency, has a lower amplitude compared to the other two harmonics. The exact dimension or dimensions that start to resonate is yet unknown. We also need to further investigate what type of standing waves we are dealing with - standing waves with two closed ends or with one closed and one open end. Notwithstanding we do not know the exact type and mode of the developed standing waves we observe, we clearly see that using the recorded standing waves we can estimate the depth of the water-mud interface. In fact, the estimate is very accurate with an accuracy of approximately 2 cm. Such an uncertainty is far smaller compared to the uncertainty of the standard non-intrusive methods used now in ports and waterways. [21] showed that the depth of the water-mud interface can also be estimated from the observations of the recorded propagating P-waves. The accuracy they achieved is 1.2 cm.

3.5. DISTRIBUTED ACOUSTIC SENSING USING PASSIVE NOISE

Above, we showed that standing waves that have developed in the water layer from an active source, like the dual frequency echo-sounder, can be very effectively used to estimate the depth of the water-mud interface. Ideally, one would like to operate a source remotely and on demand. However, permanent active installations at the water surface are not only expensive, but are also undesirable since they would form an obstruction for the shipping vessels; hence, a submerged measuring system is more desired. An interesting alternative as a source would be utilizing the noise generated by passing or idle vessels. Using a ship's propeller noise as a source has already been proposed by [22], for marine imaging. In their work, the frequency spectrum generated by the propeller's sheet cavitation, from a standard exploration vessel, is compared to the spectrum generated by a conventional 33 L air gun, as can be seen in Figure 3.8. The propellers generated a noise with a broad frequency spectrum. Such a noise is promising as a source for developing standing waves. Choosing specific frequency bands, one could check whether standing waves have developed.

In our laboratory experiment, standing waves could develop between the water

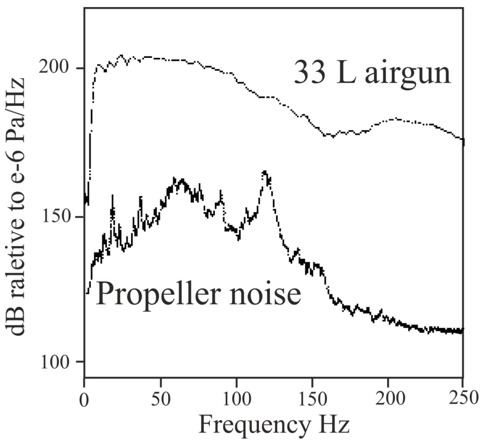

Figure 3.8: Comparison of the amplitude spectrum between cavitation sweep and an airgun array (modified from[22]).

surface and the water-mud interface, but also between the walls of the column. In contrast to that, in ports and waterways standing waves will develop only between the water surface and the water-mud interface. Because of this, they will be characterized by one closed end (the water surface) and one either open - or closed end (the water-mud interface). Knowing this, one can calculate what standing-wave modes could be developed for specific frequencies assuming certain depths. We take as examples the Port of Rotterdam and the Port of Hamburg with example depths to the water-mud interface of 22.5 m and 17 m, respectively. For such depths and velocity of the P-waves in the water layer of 1460 m s^{-1}, we calculate the first four modes of the possible standing waves with two closed ends, see Table

3.1. We can see that the calculated frequencies fall within the frequency range of

Table 3.1: Frequencies of the first four modes of standing waves that could develop in the Port of Rotterdam and Port of Hamburg with a depth of 22.5 m and 17 m, respectively.

Harmonic	1	2	3	4
Port of Rotterdam Hz	32	65	97	130
Port of Hamburg Hz	42	83	125	167

the noise produced by the propellers. This shows that the propeller noise should cause standing waves to develop in ports. Because of this, we strongly believe that we could use standing waves to accurately estimate the depth of the water-mud interface in ports using ambient noise, e.g., from propellers, where the estimation could be done remotely and on demand.

3.6. CONCLUSION

Using the results of our laboratory experiment, we showed the potential of using distributed acoustic sensing to record standing waves. We used a single-mode optical fibre to record signals from a dual frequency echo-sounder with center frequency of 38 kHz. Our laboratory experiments show that standing waves are bound to water, therefore standing waves can be used to accurately estimate the depth of the water-mud interface. Furthermore, we showed that the standing waves are easy to identify due to their high energy at the frequencies at which they develop, and due to the high apparent velocity they exhibit, which far exceeds the velocity of any other arrival.

Analyzing ambient noise from cavitation of propellers in ports, we proposed that standing waves are likely present in ports and waterways. This implies that standing waves could be used in practice to monitor the depth of the water-mud interface. Unlike conventional surveying methods, the method we propose, i.e., using standing waves in the later layer from ambient noise, would be repeatable, non-intrusive, on demand and can be operated remotely. This could increase the availability of crowded docks, where there is limited accessibility for a dredging or surveying vessel. Furthermore, our proposed method could reduce costs, increase safety, and reduce CO2 emissions because no surveying vessel is required on site.

REFERENCES

[1] M. Buisman, E. Martuganova, T. Kiers, D. Draganov, and A. Kirichek. "Continuous monitoring of the depth of the water-mud interface using distributed acoustic sensing". In: *Journal of Soils and Sediments* 22.11 (2022), pp. 2893–2899.

[2] A. Kirichek, C. Chassagne, H. Winterwerp, and T. Vellinga. "How navigable are fluid mud layers?" In: *Terra et Aqua* (Aug. 2018), pp. 6–18.

[3] I. Fadel, A. Kirchek, M. Buisman, K. Heller, and D. Draganov. "Monitoring Settling and Consolidation of Fluid Mud in a Laboratory Using Ultrasonic Measurements". In: *82nd EAGE Conference and Exhibition* (Amsterdam, The Netherlands). Expanded Abstracts. European Association of Geoscientists & Engineers, 2021, pp. 1–5. DOI: https://doi.org/10.3997/2214-4609.202120168.

[4] X. Ma, A. Kirichek, A. Shakeel, K. Heller, and D. Draganov. "Laboratory seismic measurements for layer-specific description of fluid mud and for linking seismic velocities to rheological properties". In: *The Journal of the Acoustical Society of America* 149.6 (2021), pp. 3862–3877. DOI: https://doi.org/10.1121/10.0005039.

[5] N. Lindsey, E. Martin, D. Dreger, B. Freifeld, S. Cole, S. James, B. Biondi, and J. Ajo-Franklin. "Fiber-optic network observations of earthquake wavefields: Fiber-optic earthquake observations". In: *Geophysical Research Letters* 44.23 (Nov. 2017), pp. 11, 792–11, 799. DOI: https://doi.org/10.1002/2017GL075722.

[6] P. Jousset, T. Reinsch, T. Ryberg, H. Blanck, A. Clarke, R. Aghayev, G. P. Hersir, J. Henninges, M. Weber, and C. M. Krawczyk. "Dynamic strain determination using fibre-optic cables allows imaging of seismological and structural features". In: *Nature Communications* 9.1 (2018), p. 2509. ISSN: 2041-1723. DOI: https://doi.org/10.1038/s41467-018-04860-y.

[7] J. B. Ajo-Franklin, S. Dou, N. J. Lindsey, I. Monga, C. Tracy, M. Robertson, V. Rodriguez Tribaldos, C. Ulrich, B. Freifeld, T. Daley, and X. Li. "Distributed Acoustic Sensing Using Dark Fiber for Near-Surface Characterization and Broadband Seismic Event Detection". In: *Scientific Reports* 9.1 (2019), p. 1328. ISSN: 2045-2322. DOI: https://doi.org/10.1038/s41598-018-36675-8.

[8] A. Mateeva, J. Lopez, H. Potters, J. Mestayer, B. Cox, D. Kiyashchenko, P. Wills, S. Grandi, K. Hornman, B. Kuvshinov, W. Berlang, Z. Yang, and R. Detomo. "Distributed acoustic sensing for reservoir monitoring with vertical seismic profiling". In: *Geophysical Prospecting* 62.4 (2014), pp. 679–692. DOI: https://doi.org/10.1111/1365-2478.12116.

3

[9] J. Correa, A. Egorov, K. Tertyshnikov, A. Bóna, R. Pevzner, T. Dean, B. Freifeld, and S. Marshall. "Analysis of signal to noise and directivity characteristics of DAS VSP at near and far offsets — A CO2CRC Otway Project data example". In: *The Leading Edge* 36 (Dec. 2017), 994a1–994a7. DOI: https://doi.org/10.1190/tle36120994a1.1.

[10] S. Grandi, M. Dean, and O. Tucker. "Efficient Containment Monitoring with Distributed Acoustic Sensing: Feasibility Studies for the Former Peterhead CCS Project". In: *Energy Procedia* 114 (2017), pp. 3889–3904. ISSN: 1876-6102. DOI: https://doi.org/10.1016/j.egypro.2017.03.1521.

[11] J. Götz, S. Lüth, J. Henninges, and T. Reinsch. "Vertical seismic profiling using a daisy-chained deployment of fibre-optic cables in four wells simultaneously – Case study at the Ketzin carbon dioxide storage site". In: *Geophysical Prospecting* 66.6 (2018), pp. 1201–1214. DOI: https://doi.org/10.1111/1365-2478.12638.

[12] A. Hartog, B. Frignet, D. Mackie, and M. Clark. "Vertical seismic optical profiling on wireline logging cable". In: *Geophysical Prospecting* 62.4 (2014), pp. 693–701. DOI: https://doi.org/10.1111/1365-2478.12141.

[13] W. Borland, R. Hearn, and A. Sayed. "Improving the acquisition efficiency of acquiring borehole seismic data by recording optical distributed acoustic data on a wireline hybrid electrooptical cable". In: *86th SEG Annual Meeting* (Dallas, Texas, USA). Expanded Abstracts. 2016, pp. 800–804. DOI: https://doi.org/10.1190/segam2016-13951115.1.

[14] G. Yu, Z. Cai, Y. Chen, X. Wang, Q. Zhang, Y. Li, Y. Wang, C. Liu, B. Zhao, and J. Greer. "Walkaway VSP using multimode optical fibers in a hybrid wireline". In: *The Leading Edge* 35 (July 2016), pp. 615–619. DOI: https://doi.org/10.1190/tle35070615.1.

[15] T. Daley, D. Miller, K. Dodds, P. Cook, and B. Freifeld. "Field testing of modular borehole monitoring with simultaneous distributed acoustic sensing and geophone vertical seismic profiles at Citronelle, Alabama". In: *Geophysical Prospecting* 64.5 (2016), pp. 1318–1334. DOI: https://doi.org/10.1111/1365-2478.12324.

[16] M. E. Willis, X. Wu, W. Palacios, and A. Ellmauthaler. "Understanding cable coupling artifacts in wireline-deployed DAS VSP data". In: *89th SEG Annual Meeting* (San Antonio, Texas, USA). Expanded Abstracts. 2019, pp. 5310–5314. DOI: https://doi.org/10.1190/segam2019-3208294.1.

[17] E. Martuganova, M. Stiller, K. Bauer, J. Henninges, and C. M. Krawczyk. "Cable reverberations during wireline distributed acoustic sensing measurements: their nature and methods for elimination". In: *Geophysical Prospecting* 69.5 (2021), pp. 1034–1054. DOI: https://doi.org/10.1111/1365-2478.13090.

[18] T. Daley, B. Freifeld, J. Ajo-Franklin, S. Dou, R. Pevzner, V. Shulakova, S. Kashikar, D. Miller, J. Götz, J. Henninges, and S. Lüth. “Field testing of fiber-optic distributed acoustic sensing (DAS) for subsurface seismic monitoring”. In: *The Leading Edge* 32 (June 2013), pp. 699–706. DOI: https://doi.org/10.1190/tle32060699.1.

[19] N. Lindsey, H. Rademacher, and J. Ajo-Franklin. “On the Broadband Instrument Response of Fiber-Optic DAS Arrays”. In: *Journal of Geophysical Research: Solid Earth* 125.2 (2020), e2019JB018145. DOI: https://doi.org/10.1029/2019JB018145.

[20] P. Welch. “The use of fast Fourier transform for the estimation of power spectra: A method based on time averaging over short, modified periodograms”. In: *IEEE Transactions on Audio and Electroacoustics* 15.2 (1967), pp. 70–73. DOI: 10.1109/TAU.1967.1161901.

[21] D. Draganov, X. Ma, M. Buisman, T. Kiers, K. Heller, and A. Kirichek. “Non-Intrusive Characterization and Monitoring of Fluid Mud: Laboratory Experiments with Seismic Techniques, Distributed Acoustic Sensing (DAS), and Distributed Temperature Sensing (DTS)”. In: June 2021. ISBN: 978-1-83881-119-8. DOI: https://doi.org/10.5772/intechopen.98420.

[22] K. Davies, G. Hampson, H. Jakubowicz, and J. Odegaard. “Screw seismic sources”. In: *SEG Technical Program*. Expanded Abstracts. 1992, pp. 710–711. DOI: https://doi.org/10.1190/1.1822196.

3

4

Capturing the water-mud interface in the Field using DAS

Ports and waterways, often subjected to siltation, require regular nautical depth monitoring to ensure safe vessel movement. These measurements depend on the availability of a surveying vessel and quay-wall access, limiting the temporal resolution. We propose to use distributed acoustic sensing to monitor the nautical depth using fiber-optical cables. We create a vertical seismic profile using a steel mantle coiled with a fiber, partly submerged in water and mud. We show that the large difference in attenuation between water and mud can be used with noise generated by ships for continuous monitoring of the water-mud interface with cm accuracy.

Parts of this chapter have been published in Journal of Soils and Sediments, **22**, (11) (2022) [1].
Parts of this chapter have been published in the 83rd EAGE Annual Conference & Exhibition, Vol. 2022. No. 1. European Association of Geoscientists & Engineers, 2022 (2022) [2].

4

4.1. Introduction

Ports and waterways with high siltation rates require frequent surveying to ensure the nautical depth. Currently, surveying techniques have low repeatability, are limited in accuracy, and are restricted by the availability of a surveying vessel and quay-wall access [3]. Especially at the financially most crucial quay-walls, availability for surveying is severely constrained due to the high costs of halting activities for a surveying vessel. Furthermore, substantial changes in the nautical depth can suddenly occur after storms, implying that extensive, time-consuming surveys are required again to ensure the safe navigability of vessels [3]. These surveys are time-consuming due to the large surveying area and the variation in water temperature, salinity, and (fluid) mud rheology and density. Because of these variations, even over small distances, re-calibration is often required to acquire a velocity profile for zero-offset measurements, such as with echo sounders [4]. Echo sounders operate as both a source and receiver, measuring the two-way travel time from the source to the bottom, and back to the receiver. An accurate velocity model is then used to convert the two-way travel time to depth. However, at specific locations with a mixture of sea and river water, such as estuaries, obtaining an accurate velocity profile is most challenging because of the differing P-wave velocities in the water column, leading to time-consuming calibration and a higher inaccuracy.

To tackle the limited temporal resolution and measurement accuracy, new surveying techniques are required. [1] showed that DAS can be used, combined with an active source, in a laboratory setup to measure the water-mud interface. Here, we focus on DAS for in situ nautical depth monitoring in the Port of Rotterdam. We demonstrate how passive noise from ships can be used to monitor the nautical depth with optical cables.

4.2. Distributed Acoustic Sensing

DAS interrogators convert an optical fiber into a distributed seismic array. Optical fibers offer many advantages over conventional electrical sensors, such as electric isolation and immunity to electromagnetic interference, and they are non-conductive and non-corrosive, making them well-suited for utilisation in liquids [5–7]. DAS measures the elongation or contraction of a fiber which causes an increase or decrease in optical path length, respectively. Due to density variations in the fiber, a portion of the laser sent by a source (interrogator) is backscattered in the form of Rayleigh backscattering. The exact location of such density variations is unknown; however, the total distribution is assumed to be homogenous and time-invariant [8]. Since the speed of light in a glass fiber and refractive index of glass are known, the location of a vibration, causing elongation or contraction, can be estimated by measuring the time difference between the emitted laser pulse and the recording time at the receiver. Because the density anomalies in fibers are far too frequent to be individually distinguished, an averaged phase between two points, known as the gauge length, is extracted from the backscattered signal. The response function of the gauge length varies per spatial wavelength and should ideally be optimised

to the expected recorded spatial wavelength [9]. In general, a larger gauge length usually gives a higher SNR at the expense of spatial resolution. Even though the phase difference is averaged over the gauge length, the waveforms are well preserved and have been used in various fields of research: teleseismic earthquake monitoring [10, 11], VSP [12–14], and earthquake phase identification [15].
Another interesting development in DAS is that new commercially available DAS interrogators can utilise fibers over more than 100 km [16], allowing for an extensive, cheap, and reliable (semi) permanent monitoring system, allowing to monitor large areas with a single interrogator.

Experimental Setup

We execute our experiment in the Botlek, in the Port of Rotterdam (The Netherlands). This location is chosen due to the abundance of traffic and the high sedimentation rate. The setup consists of a 24-m-long solid steel pole, driven 17 m into the subsurface to ensure a permanent position, holding a 2.4-m-long mantle coiled with a 726 m standard single-mode communication fiber with a diameter of 1.6 mm, as shown in Figure 4.1. The 726 m of fiber cover 1 m of the mantle in height, imitating a VSP geometry. With this setup, we obtain a receiver every 1.376 mm in depth. The mantle is lowered slightly beyond the water-mud interface. This way, the fibers are partly submerged in water and party immersed into (fluid) mud.

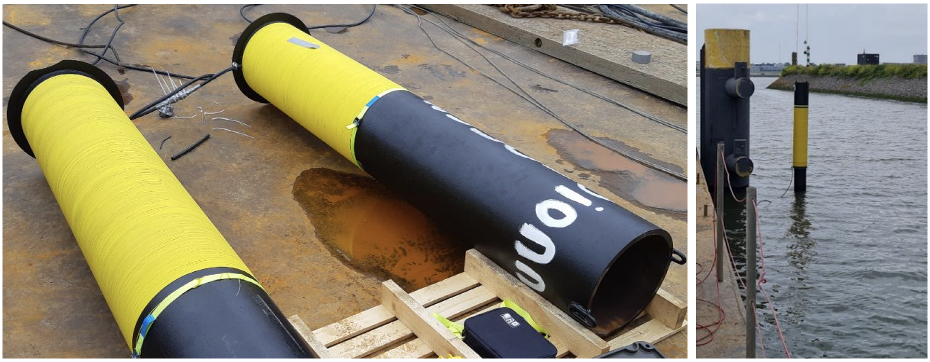

Figure 4.1: Left: two mantles of which only the right one is used. Right: picture of a mantle being installed on a pole. The diameter of the mantle is 37 cm. We use 726 m of fiber is coiled (the yellow part) around the mantle to cover 1 m of the mantle's height.

We use a Febus A1 interrogator for data acquisition, and select an 800 Hz and 2 kHz time sampling, a 2 m gauge length and a 40 m gauge length to achieve the highest spatial resolution and SNR, respectively.
The larger 40 m gauge length with the higher time sampling and a 40 m channel spacing is used to analyse the frequency spectrum of a passing vessel. The 2 m gauge with the lower time sampling provides a higher spatial resolution. With the 2

m gauge length, a finer channel spacing of 1 m is used. The lower time sampling is chosen to limit the data size. We were only able to measure for a limited amount of time due to an absence of a safe place to store the interrogator.

WATER-DEPTH ESTIMATIONS BASED ON FREQUENCY CONTENT

The depth of the water-mud interface varies due to sedimentation and dredging in the vicinity of an observation point. A sharp transition in acoustic attenuation can be expected due to drag forces and gas pockets in mud caused by bio-degradation [1, 4].

The results in Figure 4.2, a PSD plot calculated using Welch's method [17], show that DAS can measure noise from passing vessels. During the recording time shown in Figure 4.2, one ship passed between minutes 8 and 14, and one approached the sensing mantle at the end of the recording. Clear constructive and destructive

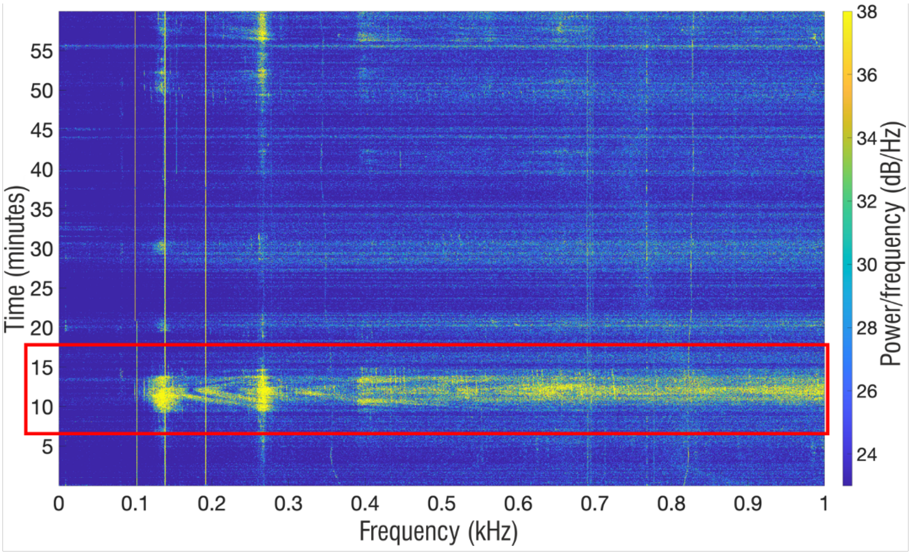

Figure 4.2: Spectrogram of channel 16, located in water, with a gauge length of 40 m and a time sampling frequency of 2 kHz. During this hour-long recording, a boat passed between minutes 8 and 14. Another boat passed at the end of the recording, which is why it is partly recorded after minute 50. In addition, one can observe various machine-noise frequencies, such as at 0.1 kHz, 0.13 kHz and 0.2 kHz. The red rectangle indicates the PSD of a passing vessel.

interference patterns with high amplitudes are observable as the ship passes. We also observe a fundamental mode of vibration at 130 Hz, and at least two overtones in the PSD are visible. These resonances are likely originating from the pole. Shipping noise has been monitored during multiple tidal windows to investigate whether the water column height changes in [18]. This research found that only much lower

frequencies change due to changes in the water column height.
Our measurements contain consistent noise, likely from the interrogator itself. This can be observed in Figure 4.2 as straight lines throughout the spectrogram at 100 Hz, 133 Hz, and 190 Hz. In addition, noise likely related to the cooling fans inside the interrogator was observed around 360 Hz increasing and decreasing due to a change in ambient temperature. Interestingly enough, a reversed temperature effect can be observed around 820 Hz, decreasing and increase with changing ambient temperatures. This mirrored effect is especially prominent in the first five minutes of Figure 4.2. Finally, also continuous noise was observed at 700 Hz from an unknown source.
When we zoom in on the frequency range of the fundamental mode and the first overtone for all channels and select the time window of 8 to 14 minutes, we notice a distinct difference in the frequency content beyond a depth of 5.7 m, see Figure 4.3. This contrast in frequency content becomes even more apparent with a gauge length

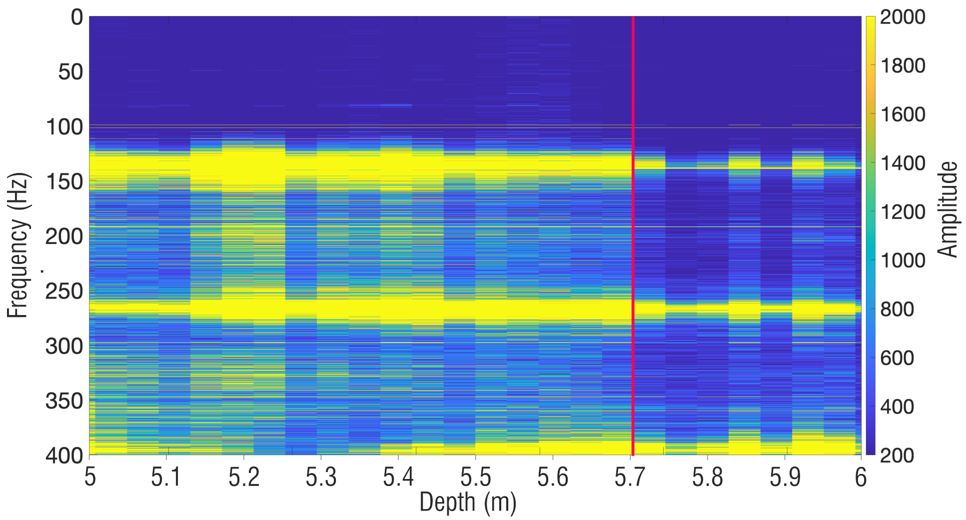

Figure 4.3: Power spectral density of minutes 8 to 14 during which a boat passes, as shown in Figure 4.2, for all channels with a 40 m gauge length, 2 kHz time sampling, and 40 m channel spacing. A change in frequency amplitude content can be observed around 5.7 m depth.

of 2 m, as shown in Figure 4.4, where we observe a sharp boundary in signal energy at a depth of 5.66 m. The difference in transition is likely related to the smaller gauge length, implying more measurement points in depth and, thus, less averaging at the transition zone. After one month of measuring, the mantle is raised for visual inspection to ensure that the mantle is partly immersed in mud. Barnacles that grew on our mantle, together with an unsightly brown coating, confirmed that our setup was indeed partly immersed in mud. Based on the visual observation of our sensing pole, we expect the depth of the water-mud interface to be at a depth of between

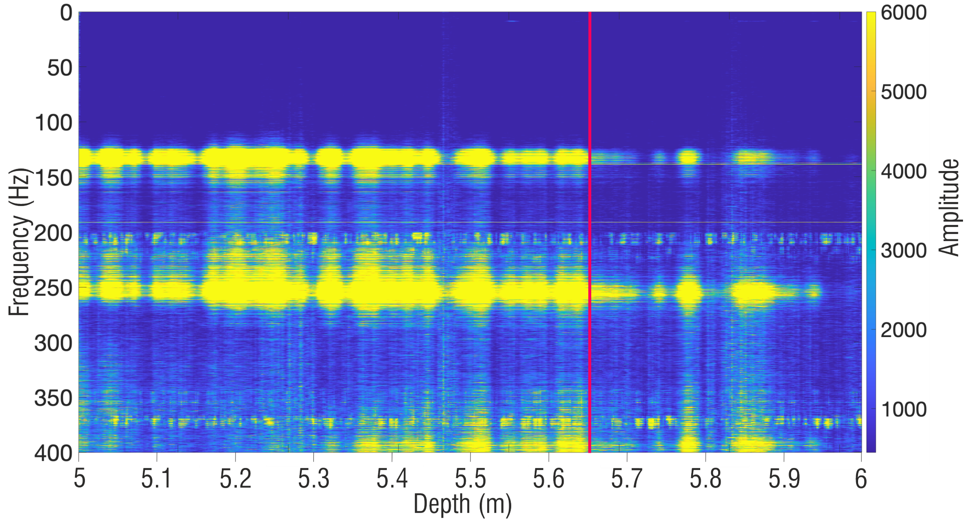

Figure 4.4: Power spectral density plot of a 120-s-long recording with an 800 Hz time sampling, a 2-m gauge length, and 2 m channel spacing during which a vessel passed. At a depth of 5.66 m, there appears to be a sharp boundary, likely the water-mud interface.

5.60 m and 5.8 m. Our 2-meter gauge length measurements show a sharp boundary at 5.66 m depth, which is well within our expectations based on visual inspection by raising the mantle and sending an underwater drone. Therefore, we assume that the difference we observe in the PSD at 5.66 m indicates the water-mud boundary. A more accurate measurement would require sending a diver.

Besides a PSD, we stack 41 traces, similar to 5 cm in height, well above the boundary, 41 traces just above the boundary, 41 traces just below the boundary, and 41 traces well below the boundary using the measurement obtained with the 2-meter gauge length (Figure 4.5). We stack 41 to increase the SNR, because individual DAS traces can differ substantially in SNR. We can observe in Figure 4.5 that the general shape of the amplitude spectra of the four stacked results are very similar. However, we see a striking difference in the amplitudes of the stacked results for traced above and for traces below the water-mud boundary. This difference in amplitude further suggests that the two pairs of stacked results are using traces recorded in different fluids - water and fluid mud. Finally, if we compare the ratio of a stationary long-term-average window with a sliding short-term-average window, we can observe a sharp increase in ratio at 5.6 m depth, as shown in Figure 4.6. A frequency band of 100 Hz - 195 Hz has been selected for these windows, and then an amplitude ratio between the long window, consisting of 10 cm depth at 5.27 m - 5.37 m, and a sliding short-term-average window of 2.07 cm along the whole pole is calculated. The expected ratio between the long-term-average and short-term-average window is 4.9 since the long-term-average window is 4.9 times longer than the short-term-average

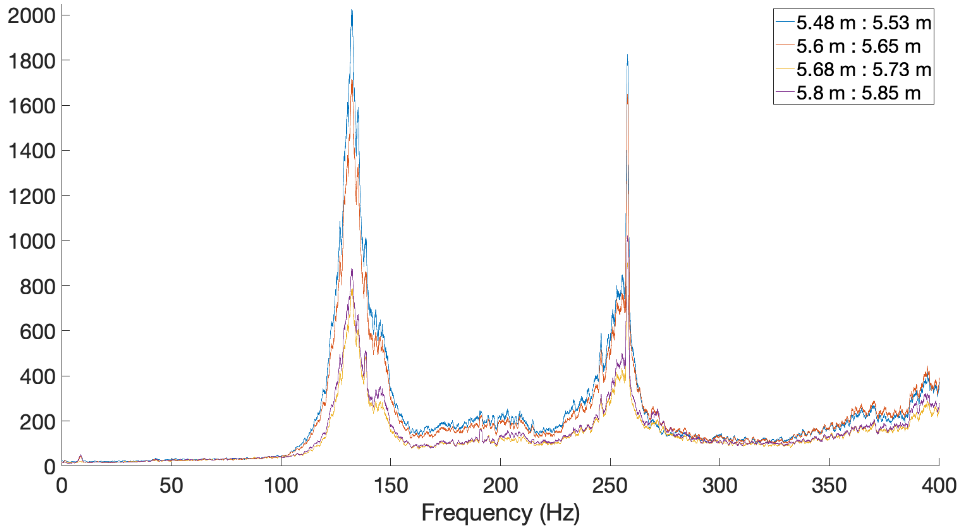

Figure 4.5: Amplitude spectrum of the stacking result of 36 traces, equal to about 5 cm depth, at four different depths, namely well above the water-mud interface, just above the water-mud interface, just below the water-mud interface, and well below the water-mud interface. The inset shows the colour-coding of the four depth intervals.

window. Initially, we can observe the window ratio oscillating around the expected average, indicating water. At 5.6 m depth the ratio starts increasing sharply; we can observe that it almost doubles and oscillates around 8.1, which value is reached at 5.65 m. Thus, the increased values of the ratio between 5.62 and 5.65 m indicate the water-mud interface. Our VSP measurements show the potential of monitoring the nautical depth using passive noise. A similar setup could be used in waterways with much traffic to monitor the nautical depth remotely and continuously. The large difference in amplitudes in recorded passive noise could be relatively easily used to pick the water-mud interface. Though our VSP is still a point measurement, the results could serve as a base for a more elaborate experiment, including a network of horizontal fibers. Based on the recorded signals from passing vessels, a horizontal fiber could most likely be efficiently utilised for monitoring the nautical depth using a similar attenuation-based approach, allowing for a broad coverage without interfering with traffic. Additionally, DAS can be used remotely and continuously, hence DAS could solve the temporal resolution problems of monitoring the nautical depth from which current surveying measurements suffer.

4.2.1. CONCLUSIONS

We recorded passive noise from vessels in the Botlek, in the Port of Rotterdam, using optical fibers and distributed acoustic sensing (DAS). We mimicked a vertical seismic profile by wrapping a standard communication fiber around a mantle that

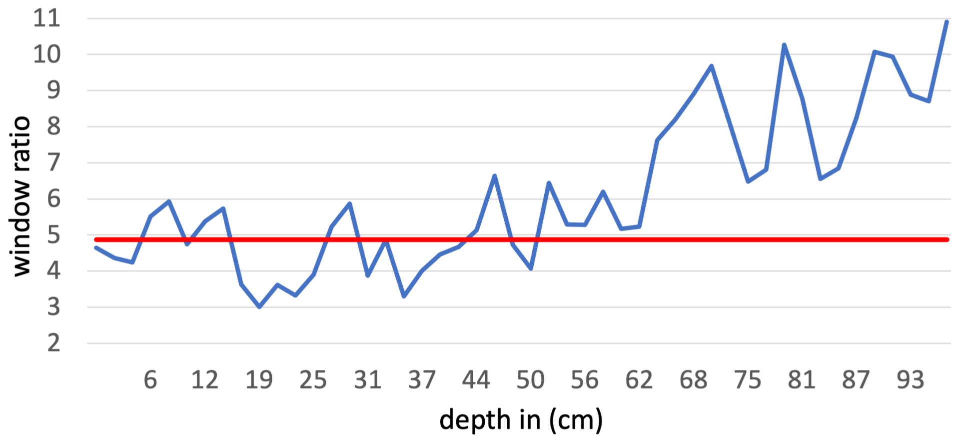

4

Figure 4.6: The ratio between the stationary long-term-average window and the short-term-average window. A frequency band of 100 Hz - 195 Hz is selected for both the short and long window. The stationary long-term-average window consists of a 10 cm depth interval at 5.27 m - 5.37 m depth. The sliding short-term-average window is taken from 5 m - 6 m depth in increments of 2.07 cm. The blue line indicates the ratio, and the red line shows the average ratio of 4.9 between the long window and short window for the interval before the sharp increase.

was partly submerged in water and mud. We showed the potential of using DAS for continuous water-depth monitoring by analysing the difference in amplitude and frequency content measurements in water and mud. We recorded data using gauge of 2m and 40 m. Both the 2-m and 40-m gauge length could use ambient noise sources for depth estimations. The 2-m gauge provided a more accurate estimation due to the denser spatial sampling, even with a lower signal-to-noise ratio. The advantage of our DAS method over conventional methods is that our method can be used continuously and remotely, given that there is water traffic nearby. Additionally, due to the low cost of fibers and the far-reaching dynamic range of interrogators, DAS could be a most attractive alternative for water-depth monitoring using propeller noise in shallow marine environments, ports and waterways. Monitoring the water-mud interface with DAS could resolve temporal resolution problems at a relatively low expense. With this new monitoring setup, berth occupancy can be optimised, safety can increase due to a reduction in surveying vessel movement, and CO_2 emissions can be reduced by optimising dredging strategies.

REFERENCES

[1] M. Buisman, E. Martuganova, T. Kiers, D. Draganov, and A. Kirichek. “Continuous monitoring of the depth of the water-mud interface using distributed acoustic sensing”. In: *Journal of Soils and Sediments* 22.11 (2022), pp. 2893–2899.

[2] M. Buisman, E. Martuganova, A. Kirichek, and D. Draganov. “Water-depth estimation using propeller noise by distributed acoustic sensing”. In: *83rd EAGE Annual Conference & Exhibition*. Vol. 2022. 1. European Association of Geoscientists & Engineers. 2022, pp. 1–5.

[3] W. H. McAnally, A. Teeter, D. Schoellhamer, C. Friedrichs, D. Hamilton, E. Hayter, P. Shrestha, H. Rodriguez, A. Sheremet, R. Kirby, *et al.* “Management of fluid mud in estuaries, bays, and lakes. II: Measurement, modeling, and management”. In: *Journal of Hydraulic Engineering* 133.1 (2007), pp. 23–38.

[4] A. Kirichek, C. Chassagne, H. Winterwerp, and T. Vellinga. “How navigable are fluid mud layers?” In: *Terra et Aqua* (Aug. 2018), pp. 6–18.

[5] M. Shao, X. Qiao, X. Zhao, Y. Zhang, and H. Fu. “Liquid Level Sensor Using Fiber Bragg Grating Assisted by Multimode Fiber Core”. In: *IEEE Sensors Journal* 16.8 (2016), pp. 2374–2379. DOI: https://doi.org/10.1109/JSEN.2015.2513413.

[6] W. Xu, J. Wang, J. Zhao, C. Zhang, J. Shi, X. Yang, and J. Yao. “Reflective Liquid Level Sensor Based on Parallel Connection of Cascaded FBG and SNCS Structure”. In: *IEEE Sensors Journal* 17.5 (2017), pp. 1347–1352. DOI: https://doi.org/10.1109/JSEN.2016.2629488.

[7] C. Yang, S. Chen, and G. Yang. “Fiber optical liquid level sensor under cryogenic environment”. In: *Sensors and Actuators A: Physical* 94 (Oct. 2001), pp. 69–75. DOI: https://doi.org/10.1016/S0924-4247(01)00663-X.

[8] N. Lindsey, H. Rademacher, and J. Ajo-Franklin. “On the Broadband Instrument Response of Fiber-Optic DAS Arrays”. In: *Journal of Geophysical Research: Solid Earth* 125.2 (2020), e2019JB018145. DOI: https://doi.org/10.1029/2019JB018145.

[9] T. Dean, T. Cuny, and A. H. Hartog. “The effect of gauge length on axially incident P-waves measured using fibre optic distributed vibration sensing”. In: *Geophysical Prospecting* 65.1 (2017), pp. 184–193.

[10] J. B. Ajo-Franklin, S. Dou, N. J. Lindsey, I. Monga, C. Tracy, M. Robertson, V. Rodriguez Tribaldos, C. Ulrich, B. Freifeld, T. Daley, and X. Li. “Distributed Acoustic Sensing Using Dark Fiber for Near-Surface Characterization and Broadband Seismic Event Detection”. In: *Scientific Reports* 9.1 (2019), p. 1328. ISSN: 2045-2322. DOI: https://doi.org/10.1038/s41598-018-36675-8.

[11] P. Jousset, T. Reinsch, T. Ryberg, H. Blanck, A. Clarke, R. Aghayev, G. P. Hersir, J. Henninges, M. Weber, and C. M. Krawczyk. “Dynamic strain determination using fibre-optic cables allows imaging of seismological and structural features”. In: *Nature Communications* 9.1 (2018), p. 2509. ISSN: 2041-1723. DOI: https://doi.org/10.1038/s41467-018-04860-y.

[12] T. Daley, D. Miller, K. Dodds, P. Cook, and B. Freifeld. “Field testing of modular borehole monitoring with simultaneous distributed acoustic sensing and geophone vertical seismic profiles at Citronelle, Alabama”. In: *Geophysical Prospecting* 64.5 (2016), pp. 1318–1334. DOI: https://doi.org/10.1111/1365-2478.12324.

[13] E. Martuganova, M. Stiller, K. Bauer, J. Henninges, and C. M. Krawczyk. “Cable reverberations during wireline distributed acoustic sensing measurements: their nature and methods for elimination”. In: *Geophysical Prospecting* 69.5 (2021), pp. 1034–1054. DOI: https://doi.org/10.1111/1365-2478.13090.

[14] A. Mateeva, J. Lopez, H. Potters, J. Mestayer, B. Cox, D. Kiyashchenko, P. Wills, S. Grandi, K. Hornman, B. Kuvshinov, W. Berlang, Z. Yang, and R. Detomo. “Distributed acoustic sensing for reservoir monitoring with vertical seismic profiling”. In: *Geophysical Prospecting* 62.4 (2014), pp. 679–692. DOI: https://doi.org/10.1111/1365-2478.12116.

[15] N. Lindsey, E. Martin, D. Dreger, B. Freifeld, S. Cole, S. James, B. Biondi, and J. Ajo-Franklin. “Fiber-optic network observations of earthquake wavefields: Fiber-optic earthquake observations”. In: *Geophysical Research Letters* 44.23 (Nov. 2017), pp. 11, 792–11, 799. DOI: https://doi.org/10.1002/2017GL075722.

[16] O. H. Waagaard, E. Rønnekleiv, A. Haukanes, F. Stabo-Eeg, D. Thingbø, S. Forbord, S. E. Aasen, and J. K. Brenne. “Real-time low noise distributed acoustic sensing in 171 km low loss fiber”. In: *OSA Continuum* 4.2 (Feb. 2021), pp. 688–701. DOI: https://doi.org/10.1364/OSAC.408761.

[17] P. Welch. “The use of fast Fourier transform for the estimation of power spectra: A method based on time averaging over short, modified periodograms”. In: *IEEE Transactions on Audio and Electroacoustics* 15.2 (1967), pp. 70–73. DOI: 10.1109/TAU.1967.1161901.

[18] M. Buisman, D. Draganov, and A. Kirichek. “Monitoring tidal water-column changes in ports using distributed acoustic sensing”. In: *84th EAGE Annual Conference & Exhibition*. Vol. 2023. 1. European Association of Geoscientists & Engineers. 2023, pp. 1–5.

4

5

Detection of Shear-Stress Changes and Optical Fibres

As already shown, optical fibres in VSP configuration could be used to estimate the water-mud interface. However, it is also important to know the shear stress of fluid mud.

This study delves into the methodology of nautical depth measurement, highlighting the potential of estimating shear stresses through distributed acoustic sensing. Laboratory experiments, utilizing both natural and synthetic sediment suspensions, employ an optical fiber wrapped around a PVC pipe to gauge variations in acoustic attenuation. Initial measurements taken an hour post-mixing, depicting a shear strength of 17 Pa, exhibit pronounced signal attenuation. Subsequent tests conducted 24 hours post-mixing, revealing a shear strength of 48 Pa, display a substantial reduction in signal attenuation, consequently amplifying the amplitude.

Field experiments corroborate these findings, demonstrating an amplitude increase correlated with increased shear strength while recording propeller noise from passing vessels at frequencies < 60 Hz. Conversely, frequencies > 100 Hz reveal a contrasting trend. This amplitude differentiation with depth potentially relates to variations in fibre coupling and acoustic wave attenuation. Furthermore, the field experiment showcases the prospective application of distributed acoustic sensing for continuous depth measurements.

Parts of this chapter have been published in Proceedings to WODCON XXIII (2022) [1].

5

5.1. Research Objective

Ports and Waterways subjective to high siltation rates must be regularly surveyed to ensure safe passage of vessels. Dredging maintenance must be carried out to ensure that the navigability of ports and waterways is maintained. Various port authorities apply different techniques to monitor the water depth and have different definitions of the nautical depth. For example, the navigable depth criterion of the Port of Rotterdam and the Port of Lianyungang is based on a density of 1.2 kgl^{-1} and 1.25-1.3 kgl^{-1}, respectively, whereas the Port of Emden has a nautical bottom definition derived from a yield stress of 100 Pa [2]. This difference in nautical criterion and surveying techniques can be related to the variety of the sediments that deposits due to natural processes, often in the form of (fluid) mud. The relation between fluid mud's density and shear strength is non-linear [3]. The properties of the fluid mud can differ substantially over short distances [4]. In addition, the properties are affected by the organic-matter content, which plays a significant role in flocculation and sediment transport processes [5]. Decaying organic matter creates gas pockets in the mud layers. These gas pockets hinder surveying methods based on P-waves due to the attenuation of these waves when passing through the gas. Furthermore, the organic-matter content in fluid mud affects the shear and yield stresses of the fluid mud. Especially the latter case is interesting because it affects the navigability of the fluid-mud layers. Currently, the nautical-depth estimation is often based on density, mainly because of practical reasons [6]. A critical aspect of measuring shear stresses with conventional laboratory methods is that once the mud has been sampled, the yield stresses of a sample are changed, making it an ambiguous and challenging process to standardise. Therefore, non-invasive in-situ methods are desired. Recent developments in this field include measuring S-waves, as described by [7] and [8]. S-waves can be of great use for estimating shear stresses in fluid mud because they only depend on the shear moduli and density. Conversely , the P-waves depend on the bulk moduli, shear moduli, and density:

$$C_p = \sqrt{\frac{K + \frac{4}{3}}{\mu}\rho}, \tag{5.1}$$

$$C_s = \sqrt{\frac{\mu}{\rho}}, \tag{5.2}$$

where c_p, c_s, K, μ, and ρ represent the P-wave velocity, S-wave velocity, bulk modulus, shear modulus, and density, respectively. The relation between an increase in shear strength (fluidic yield stress) and an increase in shear-wave velocity over time was shown in [9] for two different types of mud samples. Since S-waves cannot propagate through liquids or gases, they can only propagate through the solid parts of the fluid mud. Therefore, S-waves are almost unaffected by gas pockets in the fluid mud, which is not the case for conventional echo-sounder surveying techniques that rely on pressure waves. [8] used a piezoelectric S-wave transducer as a source and receiver. They observed an increase in shear-wave velocity in fluid mud during the sedimentation and consolidation processes. The interesting part about using shear-wave velocities is that this method is non-intrusive. Because of this, one could repeat such measurements on the same sample, opposed to conventional methods that often involve a rheometer that damage the sample. [7] used a similar laboratory setup to estimate shear stresses as[8]. One key difference is [7] used pressure transducers and estimated S-wave velocity from converted pressure to S-waves. Using pressure sources allows placing sources in the water instead of directly in the mud, making it a more realistic approach for in the field. Additionally, this setup mimics a marine seismic survey, often used by surveying companies for subsurface imaging. These measuring layouts usually consist of one or multiple sources (airguns) and multiple hydrophones (streamers) lines. The length of the streamers is often equal to the maximum exploration depth and could potentially be used in rivers. Using conventional marine seismic methods would not be without practical challenges (the most challenging is surveying transitional zones, where the depth is too shallow for marine seismic methods), such as the need to sail in a straight line and the need for a high frequency source with a large beam angle. Buisman et al. (2022) [10] showed that DAS could be used to measure the water-mud interface using a laboratory setup. A similar approach was applied for data recorded in the Port of Rotterdam. Buisman et al. (under review) showed that ambient noise generated by propellers of passing vessels and recorded by DAS could be used to (continuously) estimate the water-mud interface. An essential advantage of DAS over conventional surveying techniques is that fibres can be (semi) permanently installed, allowing for continuous or on-demand measurements. Furthermore, DAS does not require a surveying vessel and can be used even when a quay wall is occupied. It is important to note that heavily occupied quay walls are often unavailable for surveying vessels. Additionally, storms can cause significant bathymetrical changes over large areas, requiring extensive and time-consuming surveying. Below, we give a proof of concept for estimation of the shear stresses of bentonite clay in a laboratory setup and estimation of the shear stresses of (fluid) mud in the Port of Rotterdam based on signal penetration and coupling conditions of the fibre to its surrounding.

5.1.1. Overview of Distributed Acoustic Sensing

DAS is a relatively novel technology that allows using optical fibres to measure vibrations. The vibrations cause the fibre to elongate or contract, causing an increase or decrease in optical path length, respectively. Due to density variations in the fibre, a portion of the laser sent by a source (interrogator) is backscattered in the form of Rayleigh backscattering. The exact location of such density variations is unknown; however, the total distribution is assumed to be homogenous and time-invariant. The enthusiastic reader is referred to [11] for an overview of how single-pulse coherent light DAS interrogators work. In the experiments we describe below, we use two DAS interrogators of this type – Silixa iDAS v2 and Febus A1. There has been a large increase in the number of DAS applications over the last few years, for example, in teleseismic earthquake monitoring [12–14]), VSP [15–17], and earthquake phase identification [12, 18]. One of the reasons why DAS has gained a lot of attention is because standard telecommunication fibres can be used with DAS interrogators to form a seismic array. By using out-of-service telecommunication fibres, so-called "dark fibres", seismic arrays can be formed that used to be prohibitive in cost, such as described in [19], where an pre-existing ocean-bottom fibre was used to create a dense broadband array for submarine structural characterization. Due to the large dynamic range of the DAS interrogators, which have been reported to be up to 171 km [20], there are even ideas to implement DAS to create underwater seismic monitoring for an earthquake early warning system [21].

5.1.2. The Laboratory Setup

To show the potential of the DAS measurement techniques for estimation of shear stresses, we perform both a laboratory experiment and a pilot field experiment in the Botlek, Rotterdam, the Netherlands. The laboratory setup consists of an optical fibre with a length of 140 m tightly wrapped around a PVC pipe of 0.8 m in height and a diameter of 0.125 m; the wrapped cable thus covers 0.5 m of the height of the PVC pipe. This PVC pipe is then installed inside a transparent cylindrical tank with a height of 1.1 m and a diameter of 0.4 m, filled at the bottom with sand, followed by a suspension of bentonite in water, and finally a pure water layer as shown on Figure 5.1, (left).

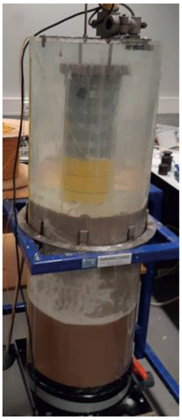

Figure 5.1: Left: A picture of the laboratory setup. A transparent cylindrical tank was filled with the following layers: sand at the bottom, a bentonite suspension, and water. Right: A picture of the mixer used to homogenize the bentonite suspension.

In this way, the acquisition scheme imitates vertical seismic profiling (VSP). It allows having a dense array of receivers with a very short vertical spacing of 1 mm while permitting visual confirmation of the location of the suspension. As a source, a piezoelectric transducer with a center frequency of 200 kHz frequency was used in combination with a wave generator and an amplifier. The source sends pulses with a center frequency of 40 kHz. Synthetic bentonite suspension displays thixotropic behaviour along with high values of shear stresses and yield stresses even at low concentrations [22, 23]. We use this type of suspension in our experiments because the shear strength increases over a short period, while other parameters, such as density, remain constant. We create this bentonite suspension by partly filling up a separate column with a mixture of bentonite and water. After a failed attempt to create a homogenous mixture with a hand drill, which broke down and had to be thrown away, we used a powerful mixer to create a homogenous bentonite suspension (Figure 1, right). After the suspension becomes homogenous, we measure the density and the shear strength of the suspension; we then put the suspension in our measuring tank and use water to fill up the measuring tank completely. We then let the shear strength build-up for three days and measure the density and the shear strength once a day. This allows us to track the rheological changes and relate these changes to the difference in signal attenuation from our DAS recordings. We perform DAS recordings with a duration of 0.1 s using a Silixa iDAS v2 interrogator, during which we send ten source pulses. The measurements from the individual pulses are summed together to obtain a final signal with an increased SNR.

5.1.3. The Field Experiment

For our field measurements, we use a similar approach as with our laboratory setup. We again tightly coil a fibre, but this time around a steel mantle. We use 750 m of fibre to cover 1 m in height of the steel mantle, as shown in Figure 5.2 This mantel

Figure 5.2: The measurement setup used for a field test in the Botlek, Rotterdam, the Netherlands. Left: a picture of two steel mantels with a fibre optical cable partially wrapped around them to form a receiver array for the experiment. Right: One of the sensing mantels is lowered onto a massive steel pole for continuous monitoring.

is lowered onto a steel pole until it is completely submerged in mud. This allows us to record in the upper 1 m of (fluid) mud. Afterwards, the mantel is raised by 90 cm, such that the upper 66 cm is in water, and the bottom 34 cm is in mud. With this setup, we can measure with different coupling conditions, namely, in water, where our fibre can move to a certain extent, in fluid mud, where our fibre is more fixed in place, and in consolidated mud, where the fibre is almost completely fixed in place. Compared to the laboratory setup, we now use ambient noise instead of a controlled transient source, and we use a Febus A1 interrogator, instead of the Silixa iDAS v2 interrogator, to record for various days. A more detailed description of this setup can be found in Buisman et al. (submitted).

5.2. Results

5.2.1. Laboratory Experiments

The shear strength of the bentonite suspension is measured with a rotational rheometer equipped with a vane (controlled stress sweep test). As expected, the density remains constant at 1.036 kgl^{-1}. This agrees with the observations of our cylindrical tank, where we can visually confirm that the level of the bentonite suspension remains constant. From our initial experience, we expect that the changes in shear strength occur during the first 24 hours after mixing. Afterwards, little to no change is expected in shear strength. Again, this is confirmed by performing the third consistent stress sweep test that indicated the same shear strength. Although the density of our bentonite suspension differs only little from that of water, the shear strength of our bentonite suspension - 16-18 Pa – is only slightly different on the first day from the shear strength of a fluid-mud sample from the Port of Hamburg – 20.5–22.5 Pa [24]. The shear strength tripled in value to 48 Pa on the second day. This drastic increase in shear strength can be seen in our acoustic measurements in Figures 5.3 and 5.4. Our first DAS measurement is taken one hour after the column is filled with the bentonite suspension and water, allowing any suspended matter to settle. We observe in Figure 5.3 that the source signal is immediately attenuated once it reaches the bentonite suspension, indicated by the blue vertical line. On the other hand, 23 hours later, i.e., on the second day, the attenuation of the source signal in the bentonite is only slightly higher than that in the water. This can be observed in Figure 5.4, where we notice that the source signal easily reaches the bottom of our sensing fibre.

5.2.2. Field Experiment

With the field experiment, we face different layers with unknown shear strength. Furthermore, the coupling conditions differ, our medium is inhomogeneous; our source is unknown (noise), and the sediments in the Botlek contain organic matter. Nonetheless, we can assume that the shear strength increases with increasing depth because of consolidation processes. Therefore, we expect increasing amplitudes of the recorded signals with increasing depth. However, our laboratory experiments already showed that the signal attenuation could be substantial in the upper unconsolidated layer, which raises the question of how much signal will be left to reach the bottom of our sensing mantel. To visualize the acoustic energy, we transform the data from the time domain to the frequency domain using Welch's method [25]. This frequency-domain data thus shows the recorded frequencies at all the channels. Despite the possibility of high attenuation in the upper unconsolidated layer, our results in Figures 5 and 6 still agree with our expectations of having higher-amplitude data with depth due to the higher shear stresses in the lower frequency spectrum, i.e., < 60 Hz. On the other hand, Figure 7 shows higher amplitudes in water for the higher frequencies, i.e., > 100 Hz. However, the low frequencies shown in Figure 6, namely < 60 Hz, seem to be absent in water. Besides, when we look at a depth of 5.5 m in Figure 7, where we observe an anomaly. This anomaly is in water and does not occur at the same position in Figures 5 and 6 when

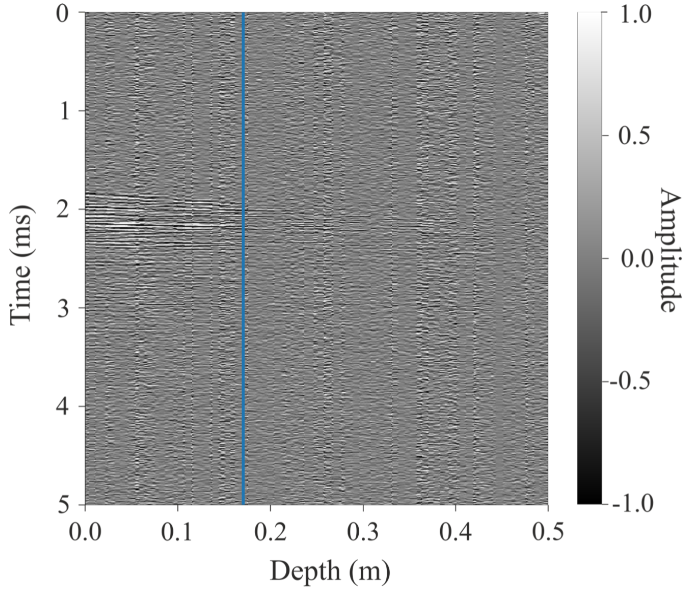

Figure 5.3: A common-source VSP gather recorded one hour after mixing the bentonite suspension. The gather is generated by stacking recordings from 10 separate source bursts. The source frequency is set at 40 kHz, the time sampling is 100 kHz. The blue line indicates the water-bentonite suspension boundary. A clear difference in acoustic attenuation is visible between the water layer and the bentonite suspension.

our sensing mantle was in the mud. This is related to repair works at this location. Unfortunately, our fibre broke due to unknown circumstances. After repairing the fibre with a fusion splice, we used some expensive high quality elastic tape covering about 4 m of fibre and, by doing so, unintentionally created a control experiment to see how the coupling condition affects the low-frequency content of our VSP data.

5.3. INTERPRETATION

5.3.1. LABORATORY EXPERIMENTS

We were limited by the maximum time sample of 100 kHz. Therefore, we are very close to the Nyquist criterion with our source center frequency of 40 kHz, making our data partly aliased. Nevertheless, our laboratory DAS data shows a tremendous difference in signal attenuation due to increased yield stress. In the laboratory, we can quantify this change in the shear strength and relate a change in amplitude predominantly to a change in signal attenuation. Additionally, the coupling condition improves over time in our laboratory experiment, leading to even higher amplitudes with a higher yield stress. It is most likely that the change in coupling conditions can be disregarded in our laboratory setup. The reason for this is that our source

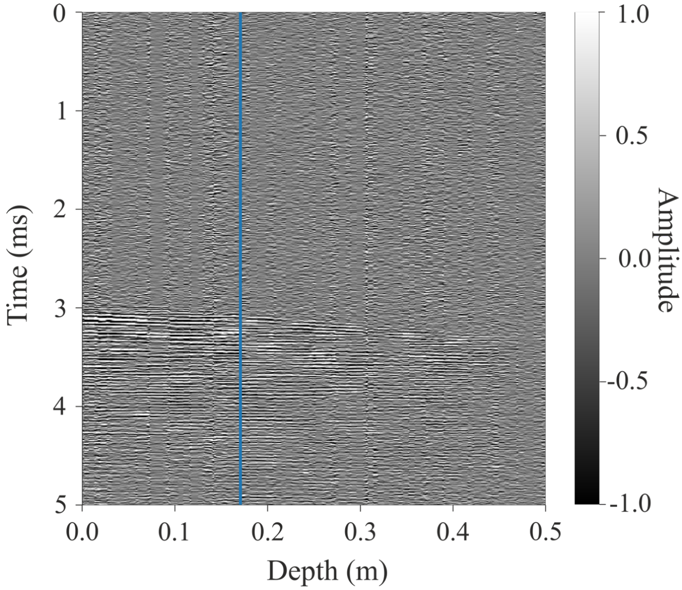

Figure 5.4: A common-source VSP gather recorded 24 hours after mixing the bentonite suspension. The gather is generated by stacking recordings from 10 separate source bursts. The source frequency is set at 40 kHz, the time sampling is 100 kHz. The blue line indicates the water-bentonite suspension boundary. The arrival time at depth 0 differs due to the absence of a trigger, which is why the signal starts at 3 ms in comparison with 1.9 ms for the recording presented in Figure 5.3.

signal was almost completely attenuated just after reaching the bentonite suspension on the first day. In this case, the difference in attenuation between water and bentonite suspension can predominantly be related to a difference in rheological properties since our coupling conditions in the bentonite suspension was equal, if not better, in comparison with the coupling conditions in the water. In contrast to our measurement on the first day, our source signal on the second day easily propagates through the whole column. This shows that the acoustic attenuation decreases dramatically with increased shear strength.

5.3.2. Field Experiment

Our field experiment shows similar results as our laboratory experiments for the lower frequency spectrum of < 60 Hz. Since we use ambient noise sources, a similar setup as our field experiment could be used for continuous measurements, given that there is traffic nearby. Unlike our laboratory experiment, the signal from ambient sources propagates (almost) horizontally because our depth ranges from 5 to 6.7 m, and our noise source can be as far as 1 km away. Because the signal from propellers propagates close to horizontal, it is plausible that both guided waves

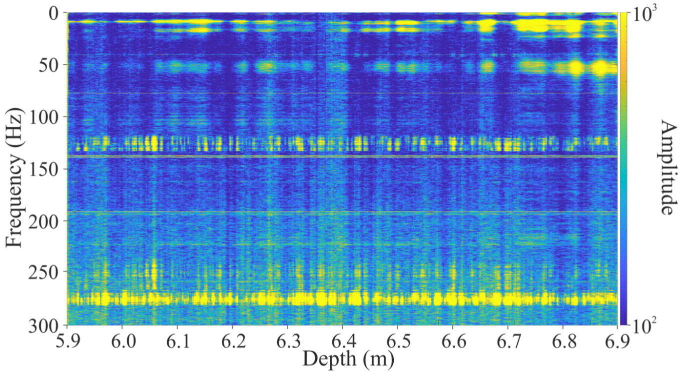

Figure 5.5: Power spectral density calculated from data acquired in the field experiment in Botlek, Rotterdam, the Netherlands. An increase in the amplitude of the spectral values can be noticed with an increase of the depth for the frequency range < 60 Hz. Furthermore, there are faint signals around 108 Hz at the depth interval from 5.9 m to 6.35 m. Unlike the lower frequencies, these signals do not increase in amplitude with depth. Additionally, machine noise can be observed around 130 Hz and 270 Hz.

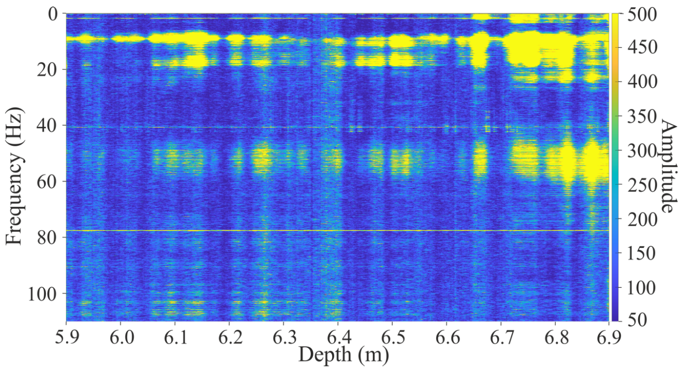

Figure 5.6: A zoom-in of Figure 5.5 to show the difference in amplitude increase with depth for frequencies < 60 Hz and in amplitude decrease for frequencies > 100 Hz.

and surface-waves, such as Scholte waves, propagate through the mud layers, which could explain why we observe an increase in amplitude in the deeper section.

Another plausible reason is the difference in the coupling condition of our fibre. The importance of coupling is validated by the section covered in tape. This section appears as an anomaly in the low-frequency content of the VSP data. The improved coupling conditions due to the tape are clearly visible in the lower

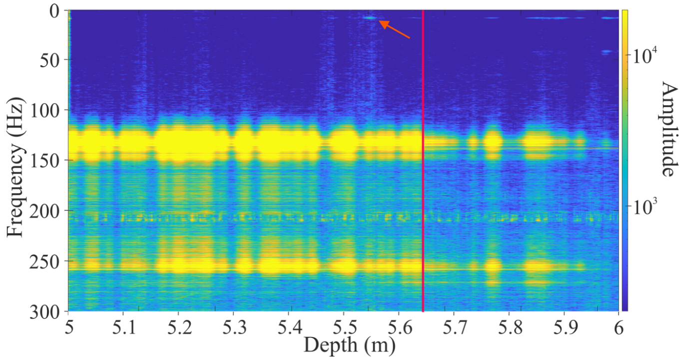

Figure 5.7: Power spectral density calculated for the field-experiment data from Botlek, Rotterdam, after the sensing mantel was raised by 90 cm. The red line indicates the water-mud interface, and the red arrow shows the anomaly caused by improved coupling obtained by the tape wrapped around this depth section. It can be noticed that in water there are mainly frequencies ranging from 110 Hz till 260 Hz. Low frequencies start to occur at a measuring depth of about 5.75 m.

frequency spectrum yet seems to have little to no effect in the higher frequency content. A possible explanation for the difference in coupling conditions in the lower frequencies could be because the fibre might be moved by low-frequency vibrations when poorly coupled; such is the case in the water. Poor coupling conditions can cause the fibre to displace rather than be elongated and compressed, and our interrogator cannot measure this displacement. When the fibre is fixed in consolidated mud, the coupling conditions improve, and thus the fibre is less likely to be displaced. The exact effect of the coupling conditions on the frequency content is still unclear. Nevertheless, what is interesting to note is that the frequency content increases in the lower frequency spectrum < 60 Hz but decreases in the high frequencies > 100 Hz. The difference in signal attenuation could potentially be used to estimate shear stresses and distinguish between water and mud.
Furthermore, the lower frequencies could indicate surface waves, commonly used to perform a surface wave inversion for estimation of the S-waves velocities.

5.3.3. Conclusion

We have shown that DAS can estimate the shear strength of non-Newtonian fluids. Our laboratory results show vastly different results in terms of attenuation caused by a change of shear strength in the bentonite suspension. Additionally, we show that DAS can be used in the field for estimating the shear strength of fluids using ambient noise. Our field results also show the complexity of using ambient noise to estimate shear strength. Although there is a clear difference in both the frequency content and amplitudes between water and (fluid) mud, and while this difference can likely be used to estimate shear strength to measure both the location of the water-mud interface, as well as estimating the shear parameters of fluid mud, the very nature of what causes this difference is still unknown. The results clearly show that the low frequencies < 60 Hz increase in amplitude when the fibre is tightly coupled to the surrounding medium, as is the case for consolidated mud. The increase in low frequencies due to an improvement of coupling is validated by the part taped to the sensing mantle, improving the coupling conditions of the fibre mantle.

For higher frequencies > 100 Hz, the reverse trend can be observed. While coupling conditions do improve when the fibre is embedded in mud, the higher frequencies are likely attenuated to such an extent that these frequencies dissipate in mud and thus are not measured.

REFERENCES

[1] M. Buisman, E. Martuganova, D. Draganov, and A. Kirichek. "Monitoring shear-stress changes using seismic measurements from controlled sources and ambient noise and optical fibres". In: *Proceedings to WODCON XXIII* (2022).

[2] W. H. McAnally, A. Teeter, D. Schoellhamer, C. Friedrichs, D. Hamilton, E. Hayter, P. Shrestha, H. Rodriguez, A. Sheremet, R. Kirby, *et al.* "Management of fluid mud in estuaries, bays, and lakes. II: Measurement, modeling, and management". In: *Journal of Hydraulic Engineering* 133.1 (2007), pp. 23–38.

[3] A. Kirichek, C. Chassagne, H. Winterwerp, and T. Vellinga. "How navigable are fluid mud layers?" In: *Terra et Aqua* (Aug. 2018), pp. 6–18.

[4] A. Shakeel, A. Kirichek, and C. Chassagne. "Is density enough to predict the rheology of natural sediments?" In: *Geo-Marine Letters* 39 (2019), pp. 427–434.

[5] C. Chassagne and Z. Safar. "Modelling flocculation: Towards an integration in large-scale sediment transport models". In: *Marine Geology* 430 (2020), p. 106361. DOI: https://doi.org/10.1016/j.margeo.2020.106361.

[6] W. H. McAnally, R. Kirby, S. H. Hodge, T. L. Welp, N. Greiser, P. Shrestha, D. McGowan, and P. Turnipseed. "Nautical depth for US navigable waterways: A review". In: *Journal of Waterway, Port, Coastal, and Ocean Engineering* 142.2 (2016), p. 04015014.

[7] X. Ma, A. Kirichek, A. Shakeel, K. Heller, and D. Draganov. "Laboratory seismic measurements for layer-specific description of fluid mud and for linking seismic velocities to rheological properties". In: *The Journal of the Acoustical Society of America* 149.6 (2021), pp. 3862–3877. DOI: https://doi.org/10.1121/10.0005039.

[8] I. Fadel, A. Kirchek, M. Buisman, K. Heller, and D. Draganov. "Monitoring Settling and Consolidation of Fluid Mud in a Laboratory Using Ultrasonic Measurements". In: *82nd EAGE Conference and Exhibition* (Amsterdam, The Netherlands). Expanded Abstracts. European Association of Geoscientists & Engineers, 2021, pp. 1–5. DOI: https://doi.org/10.3997/2214-4609.202120168.

[9] M. Buisman. "Seismic analysis of fluid mud". MA thesis. Delft University of Technology, 2019. URL: http://resolver.tudelft.nl/uuid:1c2af380-8dd4-4321-9f78-e5cb66def6d2.

[10] M. Buisman, E. Martuganova, T. Kiers, D. Draganov, and A. Kirichek. "Continuous monitoring of the depth of the water-mud interface using distributed acoustic sensing". In: *Journal of Soils and Sediments* 22.11 (2022), pp. 2893–2899.

[11] N. Lindsey, H. Rademacher, and J. Ajo-Franklin. “On the Broadband Instrument Response of Fiber-Optic DAS Arrays”. In: *Journal of Geophysical Research: Solid Earth* 125.2 (2020), e2019JB018145. DOI: https://doi.org/10.1029/2019JB018145.

[12] N. Lindsey, E. Martin, D. Dreger, B. Freifeld, S. Cole, S. James, B. Biondi, and J. Ajo-Franklin. “Fiber-optic network observations of earthquake wavefields: Fiber-optic earthquake observations”. In: *Geophysical Research Letters* 44.23 (Nov. 2017), pp. 11, 792–11, 799. DOI: https://doi.org/10.1002/2017GL075722.

[13] P. Jousset, T. Reinsch, T. Ryberg, H. Blanck, A. Clarke, R. Aghayev, G. P. Hersir, J. Henninges, M. Weber, and C. M. Krawczyk. “Dynamic strain determination using fibre-optic cables allows imaging of seismological and structural features”. In: *Nature Communications* 9.1 (2018), p. 2509. ISSN: 2041-1723. DOI: https://doi.org/10.1038/s41467-018-04860-y.

[14] J. B. Ajo-Franklin, S. Dou, N. J. Lindsey, I. Monga, C. Tracy, M. Robertson, V. Rodriguez Tribaldos, C. Ulrich, B. Freifeld, T. Daley, and X. Li. “Distributed Acoustic Sensing Using Dark Fiber for Near-Surface Characterization and Broadband Seismic Event Detection”. In: *Scientific Reports* 9.1 (2019), p. 1328. ISSN: 2045-2322. DOI: https://doi.org/10.1038/s41598-018-36675-8.

[15] T. Daley, D. Miller, K. Dodds, P. Cook, and B. Freifeld. “Field testing of modular borehole monitoring with simultaneous distributed acoustic sensing and geophone vertical seismic profiles at Citronelle, Alabama”. In: *Geophysical Prospecting* 64.5 (2016), pp. 1318–1334. DOI: https://doi.org/10.1111/1365-2478.12324.

[16] E. Martuganova, M. Stiller, K. Bauer, J. Henninges, and C. M. Krawczyk. “Cable reverberations during wireline distributed acoustic sensing measurements: their nature and methods for elimination”. In: *Geophysical Prospecting* 69.5 (2021), pp. 1034–1054. DOI: https://doi.org/10.1111/1365-2478.13090.

[17] A. Mateeva, J. Lopez, H. Potters, J. Mestayer, B. Cox, D. Kiyashchenko, P. Wills, S. Grandi, K. Hornman, B. Kuvshinov, W. Berlang, Z. Yang, and R. Detomo. “Distributed acoustic sensing for reservoir monitoring with vertical seismic profiling”. In: *Geophysical Prospecting* 62.4 (2014), pp. 679–692. DOI: https://doi.org/10.1111/1365-2478.12116.

[18] G. Yu, Z. Cai, Y. Chen, X. Wang, Q. Zhang, Y. Li, Y. Wang, C. Liu, B. Zhao, and J. Greer. “Walkaway VSP using multimode optical fibers in a hybrid wireline”. In: *The Leading Edge* 35 (July 2016), pp. 615–619. DOI: https://doi.org/10.1190/tle35070615.1.

[19] F. Cheng, B. Chi, N. J. Lindsey, T. C. Dawe, and J. B. Ajo-Franklin. “Utilizing distributed acoustic sensing and ocean bottom fiber optic cables for submarine structural characterization”. In: *Scientific Reports* 11.1 (2021), pp. 1–14.

[20] O. H. Waagaard, E. Rønnekleiv, A. Haukanes, F. Stabo-Eeg, D. Thingbø, S. Forbord, S. E. Aasen, and J. K. Brenne. “Real-time low noise distributed acoustic sensing in 171 km low loss fiber”. In: *OSA Continuum* 4.2 (Feb. 2021), pp. 688–701. DOI: https://doi.org/10.1364/OSAC.408761.

[21] I. Lior, A. Sladen, D. Rivet, J. P. Ampuero, Y. Hello, C. Becerril, H. F. Martins, P. Lamare, C. Jestin, and S. Tsagkli. "On the detection capabilities of underwater distributed acoustic sensing". In: *Journal of Geophysical Research: Solid Earth* 126.3 (2021), e2020JB020925.

[22] S. Abend and G. Lagaly. "Sol–gel transitions of sodium montmorillonite dispersions". In: *Applied Clay Science* 16.3 (2000), pp. 201–227. DOI: https://doi.org/10.1016/S0169-1317(99)00040-X.

[23] R. Goh, Y.-K. Leong, and B. Lehane. "Bentonite slurries—zeta potential, yield stress, adsorbed additive and time-dependent behaviour". In: *Rheologica Acta* 50.1 (2011), pp. 29–38.

[24] A. Shakeel, A. Kirichek, and C. Chassagne. "Rheological analysis of mud from Port of Hamburg, Germany". In: *Journal of Soils and Sediments* 20.6 (2020), pp. 2553–2562. DOI: 10.1007/s11368-019-02448-7.

[25] P. Welch. "The use of fast Fourier transform for the estimation of power spectra: A method based on time averaging over short, modified periodograms". In: *IEEE Transactions on Audio and Electroacoustics* 15.2 (1967), pp. 70–73. DOI: 10.1109/TAU.1967.1161901.

6

HORIZONTAL FIBRES

Previous chapters have shown how attenuation can be used in a vertical setup to estimate the water-mud interface. This chapter shows how a vertical setup can be extended to a horizontal setup, mimicking a more realistic setup to be used in ports. Here five horizontal fibre segments are created at different heights between two poles to continuously record along the complete installation. Analysing these continuous recordings, it is shown the spectrum of the horizontal fibre segments can be used to monitor the water-mud interface depth with a vertical resolution around six mm. Multiple passive sources, like vessel movements and water currents, are recorded to estimate the water-mud interface.

Parts of this chapter is published in Journal of Applied Geophysics [1].

6.1. Introduction

Ports and waterways with high siltation rates require frequent surveying to ensure the fibre. In seaports with a low energetic environment, sedimentation frequently comes as large quantities of fine sediments, creating thin layers of a highly aqueous suspension known as fluid mud. The density of fluid mud is frequently used by port authorities worldwide for the nautical criterion [2, 3]. At the same time, fluid mud makes the depth measurements ambiguous since its density gradually increases from water, being 1 kg/l, to consolidated mud, with 1.3 kg/l. Furthermore, the relation between shear stresses and density in mud is non-linear [2], which is why different port authorities in various places defined their nautical bottom criterion based on local sediment characteristics and hydrodynamics [3]. Currently, surveying techniques mainly rely on acoustic methods [4] in the form of dual- or multi-frequency echo sounders. Echo sounders operate as both a source and receiver, measuring the two-way travel time from the source to the bottom and back to the receiver. An accurate velocity model is then used to convert the two-way travel time to depth [4]. However, at specific locations with a mixture of sea and river water, such as estuaries, obtaining an accurate velocity profile is most challenging because of different P-wave velocities in the water column, leading to time-consuming calibration work and a higher inaccuracy.

Additionally, the results of these echos-sounders are frequently inaccurate due to the dim reflection(s) related to the small acoustic-impedance contrast between water and fluid mud since fluid mud can have a gradual increase in density, while settling and consolidating, and a P-wave velocity approximately 3% - 9% higher than that of water [5]. These surveying techniques have low repeatability and are restricted by the availability of a surveying vessel and quay wall access. Especially at the financially crucial quay walls, availability for surveying is severely constrained due to the high costs of halting activities for a surveying vessel. Finally, substantial changes in the fibre can often occur after storms, implying that extensive, time-consuming surveys are required again to ensure the safe navigability of vessels. These surveys are time-consuming due to the large surveying area and the variation in water temperature, salinity, and (fluid) mud rheology. Because of these variations, even over small distances, re-calibration is often required to acquire a velocity profile for zero-offset measurements, such as echo sounders [3, 6, 7].

New surveying techniques are required to tackle the limited temporal resolution and measurement accuracy. [8] showed that DAS can be combined with an active source in a laboratory setup to measure the water-mud interface. [9] showed that ships can be detected using DAS. We combine both [8] and [9], and use DAS for fibre monitoring in a navigational river channel. We conduct a field study in the Port of Rotterdam and demonstrate how passive noise sources like ships can be used to monitor the fibre with optical cables in a horizontal orientation.

6.1.1. Distributed Acoustic Sensing

DAS measures the dynamic strain or strain-rate of optical fibres. Optical fibres offer many advantages over conventional electrical sensors, such as electric isolation and immunity to electromagnetic interference, and they are non-conductive and non-corrosive, making them well-suited for utilisation in liquids [10–12] and saline environments. Strain or strain-rate can be measured by the changes in photon path length of Rayleigh-backscattered light emitted by a laser source from the same interrogator and measured by a receiver in an interrogator [13]. However, the backscattered signal's phase change has a highly non-linear transfer function causing an ambiguity or an inability to precisely locate the source of the acoustic disturbance, making it unsuitable for seismic applications. Because the phase change is highly non-linear, the phase difference between two points is used instead, referred to as the gauge length [14]. Even though the phase difference is averaged over the gauge length, the location of a disturbance along the fibre and waveforms are well preserved. Because of this, DAS measurements have been successfully used in various fields of research, for example, teleseismic earthquake monitoring [15, 16], vertical seismic profile [17–19], and earthquake phase identification [20].

Conventional commercially available instruments use a short-pulse generated by a coherent laser into the fibre [13]. With such a setup, the pulse width limits the spatial resolution. Another drawback of short-pulse systems is the susceptibility to optical non-linearities, such as self-phase modulation and modulation instabilities, which further limits the interrogation-energy output of the laser per pulse and thus limits the backscattered signal [21]. To monitor large seaports, implying monitoring over large distances with a high spatial resolution, thus poses a problem for short-pulse systems. This is why we selected a system that combines coherent detection with linear frequency modulation. In such a system, the linear frequency-modulated signal is then compressed using chirp compression techniques, known from radar applications [22], into a short-pulse. By doing so, the interrogator can launch much more energy into the fibre [23], allowing it to interrogate much longer distances [24].

6.1.2. FIELD SETUP

The field setup is situated in the Botlek, located in the Port of Rotterdam, The Netherlands. The setup consists of two 24-m-long steel poles designed to hold a mantel containing the sensing fibre, as shown in Figure 6.1. Due to a sharply varying bathymetry, the steel poles were driven in at different depths. One pole was driven at a point with an approximate water depth of 5.7 m, the other - 3.2 m, resulting in lengths exposed to the air of approximately 3 m and 2.4 m, respectively. The distance between the two poles is 38 m.

The mantels are 2.4 m in height and 0.37 m in diameter. Both mantels are coiled with a standard single-mode direct-burial communication fibre with a length of 317 m that covers 1.6 m of a mantle in height, and is connected via a lead fibre of 106 m. As can be seen in Figure 6.1 b, rings are welded on the mantel. These rings are used to create horizontal lines. There are five horizontal lines, starting from the very bottom of a mantel at fibre length 423 m (106 m lead fibre + 317 coiled on the mantel), then moving up 30 cm twice, then 60 cm, and finally 40 cm, with the final position located on the top of the VSP. The mantels are carefully lowered to prevent the connecting fibre from breaking during installation. A sketch of the setup can be seen in Figure 6.1 c.

An ASN OptoDAS interrogator [24] is used for data acquisition; it converts the fibre into an array of seismic sensors. We use a gauge length, the averaged fibre length for a recording, of 3 m and a channel spacing of 1 m. The 3-m gauge length was chosen because our initial objective was to record surface waves with a short wavelength [25].

The OptoDAS interrogator is stored in a shipping container 70 m from the pole setup. We record continuously for 5.7 consecutive days using a 62.5 kHz time sampling, which then is temporally decimated 62 times to reduce data volume.

Finally, a diving inspection is performed to visually validate the locations of the horizontal parts of the fibre.

6.2. Water-depth estimations based on frequency content

The water-mud interface depth varies in this area because of sedimentation and dredging in the vicinity. Measurement of the depth at a point is thus not representative of the area. Measurement along a line would be much more representative, especially in an area subjected to fluid mud, characterized by its small shear strength. We will show that the wave propagation along a line can be very effectively monitored with high resolution using DAS measurements. One parameter of the propagating waves that can be very useful for monitoring purposes is their amplitude or energy. The energy is influenced by the specific energy loss when propagating through a specific material. We expect a sharp transition in acoustic attenuation due to the muting of cable reverberations by mud [8], as if it were a vibrating guitar string that gets muted by touching the string.

Figure 6.2 a shows a PSD plot of channel 610, located on the fifth line, which is completely suspended in water, on meter 27 from the first pole to the second pole. This figure is calculated using Welch's method [26], and shows that DAS can measure noise from passing vessels with a horizontal fibre. During the recording in Figure 6.2 a, one ship passed, which can be observed from 300 - 800 s. Clear constructive and destructive interference patterns in the shape of hyperbolas with high amplitudes are observable as the ship passes. Interestingly enough, when we compare the same recording of horizontal channels 530 and 450, which are pressed against the mud and buried in the mud, respectively, at the same horizontal distance, we can observe similar patterns, though with significantly lower amplitudes, as shown in Figure 6.2 b and c, respectively. This difference in amplitude is further validated when we combine all channels and plot the PSD for the duration of a passing vessel, as shown in Figure 6.2 d. In this figure, the start and the end of the five horizontal fibres are indicated by the yellow lines, with the lowest horizontal fibre starting at 423 m and each line consisting of 40 m of fibre, of which 38 m are between the pole, and 2 m are wrapped on the pole. In Figure 6.2 d, constructive interference patterns are in the shape of hyperbolas, for example at a fibre length of 500 m. Since the fibre goes from pole one to pole two, then from pole two to pole one, and so on, mirrored frequency patterns can be expected going from an odd to an even-numbered line. This mirroring effect is especially visible at the end of line two and the beginning of line three. The horizontal lines four and five exhibit interference patterns along their

complete lengths, whereas lines one, two and three exhibit both high amplitude constructive interference patterns and low-amplitude zones.
A dive inspection was contracted to inspect the geometry of the lines with special interest for the locations with the low-amplitude zones. The recordings made with this dive inspection revealed that line one is buried in mud at the location of these low-amplitude zones, and lines two and three are pressed against consolidated mud at the low-amplitude zones, as shown in Figure 6.1 c and in Figure 6.1 d. Furthermore, a similar pattern can be observed once we look at lower frequencies likely related to flow and wind waves. Figure 6.2 e shows similar high amplitude zones like Figure 6.2 d, but at much lower frequencies (0 - 6 Hz). In addition, amplitudes around 460 m of fibre length can be observed in this lower-frequency spectrum which is absent for the higher frequencies. The dive inspection revealed that the very end of the mantel is in water because it is installed on top of armour rock, which means that the very end of unevenly numbered lines one and three and the beginning of line two are exposed to water for the first two meters. Intuitively, if the fibre is exposed to water, it will vibrate, and we can measure these reverberations. However, because the cable reverberations for higher frequencies are likely the result of constructive and destructive interference paths in our fibre, and the length from pole two towards the sediments is only two meters, constructive and destructive interference patterns can be formed in this short section.
Finally, when we look over five days at ultra-low frequencies, < 0.03 Hz, we observe very sharp boundaries between high- and low-amplitude zones. Figure 6.2 f also exhibits low amplitudes where the fibre is touching or buried in mud, implying that these frequencies are only dominant in water. A reason for this might be due to a temperature difference, making the fibre contract and elongate. This is, however, unlikely because when the fibre is lying on top of the mud, such as for lines two and three, the temperature difference should be (very) similar to that of fibre lines four and five, which are entirely suspended in water, since both are exposed to (almost) the same medium. Furthermore, no temperature change should occur in a period of 50 s.
When we compare lines four and five, we observe high-amplitudes along the complete lines, yet we can separate two zones. The first zone is 20 m near pole one; the second zone is 20 m near pole two. This difference in amplitudes indicates that a possible source for these ultra-low frequencies is either pole swaying caused by wind and currents or seafloor compliance. Because the poles are driven into the subsurface at different locations and depths, they are likely to sway differently with different amplitudes.

6.3. DATA INTERPRETATION AND APPLICATION

The attenuation of various signals by mud gives an exceptional horizontal resolution equal to the fibre's (partial) width. Given that optical cables' widths are often no more than 1 cm, in our case 6 mm, combined with the strong attenuation of signals when the fibre is only pressed against mud, the achievable vertical resolution is in the order of mm. In practice, the vertical resolution will be lower since knowing the fibre's exact location is difficult due to, for instance, cable slacking. Nevertheless, the resolution will be high; we expect an order of 5 cm, based the cable slacking with our setup, revealed by gently pulling the horizontal fibre segments during the dive inspection. The horizontal resolution is much lower. The channel spacing of 1 m combined with the gauge length of 3 m limits the obtainable horizontal resolution. We detected the 2 m suspended fibre between the second pole and the mud anomaly, as shown in mud Figure 6.1c, giving us a minimum horizontal resolution of 2 m. For monitoring the fibre in ports and waterways, the horizontal resolution is, however, far less important than the vertical resolution since sedimentation near quay walls is gradual and lateral changes are seldom shorter than 3 m due to the liquid nature of fluid mud and gradual sedimentation of fine sediments.

Considering that the poles on which the fibres are installed likely act as a resonator is crucial. When we sum the values along the frequencies axes for each of the lines in Figures 6.2 d:f, but 0 - 100 Hz of Figure 6.2 d, we obtain Figures 6.2 g:i, respectively. In these figures, the resonating effect of the poles is visible by the amplitude drop after 19 m. It shows that the deeper pole (at 0 m horizontal distance) has more prominent resonances than the shallower pole (at 40 m distance). The stacked amplitudes for lines four and five are especially interesting since these lines are entirely suspended in water. Line four shows a clear amplitude drop that can only be related to the pole vibrations since it is completely suspended in water. Line five shows more consistent low amplitudes along the complete line and a smaller amplitude drop, likely due to more cable slacking. Lines one, two, and three exhibit a drop after 20 m to a much lower level than line four. Lines four and five also show a clear drop, but the values of these lines remain higher than the lines touching the mud.

Another way to visualise the difference in frequency content is by subtracting the result in Figure 6.2 a from that in Figure 6.2 c and visa versa. This way, we obtain the difference panels in Figures 6.3 a and b, respectively. These figures show that higher frequencies are predominately present in the water, and lower frequencies are predominately present in the mud. A noticeable exception is the frequency of 2.7 Hz, which is related to the resonance of the pole by the wind. This frequency changes with time due to a difference in exposure length of the poles caused by the tidal fluctuations, as shown in Buisman et al., (submitted). This energy propagates down the pole and is muted by mud.

Our DAS measurements along horizontal lines show the potential of monitoring the fibre using noise sources. The difference in amplitude zones related to a horizontal fibre being suspended in water, touching or buried in mud, is clearly visible in different frequency ranges. A similar setup could be used in waterways with traffic that generates propeller noise to monitor the fibre remotely and continuously. The large difference in amplitudes from noise sources could be used to pick the water-mud interface. The results of this research could be up-scaled for a more elaborate experiment, including a network of horizontal fibres. Based on the recorded signals from passing vessels, water flow, and likely pole swaying or seafloor compliance, a horizontal fibre could be efficiently utilised to monitor the fibre using

a similar attenuation approach, allowing for a broad coverage without interfering with traffic, as a surveying vessel would.
Figure 6.4 shows a possible monitoring DAS setup. In this figure, two lines are installed at different heights, with the lower line buried in mud and the shallower line suspended in water. The interrogator onshore measures small amplitudes for the line in mud and large amplitudes for the line suspended in water. This information is then passed on to the water body authorities via an internet connection. This way, the authorities can map the bathymetry even while a boat is occupying the quay wall and plan to dredge and halt activities for vessels requiring a depth of line C. Alternatively, the port authorities could still allow vessels requiring a depth level of line B without sending a surveying vessel. With this information, quay wall occupation can be improved, (surveying) vessel movements can be reduced, and dredging strategies can be further optimised.
A design of this nature could utilize one or multiple passive sources, contingent upon the volume of traffic for signals > 50 Hz, the presence or absence of flow for signals within the range of 0.5 Hz to 5.5 Hz, and the proximity to a seashore for signals < 0.025 Hz. It is important to note that frequencies might vary at distinct depths or among different structures due to varying interference patterns and resonating frequencies.
In an advanced phase, a PSD could be developed, integrating machine learning for automated signal processing, converting the frequency spectrum into fibre charts.
Additionally, it is important to acknowledge that temporal resolution varies across passive sources. Vessel noise requires the shortest time window, typically a few minutes, whereas pole swaying or seafloor compliance demands the longest, spanning days. This temporal resolution should align with the dynamic environment of the installation. However, for all passive sources, our time window was considerably shorter than the revisiting time of a surveying vessel, typically in the order of two to three weeks (as per internal discussions).

6.4. CONCLUSIONS

Our distributed acoustic sensing (DAS) results showed the potential of using measurements along horizontal fibres for high temporal resolution water-depth monitoring. We showed that this is achieved by using the difference in frequency and amplitude content of signals from noise sources like passing ships and currents in water and mud. The frequency patterns created by passing vessels, > 100 Hz, were clearly visible in a fibre suspended in water and exhibited clear constructive interference patterns. These same patterns were also observed when the fibre was pressed against or buried in mud, yet with much lower amplitudes due to the muting of cable reverberations by mud. In addition, low frequencies, 1 Hz - 5 Hz, showed a similar amplitude spectrum as the higher frequencies from passing vessels. Wind and flow are likely the sources of the lower frequencies, which are notably more pronounced in the fibre suspended in water compared to the fibre placed on or in mud. Furthermore, our findings indicate that the most distinct boundaries between water and mud manifest at ultra-low frequencies, plausibly originating from pole swaying or seafloor compliance. These pronounced transitions can be attributed to the extended recording period of 5.7 days. In contrast, vessel noise, with a recording duration as short as 15 minutes, exhibits more gradual transitions. This discrepancy in resolution underscores the inherent trade-off between temporal and spatial resolution.

The advantage of our DAS method over conventional methods is that our method can be used continuously and remotely, given that there is a current, or traffic nearby. The horizontal resolution up to a few mm far outperforms other acoustic/seismic depth monitoring methods. Due to the low cost of optical fibres and the far-reaching dynamic range of interrogators, DAS could be a most attractive alternative for water-depth monitoring using propeller noise or natural currents in shallow marine environments such as ports and waterways. Monitoring the water-mud interface with DAS could resolve temporal resolution problems related to surveying vessel availability and quay wall accessibility at a low expense. With this new monitoring setup, the depth can be monitored without affecting traffic at quay walls. This allows for optimisation of occupancy, increased by reducing surveying vessel movement, and reduced CO2 emissions by optimising dredging strategies.

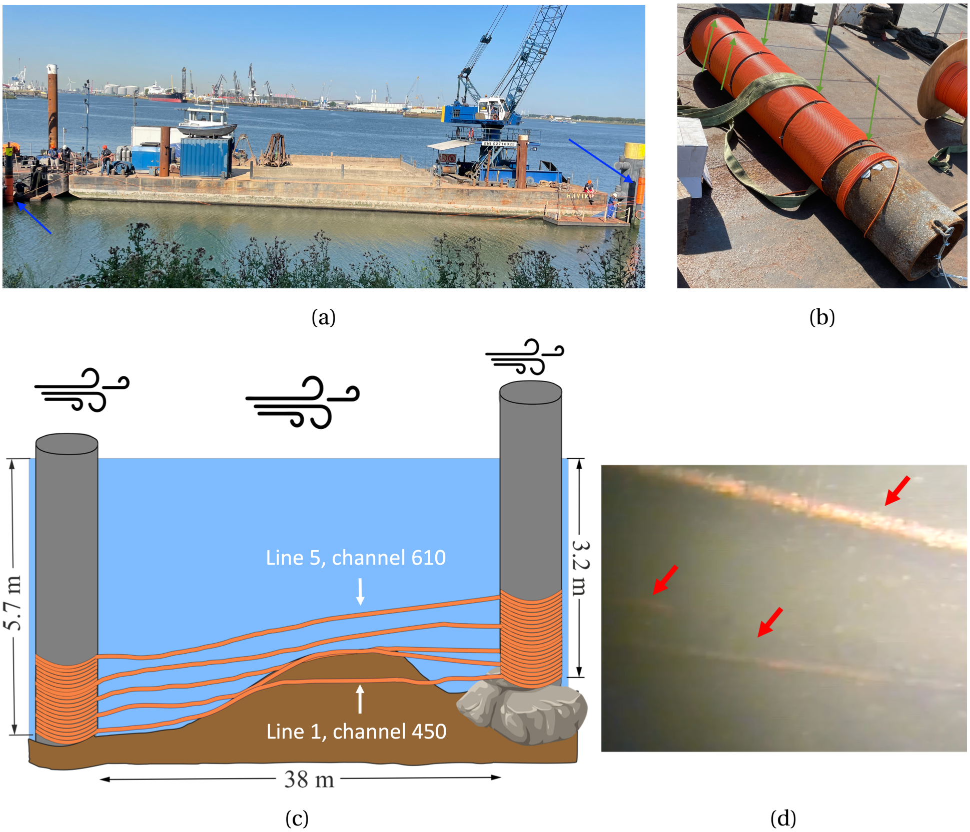

Figure 6.1: a): Two mantels with the direct-burial single-mode fibre being lowered onto the steel poles. The blue arrows show the location of the mantles. The platform was used for installation only. b): A photo of a mantel with the fibre. The exposed lines are where rings have been welded on, indicated by the green arrows, that are used to guide the fibre through. These rings are used to create horizontal lines at different heights that can be seen on a). Later, the horizontal lines are tightened to reduce cable slacking. c): Sketch of the fibre installation and bathymetry. d): Picture of the dive inspection where line one, the middle line on the left, enters the mud, and lines two and three are on top of the mud. The red arrows point towards the fibres.

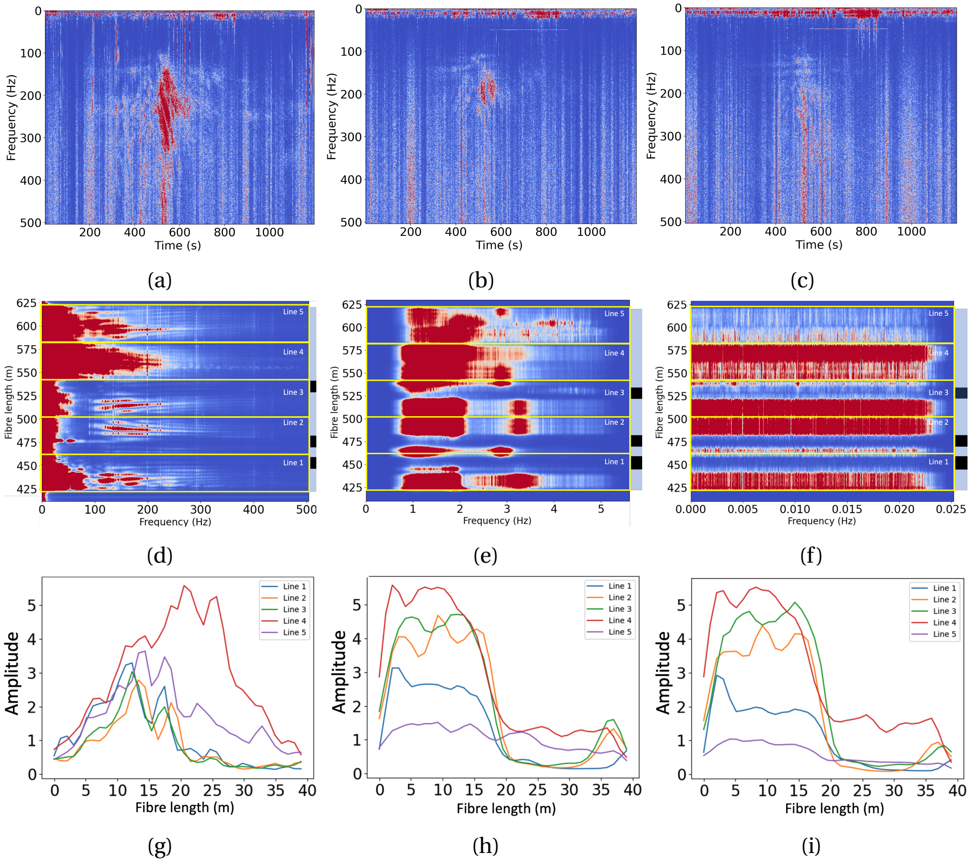

Figure 6.2: a): Spectrogram of channel 610, located in water on line 5, with a gauge length of 3 m. The exact location of channel 610 is shown in Figure 6.1 c. During this 20-minute-long recording, a ship passed between 300 - 800 s. Clear interference patterns can be observed in the shape of hyperbolas that have a mid-point at 500 s. b and c): Similar to a, but for channel 530, located on line 3, which is pressed against the mud, and for channel 450 located in mud, respectively. d): PSD of all five horizontal lines. Each yellow box represents one line, with the first line, denoted by the number "1", being the lowest line, and the fifth line being, denoted by the number "5", being nearest to the water surface. Each line consists of 38 m cable between the poles and 2 m on the poles. The water and mud locations are shown on the right of the PSD in blue and black, respectively. e and f): Like d, but for 0 - 6 Hz and 0 - 0.025 Hz, respectively. g:i) Stacked amplitudes of 100 Hz - 504 Hz, 0 - 6 Hz and 0 - 0.025 Hz, respectively, along all lines for each meter. The beginning and end of lines two and four have been flipped aligning them with lines one, three and five.

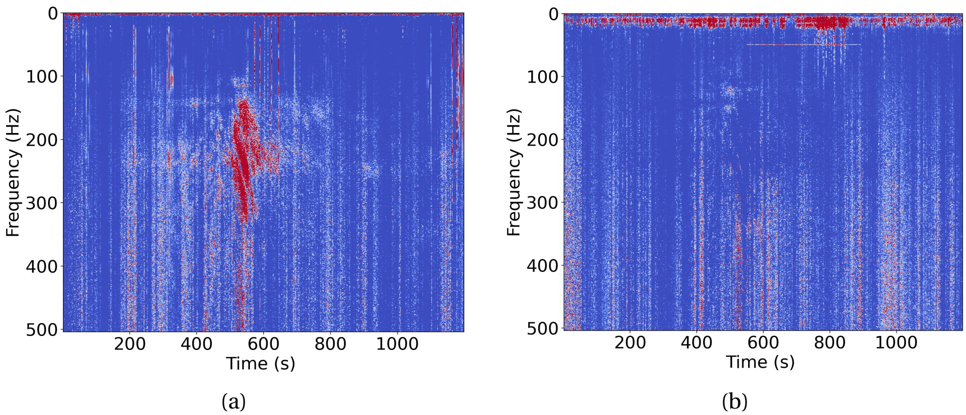

Figure 6.3: a): Frequency content of water, calculated by subtracting channel 450, buried in mud, from channel 610, located in water, and b) frequency content of mud, calculated by subtracting channel 610 from channel 450.

Figure 6.4: Potential setup for monitoring the water-mud interface. Here A is an observation station with a DAS interrogator onshore, B is the line suspended in water in this particular situation, and C is a line in (fluid) mud.

REFERENCES

[1] M. Buisman, D. Draganov, and A. Kirichek. “Near real-time nautical depth mapping via horizontal optical fibers and distributed acoustic sensing”. In: *Journal of Applied Geophysics* (2024), p. 105377.

[2] W. H. McAnally, A. Teeter, D. Schoellhamer, C. Friedrichs, D. Hamilton, E. Hayter, P. Shrestha, H. Rodriguez, A. Sheremet, R. Kirby, *et al.* “Management of fluid mud in estuaries, bays, and lakes. II: Measurement, modeling, and management”. In: *Journal of Hydraulic Engineering* 133.1 (2007), pp. 23–38.

[3] A. Kirichek, C. Chassagne, H. Winterwerp, and T. Vellinga. “How navigable are fluid mud layers?” In: *Terra et Aqua* (Aug. 2018), pp. 6–18.

[4] W. H. McAnally, A. Teeter, D. Schoellhamer, C. Friedrichs, D. Hamilton, E. Hayter, P. Shrestha, H. Rodriguez, A. Sheremet, R. Kirby, *et al.* “Management of fluid mud in estuaries, bays, and lakes. II: Measurement, modeling, and management”. In: *Journal of Hydraulic Engineering* 133.1 (2007), pp. 23–38.

[5] X. Ma, A. Kirichek, K. Heller, and D. Draganov. “Estimating P-and S-Wave Velocities in Fluid Mud Using Seismic Interferometry”. In: *Frontiers in earth science* 10 (2022), p. 251.

[6] A. Shakeel, A. Kirichek, and C. Chassagne. “Is density enough to predict the rheology of natural sediments?” In: *Geo-Marine Letters* 39 (2019), pp. 427–434.

[7] A. Shakeel, A. Kirichek, and C. Chassagne. “Rheological analysis of mud from Port of Hamburg, Germany”. In: *Journal of Soils and Sediments* 20 (2020), pp. 2553–2562.

[8] M. Buisman, E. Martuganova, T. Kiers, D. Draganov, and A. Kirichek. “Continuous monitoring of the depth of the water-mud interface using distributed acoustic sensing”. In: *Journal of Soils and Sediments* 22.11 (2022), pp. 2893–2899.

[9] D. Rivet, B. de Cacqueray, A. Sladen, A. Roques, and G. Calbris. “Preliminary assessment of ship detection and trajectory evaluation using distributed acoustic sensing on an optical fiber telecom cable”. In: *The Journal of the Acoustical Society of America* 149.4 (2021), pp. 2615–2627.

[10] M. Shao, X. Qiao, X. Zhao, Y. Zhang, and H. Fu. “Liquid Level Sensor Using Fiber Bragg Grating Assisted by Multimode Fiber Core”. In: *IEEE Sensors Journal* 16.8 (2016), pp. 2374–2379. DOI: https://doi.org/10.1109/JSEN.2015.2513413.

[11] W. Xu, J. Wang, J. Zhao, C. Zhang, J. Shi, X. Yang, and J. Yao. "Reflective Liquid Level Sensor Based on Parallel Connection of Cascaded FBG and SNCS Structure". In: *IEEE Sensors Journal* 17.5 (2017), pp. 1347–1352. DOI: https://doi.org/10.1109/JSEN.2016.2629488.

[12] C. Yang, S. Chen, and G. Yang. "Fiber optical liquid level sensor under cryogenic environment". In: *Sensors and Actuators A: Physical* 94 (Oct. 2001), pp. 69–75. DOI: https://doi.org/10.1016/S0924-4247(01)00663-X.

[13] N. Lindsey, H. Rademacher, and J. Ajo-Franklin. "On the Broadband Instrument Response of Fiber-Optic DAS Arrays". In: *Journal of Geophysical Research: Solid Earth* 125.2 (2020), e2019JB018145. DOI: https://doi.org/10.1029/2019JB018145.

[14] A. Hartog, B. Frignet, D. Mackie, and M. Clark. "Vertical seismic optical profiling on wireline logging cable". In: *Geophysical Prospecting* 62.4-Vertical Seismic Profiling and Microseismicity Frontiers (2014), pp. 693–701.

[15] J. B. Ajo-Franklin, S. Dou, N. J. Lindsey, I. Monga, C. Tracy, M. Robertson, V. Rodriguez Tribaldos, C. Ulrich, B. Freifeld, T. Daley, and X. Li. "Distributed Acoustic Sensing Using Dark Fiber for Near-Surface Characterization and Broadband Seismic Event Detection". In: *Scientific Reports* 9.1 (2019), p. 1328. ISSN: 2045-2322. DOI: https://doi.org/10.1038/s41598-018-36675-8.

6

[16] P. Jousset, T. Reinsch, T. Ryberg, H. Blanck, A. Clarke, R. Aghayev, G. P. Hersir, J. Henninges, M. Weber, and C. M. Krawczyk. "Dynamic strain determination using fibre-optic cables allows imaging of seismological and structural features". In: *Nature Communications* 9.1 (2018), p. 2509. ISSN: 2041-1723. DOI: https://doi.org/10.1038/s41467-018-04860-y.

[17] T. Daley, D. Miller, K. Dodds, P. Cook, and B. Freifeld. "Field testing of modular borehole monitoring with simultaneous distributed acoustic sensing and geophone vertical seismic profiles at Citronelle, Alabama". In: *Geophysical Prospecting* 64.5 (2016), pp. 1318–1334. DOI: https://doi.org/10.1111/1365-2478.12324.

[18] E. Martuganova, M. Stiller, K. Bauer, J. Henninges, and C. M. Krawczyk. "Cable reverberations during wireline distributed acoustic sensing measurements: their nature and methods for elimination". In: *Geophysical Prospecting* 69.5 (2021), pp. 1034–1054. DOI: https://doi.org/10.1111/1365-2478.13090.

[19] A. Mateeva, J. Lopez, H. Potters, J. Mestayer, B. Cox, D. Kiyashchenko, P. Wills, S. Grandi, K. Hornman, B. Kuvshinov, W. Berlang, Z. Yang, and R. Detomo. "Distributed acoustic sensing for reservoir monitoring with vertical seismic profiling". In: *Geophysical Prospecting* 62.4 (2014), pp. 679–692. DOI: https://doi.org/10.1111/1365-2478.12116.

[20] N. Lindsey, E. Martin, D. Dreger, B. Freifeld, S. Cole, S. James, B. Biondi, and J. Ajo-Franklin. "Fiber-optic network observations of earthquake wavefields: Fiber-optic earthquake observations". In: *Geophysical Research Letters* 44.23 (Nov. 2017), pp. 11, 792–11, 799. DOI: https://doi.org/10.1002/2017GL075722.

[21] J. Toulouse. “Optical nonlinearities in fibers: review, recent examples, and systems applications”. In: *Journal of lightwave technology* 23.11 (2005), pp. 3625–3641.

[22] M. A. Richards. *Fundamentals of radar signal processing*. McGraw-Hill Education, 2014.

[23] S. Wang, X. Fan, Q. Liu, and Z. He. “Distributed fiber-optic vibration sensing based on phase extraction from time-gated digital OFDR”. In: *Optics Express* 23.26 (2015), pp. 33301–33309.

[24] O. H. Waagaard, E. Rønnekleiv, A. Haukanes, F. Stabo-Eeg, D. Thingbø, S. Forbord, S. E. Aasen, and J. K. Brenne. “Real-time low noise distributed acoustic sensing in 171 km low loss fiber”. In: *OSA Continuum* 4.2 (Feb. 2021), pp. 688–701. DOI: https://doi.org/10.1364/OSAC.408761.

[25] T. Dean, T. Cuny, and A. H. Hartog. “The effect of gauge length on axially incident P-waves measured using fibre optic distributed vibration sensing”. In: *Geophysical Prospecting* 65.1 (2017), pp. 184–193.

[26] P. Welch. “The use of fast Fourier transform for the estimation of power spectra: A method based on time averaging over short, modified periodograms”. In: *IEEE Transactions on Audio and Electroacoustics* 15.2 (1967), pp. 70–73. DOI: 10.1109/TAU.1967.1161901.

7

Vortex Induced Vibrations and Water Column Height

Water-flow and water-column height measurements play a critical role in various industries and sectors, ranging from environmental monitoring and resource management to industrial processes and infrastructure maintenance. Accurate and real-time measurement of water-flow is essential for ensuring the efficient use of water resources, early detection of potential issues such as leaks, erosion, or blockages, oceanography, and safeguarding the environment. Fiber optical cables have emerged as a promising technology for water-flow measurements due to their numerous advantages, including high sensitivity, immunity to electromagnetic interference, and the ability to cover long distances.
We show how vortex-induced vibrations, measured by using distributed acoustic sensing, can be used to measure the water-column height, and give information about the waterflow, by relating frequency oscillation and amplitude differences to tidal and flow measurements in a shallow marine setting.

Parts of this chapter have been published in the 84th EAGE Annual Conference & Exhibition (2023) [1] and is submitted to First Break.

7.1. Introduction

Monitoring and managing water resources is of great importance in our increasingly water-stressed world. Effective and precise measurements of water-column height and flow velocity are essential for a wide range of applications, including flood prediction, hydroelectric power generation, environmental conservation, cable integrity, and water supply management. Traditional methods of water monitoring have their limitations, often constrained by cost, spatial coverage, and the need of swapping batteries and/or retrieving data from sensors placed at specific locations. In recent years, DAS technology has emerged as a tool capable of monitoring the water depth [2] and flow velocity with great precision [3].

DAS converts optical fibers into distributed sensors capable of detecting perturbations along the cable's entire length [4]. In the context of water monitoring, DAS systems can be deployed within water bodies, providing a continuous and high-resolution picture of water dynamics. Unlike conventional point sensors, DAS offers the advantage of real-time, continuous, and distributed monitoring over long distances, making it a powerful tool for understanding and managing complex hydrological systems. In this express letter, we explore the applications in water height and flow monitoring using DAS. By harnessing the capabilities of DAS, we aim to contribute to a more comprehensive and accurate understanding of ocean and river water dynamics.

We focus on vortex-induced vibrations (VIVs) which are known to cause cable erosion, and cable-soil coupling failure [5]. We identify two different VIVs bandwidths at different depths and relate their frequency oscillations to the changing water-column height due to the tides. Moreover, we show the complex relation between the frequency spectrum and the flow velocity.

7.1.1. Experimental setup

The experimental setup is located within the Botlek area in the Port of Rotterdam, The Netherlands. It comprises of a pair of steel poles, each measuring 24 m in length and 0.35 m in diameter, purposefully designed to support a mantle housing a sensing fiber. A schematic overview of the setup can be seen in Figure 7.1. This setup serves a dual purpose by facilitating VSP, alongside horizontal fibers that demonstrate the potential for large-scale areal monitoring. Due to the different water depths and subsurface at the site, the steel poles were driven in at different depths. One pole was driven at a location with a water depth of 5.7 m, while the other pole's water depth was at 3.2 m. Consequently, the exposed portions of the poles above the water surface measured approximately 3 m and 2.4 m, respectively. The horizontal distance between the poles was 38 m.

The mantles have dimensions of 2.4 m in height and 0.37 m in diameter. Each mantle is coiled with a standard single-mode direct-burial communication fiber, with a diameter of 6 mm, extending 317 m in length, covering 1.6 m of the mantle's height. To connect the fiber to the mantle, a lead fiber spanning 106 m is used, which leads to a container where the interrogator is stored. For clarity, Figure 7.1 offers a visual depiction of the setup.

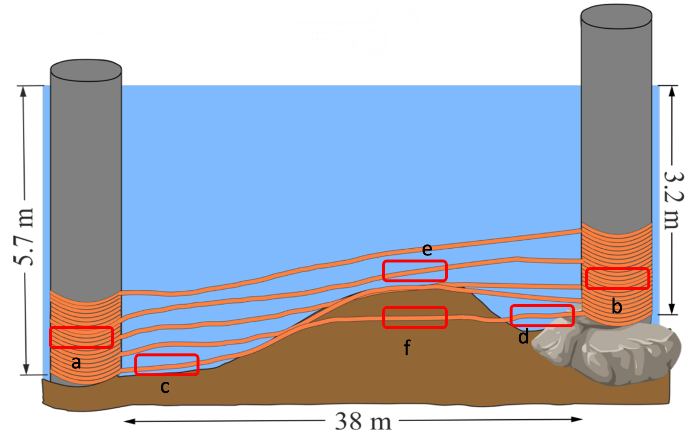

Figure 7.1: Illustration of the setup as observed by a dive inspection. a) Channel location coiled along the deeper pole. b) Channel location coiled along the shallower pole. c) Channel location along a straight fiber in water near the deeper pole. d) Channel location along a straight fiber in water near the shallower pole. e) Straight-fiber channel location along the fourth line in water. f) Straight-fiber channel buried almost 5 cm in mud.

We create five horizontal lines, starting from the base of the mantle at a fiber length of 423 m (106 m for the lead fiber plus 317 m coiled around the mantle). These horizontal lines are situated at height intervals, rising by 0.3 m twice, then 0.6 m, and finally 0.4 m. Each line consists of 38 m of fiber between the poles and 1 m coiled on each pole, giving a length of 40 m in total per line and 200 m total of horizontal fiber length. The shallowest line is positioned at the apex of the VSP. Particular care is exercised during the lowering of the mantles to ensure the integrity of the fiber is maintained throughout the installation process.

For data acquisition, an ASN OptoDAS interrogator [6] is used during the start of the autumn season, the 21st of September at 16:28, over a duration of 6 days. A gauge length of 3 m is chosen for recording, with channel spacing set at 1 m. The selection of a 3-meter gauge length is motivated by the initial objective of capturing surface waves characterized by short wavelengths. The time sampling is set at 62.5 kHz, and decimated 62 times to reduce data volume.

7.2. RESULTS

Our recorded data, as presented in Figures 7.2 - 7.4, reveals the presence of frequency oscillations characterized by a periodicity of 12 hours and 25 minutes. Remarkably, this periodicity aligns with the double tidal cycle occurring along the Dutch coastline. Furthermore, our observations highlight a clear correlation between the frequency oscillations and the water depth. Specifically, when we compare the frequency content with tidal data, as in Figure 7.5, we note that during low-tide phases, only the higher-frequencies of the oscillations are evident, whereas during high-tide phases, the frequencies are comparatively lower.

Additionally, it is noteworthy that the pole positioned in shallower water exhibits a larger and higher frequency band than the pole located in deeper waters, albeit with a reduced amplitude. This can be seen in Figure 7.2. When we focus on the straight channel marked c in Figure 7.1, situated in close proximity to the deeper pole, we observe identical frequency oscillations as those recorded by channel a in Figure 7.1, as shown in Figure 7.2a. It is essential to highlight that the amplitudes of these oscillations are four orders of magnitude higher in the horizontal channel c compared to channel a coiled on the mantle, and that less coherent oscillations emerge within the frequency range of 3 Hz to 3.5 Hz for in Figure 7.3a. These oscillations neither align with the oscillations of the shallower pole nor represent overtones of the fundamental-frequency oscillations occurring within the range of 1.67 Hz to 1.98 Hz. An overtone is discernible in Figure 7.2a, spanning from 2e5 to 3e5 seconds. Nevertheless, the 3 Hz to 3.5 Hz oscillations appears to follow the change in tidal height, as can be seen in Figures 7.2a and 7.3a.

The frequency spectrum of channel f, marked in Figure 7.1 and shown in Figure 7.3b, exhibits very low amplitudes, likely attributed to its position being buried in mud. The straight channel marked d in Figure 7.1, located near the shallower pole on line 1, shows the same frequency content similar to channel b, but with much higher amplitudes, as shown on Figure 7.3c.

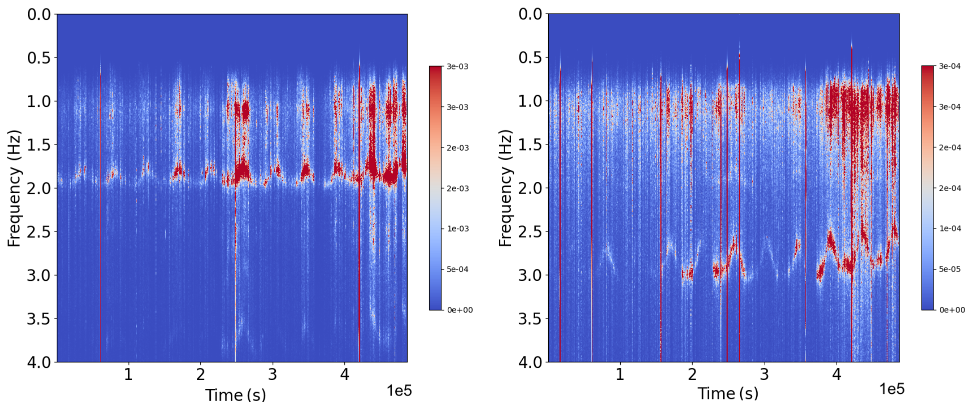

(a) (b)

Figure 7.2: a) Frequency content of channel a (marked in Figure 7.1) coiled on the deeper pole. b) Frequency content of channel b coiled on the shallower pole. Both channels show an oscillation with a period of 12 hours and 25 minutes.

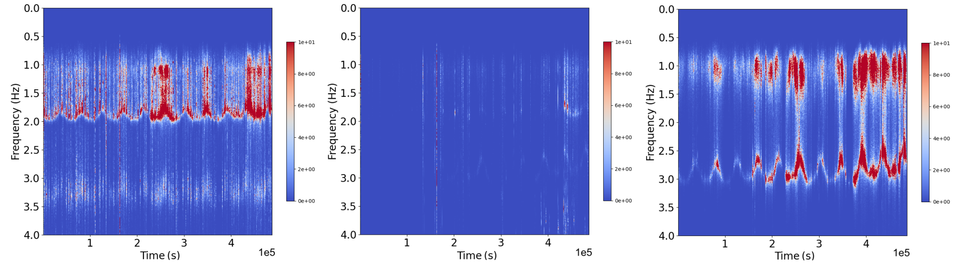

(a) (b) (c)

Figure 7.3: a) Frequency content of the straight horizontal channel c (marked in Figure 7.1) located near the deeper pole. b) Frequency content of channel f located buried in mud. c) Frequency content of channel d located near the shallower pole.

7.3. Interpretation and Discussion

Our findings show the presence of distinct frequency oscillations that exhibit a close correlation with the tidal variations. These oscillations likely stem from the fluctuations in the water-column height, which, in turn, induce changes in the vortex shedding frequency due to variations in the length of the poles exposed to water-flow.

[7] have previously suggested that it is feasible to detect VIVs in sections of offshore cables that remain exposed, meaning parts of the cable which are not buried in sedimentary layers. In our study, we validate their findings through an examination of the amplitude disparities depicted in Figure 7.3. Notably, this figure reveals that once a channel is buried, as in Figure 7.3b, the amplitude of VIVs is greatly reduced, even with the cable being buried for just 5 cm, compared to the frequency and amplitudes in Figure 7.3a and c, that are suspended in water. This observation underscores the potential utility of VIVs detection as a means to monitor the exposure of cables to prevailing currents, particularly since VIVs are recognized to be a large factor contributing to the erosion of cables and pipelines [5].

Furthermore, Figure 7.4a shows that channel c near the deeper pole has the same frequency band oscillation as channel a on the pole. The same is true for Figure 7.4c near the shallower pole. Interestingly enough, channel e in Figure 7.4b shows both oscillation bands. This is related to the location of the channel being in the middle of a straight line, allowing it to record both poles oscillating. It is worth noting the amplitude disparity in time between the lower band of 1.6 Hz - 2 Hz, and the 2.5 Hz - 3 Hz band in Figure 7.4b. The lower-frequency band, emanating from the deeper pole, exhibits higher amplitudes when the frequency band moves from the higher end towards the lower end of the frequency spectrum, which occurs during a tidal rise. Conversely, oscillations originating from the shallower pole demonstrate the opposite behavior, with increased amplitude observed when transitioning from the lower end to the higher end of the spectrum during a tidal fall. Such a change from tidal rise to fall can be observed 2.55e s in Figure 7.4b. This feature is likely

related to the alternating landwards and seawards tidal-stream direction during tidal rise and fall, respectively. Due to the reversed tidal-stream direction, the poles' VIVs alternate being inline with the horizontal lines.
However, beyond the stream direction, drawing meaningful conclusions from the amplitudes in the frequency spectrum in Figures 7.2 - 7.5 proves to be a formidable challenge. Figure 7.5 shows the frequency spectrum of channel d on Figure 7.1 with a higher gain and with modelled tidal height and tidal-stream data for our setup's location beneath the frequency oscillations as a reference. It can be observed that the frequency oscillations follow the tidal height; however, neither the amplitudes nor the frequencies follow the tidal-stream. This shows that estimating the water-flow velocity is far from trivial, at least for a shallow marine environment. An possible explanation for the amplitude behavior would be the effect of the wind; however, our fiber is located several meters below the water surface, and wind data from the Geulhaven weather station, located 200 m from our setup, showed no difference in wind speed during our measuring time.

Mata et al. [8] derived the deep ocean currents based on

$$f_{v_s} = S_t \frac{U_c}{D}. \tag{7.1}$$

In this equation, f_{v_s} is the vortex shedding frequency, S_t is the dimensionless Strouhal number, U_c is the flow velocity, and D is the diameter of the cable, or in our case, our pole. Based on [9], the Strouhal number was taken as 0.2 for seafloor cables and relevant current conditions. In our case, we have two locations and could thus have two different Strouhal numbers, but the poles are in close proximity to each other. It is, therefore, unlikely that the Strouhal number would differ substantially. Especially in between the high - and low tide, when the tidal flow is close to zero, the Strouhal number should be close to zero at the location of both poles. Furthermore, the diameter of our poles is the same. Nevertheless, our vortex shedding frequencies always differ by a factor of approximately 1.5. Furthermore, in our case, the vortex shedding frequencies follow the water height rather than the flow velocity, as shown by Figure 7.5. In this figure, the oscillation's period is clearly 12 hours and 25 minutes, not 6 hours and 12.5 minutes, which would be the case if it would follow the tidal-stream.

7.4. Conclusion

Flow measurements and water-column height monitoring are paramount across diverse sectors.
In this study, we have demonstrated how Vortex-Induced Vibrations (VIVs), measured using distributed acoustic sensing (DAS), can serve as a novel means of measuring water-column height and inferring flow velocity in a shallow marine setting. By associating frequency oscillations and amplitude differences with tidal and flow measurements in a shallow port setting, we unveiled a new perspective on water dynamics.
A purpose-built experimental setup, comprising two steel poles with differential

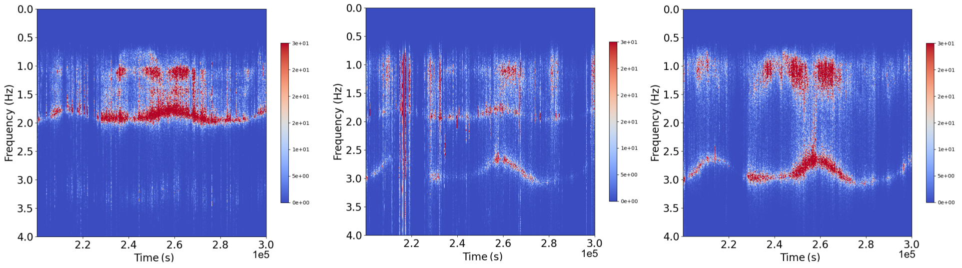

(a) (b) (c)

Figure 7.4: a): Frequency content for a shorter time window of channel c (marked in Figure 7.1). b) Frequency content for channel e. c) Frequency content of channel d.

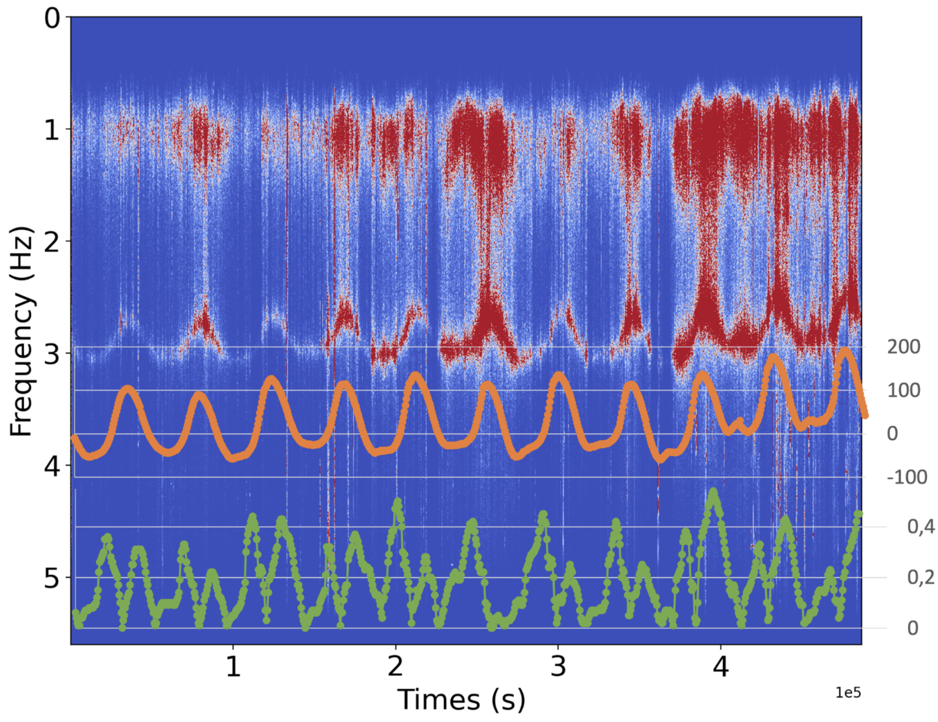

Figure 7.5: Like Figure 7.3c but with a higher gain and with, added, for comparison, modelled tidal height and tidal-stream data in orange in cm and green in ms^{-1}, respectively.

exposures above the water surface, allowed us to investigate the behavior of VIVs in response to changing tidal conditions. Our results confirmed that VIVs, previously linked to cable erosion and cable-soil coupling issues, hold immense potential for monitoring water dynamics and cable-exposure detection. We have unraveled two distinct VIVs bandwidths at different water depths and unveiled their correlation with tidal oscillations in water height. Furthermore, we highlighted the intricate relationship between the frequency spectrum and flow velocity, contributing to the understanding of how these factors interact in a dynamic shallow marine environment. Importantly, we showed that the vortex shedding frequency cannot easily be linked to the flow velocity for such shallow marine setting.

The complex interplay between VIVs, frequency oscillations, and tidal influences provides new insights into the delicate balance of factors governing the behavior of water-flow. Our water dynamic monitoring research highlights potential of using DAS in various domains where precision hydrodynamics data are essential such as industrial sectors, including environmental monitoring, resource management, industrial processes, and infrastructure maintenance.

REFERENCES

[1] M. Buisman, D. Draganov, and A. Kirichek. “Monitoring tidal water-column changes in ports using distributed acoustic sensing”. In: *84th EAGE Annual Conference & Exhibition*. Vol. 2023. 1. European Association of Geoscientists & Engineers. 2023, pp. 1–5.

[2] M. Buisman, E. Martuganova, T. Kiers, D. Draganov, and A. Kirichek. “Continuous monitoring of the depth of the water-mud interface using distributed acoustic sensing”. In: *Journal of Soils and Sediments* 22.11 (2022), pp. 2893–2899.

[3] N. Vahabi, E. Willman, H. Baghsiahi, and D. R. Selviah. “Fluid flow velocity measurement in active wells using fiber optic distributed acoustic sensors”. In: *IEEE Sensors Journal* 20.19 (2020), pp. 11499–11507.

[4] N. Lindsey, H. Rademacher, and J. Ajo-Franklin. “On the Broadband Instrument Response of Fiber-Optic DAS Arrays”. In: *Journal of Geophysical Research: Solid Earth* 125.2 (2020), e2019JB018145. DOI: https://doi.org/10.1029/2019JB018145.

[5] F. Alzabari, C. A. Wilson, and P. Ouro. “Unsteady vortex shedding dynamics behind a circular cylinder in very shallow free-surface flows”. In: *Computers & Fluids* 260 (2023), p. 105918.

[6] O. H. Waagaard, E. Rønnekleiv, A. Haukanes, F. Stabo-Eeg, D. Thingbø, S. Forbord, S. E. Aasen, and J. K. Brenne. “Real-time low noise distributed acoustic sensing in 171 km low loss fiber”. In: *OSA Continuum* 4.2 (Feb. 2021), pp. 688–701. DOI: https://doi.org/10.1364/OSAC.408761.

[7] D. Mata Flores, E. D. Mercerat, J. P. Ampuero, D. Rivet, and A. Sladen. “Identification of two vibration regimes of underwater fibre optic cables by Distributed Acoustic Sensing”. In: *J. Acoust. Soc. Am.* 71 (2023), pp. 554–564.

[8] D. Mata Flores, A. Sladen, J. P. Ampuero, E. D. Mercerat, and D. Rivet. “Monitoring deep sea currents with seafloor distributed acoustic sensing”. In: *Earth and Space Science* 10.6 (2023), e2022EA002723.

[9] T. Worzyk. *Submarine power cables: design, installation, repair, environmental aspects*. Springer Science & Business Media, 2009.

8

The Palette of DAS: Painting Diverse Measurements

This is a concluding chapter discussing the scientific and technical implications for using DAS in ports and waterways. It summarises the frequency bands and sources discovered by this research and elaborated on the preceding chapters. Furthermore, this chapter serves as a pragmatic guide on using DAS to measure the nautical depth using passive noise sources.

IEEE(2023) [1] and is submitted to First Break.

8.1. INTRODUCTION

Coastal regions, including estuaries and river deltas, are frequently subjected to large bathymetrical changes due to sediment transport. These large changes often occur after storms. Monitoring the water depth in these areas is challenging due to numerous factors such as their size, heavy shipping traffic, intricate mixing of water layers, and the highly dynamic nature of the environment. However, there is a pressing need for precise depth measurements to facilitate marine traffic, aid in water management practises, and to enhance our understanding in sediment transport. Despite the growing significance of coastal regions due to expanding trade and population growth in or near these regions, accurate shallow marine depth measurements remain challenging, with limited progress made since the previous century [2].
Buisman et al., (2022a) [3] developed a vertical seismic profile (VSP) using a coiled fibre wrapped around a PVC pipe, successfully recording an active acoustic source through distributed acoustic sensing (DAS) in a laboratory setup. Their work effectively captured the interface between water and sediment. Building upon these findings, Buisman et al., (2022b) [4] demonstrated the applicability of a similar setup to measure the water-sediment interface in a river channel using passive noise. Furthermore, Buisman et al., (2023) [5] showed that the same setup can be used to monitor the water column height. In a subsequent study by Buisman et al., (submitted), the use of horizontal fibres was explored. In this work, we integrate these previous discoveries and showcase how DAS, in conjunction with passive noise, can be employed to monitor water depth on a large scale, including both the water column height and the sediment-water interface, utilizing frequency and amplitude characteristics. Additionally, we focus on all the physical creating passive noise, and how this can be applied for various purposes.

8.2. WATER HEIGHT BASED ON FREQUENCY CONTENT

When a single channel is selected on a pole, and a spectrogram is plotted for a duration of 400,000 s (equivalent to 4.6 days), we obtain Figure 8.1. Thus figure depict oscillating frequency patterns, characterized by a dominant period of 12 hours and 25 minutes. These frequency oscillations are likely attributed to the influence of tides and wind, which induce alternating flow velocities and resonances in our poles. In the port of Rotterdam, the tidal period lasts 12 hours and 25 minutes, coinciding with the observed periodicity. Furthermore, a qualitative agreement is observed when comparing the recorded data with measurements from the nearest tidal station for the same time period. Particularly, the sharp peaks and troughs are evident in both the tidal station's recordings and our frequency spectra. For instance, a trough around 250,000 s is visible in the tidal station measurement, and in our frequency spectrum. These results carry potential implications for continuous water height measurement at quay walls or docks. Existing structures such as docking poles can be repurposed as tidal stations by wrapping several tens of meters of fibre around them, and measuring the exposure length during high and low tide.

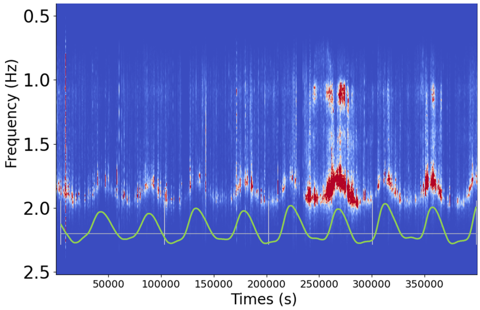

Figure 8.1: The spectrogram depicts a single channel of the left pole in the deeper water, revealing frequency oscillations characterized by a period of 12 hours and 25 minutes. Notable features observed within the frequency range of 1.75 Hz to 2 Hz include distinct sharp peaks and smooth troughs. As a reference, the accompanying measurements of the water height from a nearby tidal station are graphed in green beneath the oscillations (Modified from Buisman et al. 2023).

8.3. SEDIMENT LEVEL AMPLITUDE BASED

The results depicted in Figure 8.2 demonstrate the capability of DAS to measure noise generated by passing vessels. During the recording period illustrated in Figure 8.2, a ship passed between 4700 - 5200 s. Knowing that we are able to measure shipping noise, we use a short record time of 120 s with ample shipping noise and create a PSD, obtaining Figure 8.3. After one month, a sensing mantle was raised

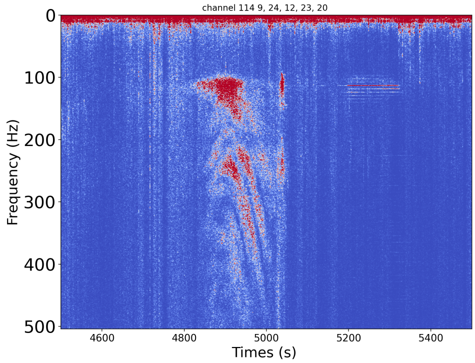

Figure 8.2: Time slice of a spectrogram of channel 114 which is located on the left pole in water, with a gauge length of 3 m. During this recording, a boat passed between 4700 s - 5100 s.

for visual inspection to verify its partial submergence in mud. The presence of barnacles and a discolored brown coating on the mantle confirmed that our setup was indeed partially submerged in mud. Consequently, we anticipate the presence of a water-sediment interface within the depth range of 5.60 m to 5.8 m. The specific depth of the water-sediment interface can vary due to sedimentation and nearby dredging activities. Due to the existence of gas pockets in the mud and the influence of drag forces, a sharp transition at the interface is expected.

By focusing on the frequency range encompassing the fundamental mode and the first overtone and narrowing our analysis to a time window with ample traffic, we obtain Figure 8.3. In this figure, we can observe a noticeable discrepancy in the frequency content beyond a depth of 5.66 m, which coincides with our visual inspection. The sharp transition is likely attributed to the small channel spacing and small gauge length, which results in more measurement points in the depth profile and consequently less averaging in the transition zone.

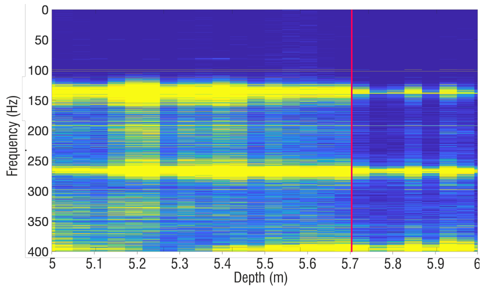

Figure 8.3: A power spectral density plot illustrating a 120 s recording obtained. Notably, at a depth of 5.66 m, a discernible sharp boundary becomes apparent, indicative of the likely interface between water and mud (Modified from Buisman et al. 2022b).

8.4. HORIZONTAL COVERAGE FOR SEDIMENT DETECTION

The depth of the water-sediment interface in many coastal areas frequently exhibits variability due to sedimentation and dredging activities in the vicinity. Hence, measuring the depth at a single point may not accurately represent the entire area, emphasizing the importance of conducting measurements along a line to achieve better spatial resolution.

A similar difference in amplitude content, as in Figure 8.3, is confirmed when combining all horizontal channels and plot the PSD for the duration of a passing vessel, as illustrated in Figure 8.4. The yellow lines indicate the start and end of the five horizontal fibres, with the lowest horizontal fibre starting at 423 m. Each line consists of 40 m of fibre, with 38 m positioned between the poles and 1 m wrapped around each pole. Constructive interference patterns in the form of hyperbolas are observable in Figure 8.4. Given that the fibre extends from one pole to the next and then reverses its path, mirrored frequency patterns are anticipated when transitioning from odd-numbered to even-numbered lines. This mirroring effect is particularly noticeable at the junction of line two and line three. Lines four and five exhibit interference patterns along their entire lengths, whereas lines one, two, and three display zones of both high-amplitude constructive interference patterns and low-amplitude regions. Furthermore, a similar pattern of lower and higher

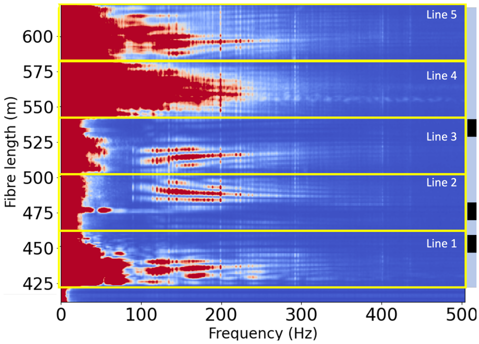

Figure 8.4: PSD plot, integrated over 600 s during which a vessel passed by, displaying all five horizontal lines for 0 - 500 Hz, generated by ships. Each yellow box represents a line from line 1 to 5, with line 1 positioned at the bottom and partially buried the mud region, while line 5 is located at the right, nearest to the water surface. Each line consists of a 38 m cable between the poles, with an additional 1 m segment each pole. Lines 4 and 5 exhibit notable energy with the highest amplitudes. In the PSD, the mud area near the right pole is visible as regions of low amplitude, specifically at the end of line 1, the beginning of line 2, and the end of line 3. The water and mud locations are visually represented in blue and black, respectively, on the right side of the PSD (Modified from Buisman et al. submitted).

amplitude zones is observed when examining lower frequencies. Figure 8.5 displays comparable high-amplitude zones to Figure 8.5 but for much lower frequencies (0.8 - 6 Hz). Additionally, amplitudes around 460 m of fibre length are visible in this lower frequency spectrum, which is absent in the higher frequency range.

Upon further examination of even lower frequencies (less than 0.025 Hz), we observe the same pattern of low amplitude and high amplitude regions, as depicted in Figure 8.6. Notably, this figure also highlights distinct boundaries between zones of high and low amplitude.

A dive inspection was conducted to visually inspect the lines, particularly the locations with low-amplitude zones. The dive inspection recordings revealed that line one is buried in mud at the positions corresponding to these low-amplitude zones, while lines two and three are pressed against consolidated mud within these areas, as demonstrated in Figure **??**. The dive inspection also revealed that the very end of the both mantles are exposed to water as it is installed on top of armor rock. Consequently, the initial two meters of unevenly numbered lines one and three, as well as the beginning of line two, are immersed in water. Intuitively, if the fibre is in contact with water, it will vibrate more than when it is pressed/in mud, allowing us to measure these reverberations. However, since cable reverberations for higher

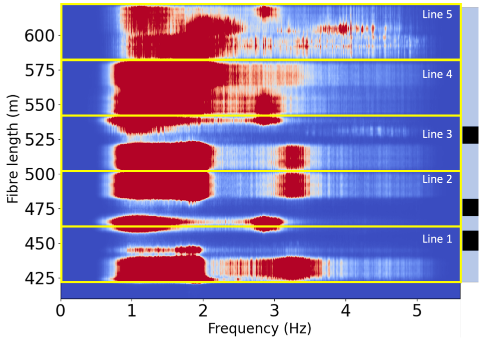

Figure 8.5: PSD plot like Figure 8.4, but for 0 - 5 Hz, and integrated over 5.7 dasys. The vibrations are likely generated by wind and currents, creating vortex-induced vibrations. Lines 4 and 5 exhibit notable energy with the highest amplitudes. In the PSD, the mud area near the right pole is discernible as regions of low amplitude, specifically close to the end of line 1, close to the beginning of line 2, and close the end of line 3. The water and mud locations are visually represented in blue and black, respectively, on the right side of the PSD (Modified from Buisman et al. submitted).

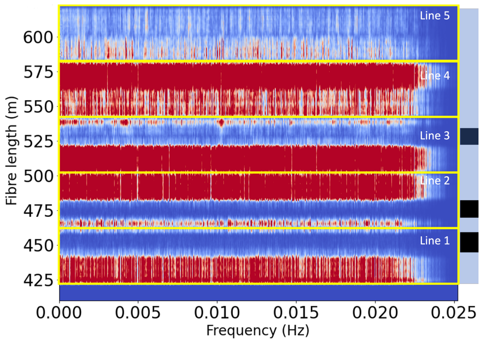

Figure 8.6: PSD plot like Figure 8.4 and 8.5, but for 0 - 0.025 Hz, and integrated over 5.7 days, The vibrations are likely generated by seafloor compliance. Lines 1, 2, and 3 exhibit large amplitude drops once the fibre is buried in mud. In the PSD, the mud area near the right pole is discernible as regions of low amplitude, specifically close to the end of line 1, close to the beginning of line 2, and close the end of line 3. The water and mud locations are visually represented in blue and black, respectively, on the right side of the PSD (Modified from Buisman et al. submitted).

frequencies are likely standing waves within our fibre, and the length from pole two towards the sediments is only two meters, a P-wave standing wave may not be formed within this short section.

Because the signals are muted once the fibre touches the sediments, a very high vertical accuracy is achieved of minimally 6 mm, equal to the fibre width. The horizontal accuracy is smaller due to the gauge length. Nevertheless, the sediment anomaly were still easily identified, and the 2 m section between the end of the pole and the beginning of the sediment anomaly is visible in the lower frequency range, giving us a minimal horizontal resolution of 2 m.

8.5. Frequencies discussion

Figures 8.1 - 8.6 showcase several salient bandwidths encompassing ultra low frequencies spanning the range of 0.001 Hz - 0.025 Hz, low frequencies spanning from 0.8 Hz - 5 Hz, and high frequencies ranging between 100 - 500 Hz. These bandwidths underscore the feasibility of sediment monitoring through diverse passive sources. The ultra low frequencies are likely generated by infra gravity waves [6], which in turn generate seafloor compliance. Similar ultra low frequencies have been observed on a soft sediment shelf [7]. It is plausible that our poles act as a resonator for the seafloor compliance, allow us to measure this phenomenon with our fibres, despite their location being 16 km distant from the shoreline. The reason for the sharp boundaries is likely related to the large integration time of 5.7 days, which accentuates even subtle disparities in amplitude over extended temporal scales.

In the context of the low frequency band, which spans 0.8 Hz to 5 Hz, it is plausible that these oscillations arise from vortex-induced vibrations. Such vibrations, previously detected offshore through using DAS, have been correlated with deep-sea currents, as documented by Mata et al. [8]. In our pilot study, the alternating currents resulting from the tidal dynamics likely play a contributory role in inducing these vibrations. Consequently, a linkage can be inferred between the fluctuations in water column height and the vortex-induced vibrations, as shown in Figure 8.1.

Finally, the high frequency group of 100 Hz - 500 Hz is traced back to vessels movements. Similar frequencies attributed to vessel-generated activities have been documented in Wittekind & Schuster, (2016) and Reis et al., (2019)[9, 10]. Furthermore, by examining a single channel, as in Figure 8.2 and visually observing traffic, we can confirm that these frequencies originate from vessel movements. Additionally, when considering a P-wave velocity of 5900 ms^{-1}[11], and our 24-meter-long steel, a fundamental mode at 123 Hz arises. This resonance frequency may account for the large amplitudes observed in proximity to the 123 Hz fundamental mode and the first overtone near 246 Hz.

8.6. Conclusion

In this study, our deployment of Distributed Acoustic Sensing (DAS) has enabled the comprehensive characterization of wide-ranging frequency bands, delineating distinct bandwidths that offer various applications. We show the plausibility of measuring, and using seafloor compliance (0.001 Hz - 0.025 Hz), vortex-induced

vibrations (0.8 Hz - 5 Hz), and vessel movements (100 - 500 Hz).
The vortex-induced vibration frequency band could be used to estimating the water column height, by relating the flow velocity to the tidal height. Furthermore, the higher frequencies from vessel movements could be used to measure the water-sediment interface with a high accuracy in a vertical setup, given there is a fine channel spacing.
Additionally, we show that horizontal fibres' have a very pronounced amplitudes drop along segments when they come into contact with sediments across all of these frequency bands. This gives us a horizontal resolution with straight fibres between poles of at least 6 mm for measuring the water-sediment interface. Using seafloor compliance we were able to image a horizontal water section of only 2 m, giving us a minimal horizontal resolution of 2 m, using the fibres spanning between two poles.
The combined DAS results show the vast potential of utilising DAS for water column monitoring and water-sediment interface detection. Different passive sources can be used for this purpose, such as: seafloor compliance, vortex-induced vibrations, and vessel movements. Because DAS can be used over large distances, it could potentially be used to monitor sediment transport, water levels and water flows at multiple sites.

REFERENCES

[1] M. Buisman. “Monitoring water column and sediments using DAS”. In: *2023 IEEE International Workshop on Metrology for the Sea; Learning to Measure Sea Health Parameters (MetroSea)*. IEEE. 2023, pp. 328–333.

[2] W. H. McAnally, A. Teeter, D. Schoellhamer, C. Friedrichs, D. Hamilton, E. Hayter, P. Shrestha, H. Rodriguez, A. Sheremet, R. Kirby, *et al.* “Management of fluid mud in estuaries, bays, and lakes. II: Measurement, modeling, and management”. In: *Journal of Hydraulic Engineering* 133.1 (2007), pp. 23–38.

[3] M. Buisman, E. Martuganova, T. Kiers, D. Draganov, and A. Kirichek. “Continuous monitoring of the depth of the water-mud interface using distributed acoustic sensing”. In: *Journal of Soils and Sediments* 22.11 (2022), pp. 2893–2899.

[4] M. Buisman, E. Martuganova, A. Kirichek, and D. Draganov. “Water-depth estimation using propeller noise by distributed acoustic sensing”. In: *83rd EAGE Annual Conference & Exhibition*. Vol. 2022. 1. European Association of Geoscientists & Engineers. 2022, pp. 1–5.

[5] M. Buisman, D. Draganov, and A. Kirichek. “Monitoring tidal water-column changes in ports using distributed acoustic sensing”. In: *84th EAGE Annual Conference & Exhibition*. Vol. 2023. 1. European Association of Geoscientists & Engineers. 2023, pp. 1–5.

[6] X. Bertin, A. de Bakker, A. Van Dongeren, G. Coco, G. André, F. Ardhuin, *et al.* “Infragravity waves: From driving mechanisms to impacts”. In: *Earth-Science Reviews* 177 (2018), pp. 774–799.

[7] W. C. Crawford, S. C. Webb, and J. A. Hildebrand. “Seafloor compliance observed by long-period pressure and displacement measurements”. In: *Journal of Geophysical Research: Solid Earth* 96.B10 (1991), pp. 16151–16160.

[8] D. Mata Flores, A. Sladen, J. P. Ampuero, E. D. Mercerat, and D. Rivet. “Monitoring deep sea currents with seafloor distributed acoustic sensing”. In: *Earth and Space Science* 10.6 (2023), e2022EA002723.

[9] D. Wittekind and M. Schuster. “Propeller cavitation noise and background noise in the sea”. In: *Ocean Engineering* 120 (2016), pp. 116–121.

[10] C. D. Reis, L. R. Padovese, and M. C. de Oliveira. “Automatic detection of vessel signatures in audio recordings with spectral amplitude variation signature”. In: *Methods in Ecology and Evolution* 10.9 (2019), pp. 1501–1516.

[11] I. Rhee, E. Choi, and Y. S. Roh. “Guided wave propagation induced by piezoelectric actuator in bolted thin steel members”. In: *KSCE Journal of Civil Engineering* 16 (2012), pp. 398–406.

8

Bibliography

[1] M. Buisman, E. Martuganova, T. Kiers, D. Draganov, and A. Kirichek. "Continuous monitoring of the depth of the water-mud interface using distributed acoustic sensing". In: *Journal of Soils and Sediments* 22.11 (2022), pp. 2893–2899.

[2] M. Buisman, E. Martuganova, A. Kirichek, and D. Draganov. "Water-depth estimation using propeller noise by distributed acoustic sensing". In: *83rd EAGE Annual Conference & Exhibition*. Vol. 2022. 1. European Association of Geoscientists & Engineers. 2022, pp. 1–5.

[3] M. Buisman, E. Martuganova, D. Draganov, and A. Kirichek. "Monitoring shear-stress changes using seismic measurements from controlled sources and ambient noise and optical fibres". In: *Proceedings to WODCON XXIII* (2022).

[4] M. Buisman, D. Draganov, and A. Kirichek. "Monitoring tidal water-column changes in ports using distributed acoustic sensing". In: *84th EAGE Annual Conference & Exhibition*. Vol. 2023. 1. European Association of Geoscientists & Engineers. 2023, pp. 1–5.

[5] M. Buisman. "Monitoring water column and sediments using DAS". In: *2023 IEEE International Workshop on Metrology for the Sea; Learning to Measure Sea Health Parameters (MetroSea)*. IEEE. 2023, pp. 328–333.

ACKNOWLEDGEMENTS

This work has been made possible by The Port of Rotterdam, Rijkswaterstaat, SmartPort, and Hamburg Port Authority. Furthermore, there are many individuals involved who saw the potential of this work, and who will always have my gratitude for placing their trust in me. First I want to thank **Evgeniia Martuganova** for all the help she has provided. Your level-headed ability to inform and to calibrate my decisions have been instrumental for this work. Not only that, your passion for science is a an attribute I always admired. My supervisors **Deyan, Alex, and Claire** have also significantly impacted this work. **Deyan**, over time, I have grown to appreciate you more and more as a supervisor. It goes without saying that scientific insights have been very valuable, but what I found most captivating when nearing the end, was your calm demeanor when facing adversity with this project, knowing that these challenges would eventually be resolved, initially conflicted with my views. As a progressed with my work, I realised that adopting your approach is what has been an important key to my growth. **Alex**, already during my MSc, you motivated me regarding research. Follow one's curiosity and see where it leads you is something that I learnt to do during my internship with you. Not only that, the combination of applied research with companies is something you showed where we can do good for society. I will try to keep follow this path. **Claire**, your compassion, curiosity and passion is why many people, including my self, gravitate towards you. You set an example without trying. When I struggled your ability to help me reflect is something I truly valued. **Guy**, thank you for your substantial contributions in the applied work, and showing me how to conduct professional surveys. Listening to your experiences and sharing views made this project much more fun, interesting, and successful. You also helped me a great deal with lifting my expertise in geophysics and DAS. **Evert** thank you for getting me into the MSc of Applied Geophysics, though I was not certain at the time, you seemed to know it would work out rather nicely. Thank you also for helping me during tough times. **Edwin Hupkes**, thank you for all the support you have shown throughout the years. Your optimism and long term vision have been instrumental for me to keep thinking bigger and bigger. **Willem**, thank you for your guidance during both my summer internship, MSc thesis and PhD. Your extensive surveying knowledge was a great addition and most useful to have. **Piet**, your compassion will always stick with me. You helped a great deal acquiring a DAS interrogator. Furthermore, I will never forget how you came to my house to give me a bingo card such that I could join the team in a game of bingo during corona. Thank you. **Stoffel** Thank you for your collaboration with Rijkswaterstaat and helping me expanding my research. **Wiebe** thank you for your support and helping me displaying my research to a broader audience. I never thought making such a video would have such an impact. **Nino** thank your support and showing how innovation can be a challenging, but most interesting journey. **Aad**, thank you for always being there for me and keeping me in check. I know I can always count on you, though I am fearful of what you will do as a paranimf. **Eric** though we are both geophysicist from Vlaardingen, we are almost polar opposites. Maybe that is why are conversations are always great. We will keep on mutually learning and growing and I can't wait to try out that jacuzzi. **Ana** Thank you for opening your hearth and the exchange of ideas on so many topics. **Aukje**, I know I complained a lot with you so thank you for listening to all of that. Also, thank you for your scientific insights. **Marat** having you around is made everything better. We instinctively align on so many things. With your seniority and experience came many interesting stories and lessons, which I highly appreciated, but at the same time, it was also really great just watching The Office with you. **Musab** Our discussions about DAS soon evolved in a whole brought range of topics. It was great to listen to get more and more into science with you. **Jingming** your calm and relaxed demeanor makes you a fantastic colleague to have a cup of tea with. Thanks for everything. **Joeri** you know that the eating contest was a tie. Better luck next time. **Manos** it was really cool to have you around during the experiments and to have a beer with. I am sure we will keep in touch and I can't wait for us to catch up again. **Edwin Obando** I remember when we met in Madrid. It was a pleasure meeting you there, and it has always been a pleasure working with you. **Brenda** training with you after a hard day of work was always something I was looking forward to, not just because of the fries. I hope many more sessions will follow. **My family** with whom I struck a fortune. **My parents** thank you for all the unwavering support and being the best. **Michelle** your ability to challenge me and to inspire me at the end of my PhD journey was invigorating, and just what I needed. I hope we will continue down this path with many adventures, making many more memories.

Curriculum Vitæ

Menno Buisman

04-01-1996	Born in Vlaardingen, The Netherlands.

Education

2014–2017	B.Sc. in Earth Science and Economics Vrije Universiteit, Amsterdam Aurau, Switzerland (2017–2019)
2017–2019	M.Sc. IDEA League in Applied Geophysics Delft University of Technology, Delft, the Netherlands Eidgenössische Technische Hochschule Schule Zürich, Switzerland Rheinisch-Westfälische Technische Hochschule, Aachen, Germany Thesis at Delft University of Technology, Delft, The Netherlands
2020 – 2024	PhD. in Applied Geophysics Delft University of Technology, Delft, The Netherlands *Thesis:* Nautical Depth Monitoring and fibre optical cables *Promotor:* dr. D.S. Draganov

Awards

2023	Best Conference Paper Award at MetroSea 2023 IEEE

List of Publications

5. M. Buisman, E. Martuganova, T. Kiers, D. Draganov, and A. Kirichek. “Continuous monitoring of the depth of the water-mud interface using distributed acoustic sensing”. In: *Journal of Soils and Sediments* 22.11 (2022), pp. 2893–2899

4. M. Buisman, E. Martuganova, A. Kirichek, and D. Draganov. “Water-depth estimation using propeller noise by distributed acoustic sensing”. In: *83rd EAGE Annual Conference & Exhibition*. Vol. 2022. 1. European Association of Geoscientists & Engineers. 2022, pp. 1–5

3. M. Buisman, E. Martuganova, D. Draganov, and A. Kirichek. “Monitoring shear-stress changes using seismic measurements from controlled sources and ambient noise and optical fibres”. In: *Proceedings to WODCON XXIII* (2022)

2. M. Buisman, D. Draganov, and A. Kirichek. “Monitoring tidal water-column changes in ports using distributed acoustic sensing”. In: *84th EAGE Annual Conference & Exhibition*. Vol. 2023. 1. European Association of Geoscientists & Engineers. 2023, pp. 1–5

1. M. Buisman. “Monitoring water column and sediments using DAS”. in: *2023 IEEE International Workshop on Metrology for the Sea; Learning to Measure Sea Health Parameters (MetroSea)*. IEEE. 2023, pp. 328–333